

AD-A241 857



DTIC

SELECTE

OCT 28 1991

S

D

D

COLLISIONAL DYNAMICS OF THE $B^3\Pi(0^+)$ STATE
OF
BROMINE MONOFLUORIDE

DISSERTATION

David W. Melton, Captain, USAF

AFIT/DS/ENP/91-01

This document has been approved
for public release and sale; its
distribution is unlimited.

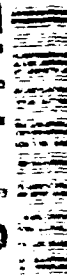
DEPARTMENT OF THE AIR FORCE
AIR UNIVERSITY

AIR FORCE INSTITUTE OF TECHNOLOGY

Wright-Patterson Air Force Base, Ohio

91 10 25 043

91-14123



1

AFIT/DS/ENP/91-01

DTIC
ELECTE
OCT 28 1991
S D

COLLISIONAL DYNAMICS OF THE $B^3\Pi(0^+)$ STATE
OF
BROMINE MONOFLUORIDE

DISSERTATION

David W. Melton, Captain, USAF
AFIT/DS/ENP/91-01

DTIC	
ELECTE	
OCT 28 1991	
S D	
By	
Distribution	
Availability Codes	
Dist	Acquisition Source
A-1	

Approved for public release; distribution unlimited

AFIT/DS/ENP/91-01

COLLISIONAL DYNAMICS OF THE $B^3\Pi(O^+)$ STATE
OF
BROMINE MONOFLUORIDE

DISSERTATION

Presented to the Faculty of the School of Engineering
of the Air Force Institute of Technology
Air University
in Partial Fulfillment of the
Requirements for the Degree of
Doctor of Philosophy

David W. Melton, B.S., M.S.

Captain, USAF

August 1991

Approved for public release; distribution unlimited

REPORT DOCUMENTATION PAGE

1. AGENCY USE ONLY (Leave blank)		2. REPORT DATE Aug 91	3. REPORT TYPE AND DATES COVERED Doctoral Dissertation, Mar 90-Aug 91
4. TITLE AND SUBTITLE COLLISIONAL DYNAMICS OF THE $B^3\Pi(0^+)$ STATE OF BROMINE MONOFLUORIDE			5. FUNDING NUMBERS PE:61101F WU:ILIR9113
6. AUTHOR(S) David W. Melton, CAPT, USAF			
7. PERFORMING ORGANIZATION NAME(S) AND ADDRESS(ES) AIR FORCE INSTITUTE OF TECHNOLOGY WRIGHT-PATTERSON AFB OH 45433-6583			8. PERFORMING ORGANIZATION REPORT NUMBER AFIT/DS/ENP/91-01
9. SPONSORING MONITORING AGENCY NAME(S) AND ADDRESS(ES) Phillips Laboratory (Dr E.A. Dorko) PL/LID Kirtland AFB NM 87117-6008			10. SPONSORING MONITORING AGENCY REPORT NUMBER
11. SUPPLEMENTARY NOTES			
12a. DISTRIBUTION AVAILABILITY STATEMENT Approved for public release; distribution unlimited.			12b. DISTRIBUTION CODE
13. ABSTRACT See Attached.			
14. SUBJECT TERMS Bromine monofluoride, chemical laser, singlet oxygen, laser induced fluorescence, collisional energy transfer, interhalogen			15. NUMBER OF PAGES 168 16. PRICE CODE
17. SECURITY CLASSIFICATION OF REPORT Unclassified	18. SECURITY CLASSIFICATION OF THIS PAGE Unclas	19. SECURITY CLASSIFICATION OF ABSTRACT Unclas	20. LIMITATION OF ABSTRACT UL

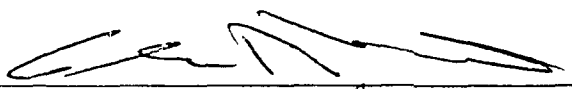
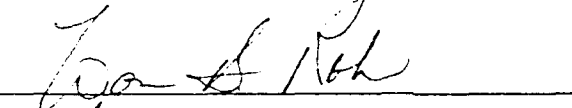
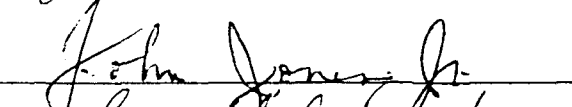

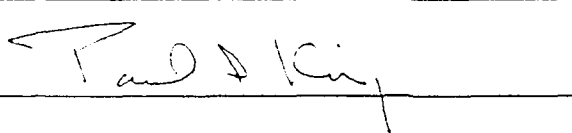
AFIT/DS/ENP/91-01

COLLISIONAL DYNAMICS OF THE $B^3\Pi(0^+)$ STATE
OF
BROMINE MONOFLUORIDE

David W. Melton, B.S., M.S.

Captain, USAF

Approved:

	<u>23 AUG 91</u>
	<u>26 Aug 91</u>
	<u>23 Aug 91</u>
	<u>28 Aug 91</u>
	<u>23 Aug 91</u>

Accepted:

	<u>2 Sept 91</u>
---	------------------

Preface

The interest and financial assistance of Phillips Laboratory and Dr. Ernest A. Dorke in support of the author's Ph.D. dissertation research at the Air Force Institute of Technology is appreciated.

The author is deeply indebted to his initial faculty advisor, Dr. Won B. Roh for his direction in selecting a topic for investigation. His support and interest during course work, qualifying exams and throughout the dissertation research was critical to the author's success.

The author is profoundly grateful to his committee chairman, Captain Glen P. Perram. Captain Perram's advice, guidance and instruction were the foundation of the author's dissertation research. Captain Perram's accessibility and attitude made him both a trusted counselor and a true friend.

The author would like to thank laboratory supervisor Bill Evans, and technicians Greg Smith, Leroy Cannon and Rick Patton for their assistance throughout this project.

Finally, the author wishes to thank his wife, Beth, and his children for their support and understanding during the long hours of this project.

David W. Melton

Table of Contents

	Page
Preface.	iii
List of Figures.	vii
List of Tables	ix
Notation	x
Abstract	xiii
I. Introduction	1
1.1 Overview.	1
1.2 Halogens and Interhalogens.	2
1.3 Bromine Monofluoride (BrF).	5
1.4 Problem Statement	8
1.5 Organization.	9
II. Background Theory.	10
2.1 Spectroscopy.	10
2.1.1 Hund's Cases	10
2.1.2 Predissociation.	14
2.2 Kinetics.	17
2.2.1 Laser Induced Fluorescence (LIF)	18
2.2.2 Energy Transfer.	19
2.3 Types of Spectra.	23
III. Singlet Oxygen Excitation of BrF $B^3\Pi(0^+)$	24
3.1 Introduction.	24
3.2 Background Theory	25
3.3 Experiment.	29
3.4 Results	33
3.4.1 Quenching of $O_2(b)$	33
3.4.2 Chemiluminescence Spectrum	39
3.4.3 Excitation Mechanism	42
3.5 Discussion.	51
3.5.1 Steady State Kinetic Analysis.	51
3.5.2 BrF(B) Excitation Rate	58
3.5.3 Energetics of the Excitation Mechanism	58
3.5.4 Singlet Oxygen Quenching Studies	59
3.5.5 Potential for a BrF(B-X) Chemical Laser.	60
3.6 Conclusions	61
IV. Collisional Energy Transfer in BrF $B^3\Pi(0^+)$	63
4.1 Introduction.	63

4.2	Experimental Arrangement.	64
4.2.1	BrF Production	64
4.2.2	Excitation System.	67
4.2.3	Detection System	68
4.3	Electronic Quenching.	69
4.3.1	Background Theory.	70
4.3.2	Experimental Results	71
4.3.2.1	Laser Excitation Spectra.	73
4.3.2.2	Electronic Quenching Experimental Procedures.	76
4.3.2.3	Mix Self Quenching.	77
4.3.2.4	Argon Quenching	79
4.3.2.5	Bromine Quenching	82
4.3.2.6	CF ₄ , CO ₂ and N ₂ Quenching.	84
4.3.2.7	Oxygen Quenching.	84
4.3.2.8	SF ₆ Quenching	85
4.3.3	Discussion of Electronic Quenching Results . .	87
4.3.3.1	Bromine Quenching	87
4.3.3.2	CO ₂ Quenching	89
4.3.3.3	SF ₆ Quenching	90
4.3.3.4	Oxygen Quenching.	92
4.3.3.5	Energy Channels	95
4.4	Vibrational Transfer.	96
4.4.1	Background Theory	96
4.4.1.1	Montroll-Shuler Model	98
4.4.2	Vibrational Transfer Experimental Results. . .	101
4.4.2.1	Experimental Procedures	102
4.4.2.2	Montroll-Shuler Data Fits	105
4.4.2.3	Stern-Volmer Analysis	110
4.4.3	Discussion of Vibrational Transfer Results . .	112
4.5	Conclusions	117
4.5.1	Electronic Quenching	117
4.5.2	Vibrational Transfer	118
V.	Conclusions.	119
5.1	Summary of Singlet Oxygen Excitation of BrF(B). . . .	119
5.2	Summary of Collisional Energy Transfer in BrF(B). . .	120
5.3	Implications for Chemical Laser Development	121
5.4	Further Studies	122
	Bibliography	123
	Appendix A BrF Spectroscopic Data	130
	Appendix B Montroll-Shuler Computer Model	138

Appendix C	Experimental Calibrations and Calculations	143
Appendix D	Systematic Error	150
Vita		152

List of Figures

<u>Figure</u>	<u>Page</u>
1	Typical interhalogen potential energy curves 3
2	Ground state interhalogen electronic configuration 13
3	Hund's cases correlation diagram 13
4	Herzberg case I(c) predissociation 16
5	Energy transfer processes 20
6	Potential energy curves for BrF 27
7	Chemiluminescent flow tube apparatus 30
8	Emission spectra for O ₂ (b-X) band 34
9	Stern-Volmer plot for quenching of O ₂ (b) by CO ₂ and CF ₄ . . . 36
10	Stern-Volmer plot for quenching of O ₂ (b) by bromine 38
11	Chemiluminescence spectrum of BrF(B-X) 40
12	Relative vibrational population distribution for BrF(B) . . . 41
13	BrF emission intensity as a function of flow time 43
14	Relationship between BrF(B) and O ₂ (b) Intensities when CO ₂ is added 46
15	BrF(B) and O ₂ (b) emission intensities as a function of molecular bromine concentration 47
16	Relationship between BrF(B) and O ₂ (b) intensities as a function of O atom concentration 49
17	Experimental LIF Apparatus 65
18	Fluorescence decay of BrF(B) with 1 mtorr of CO ₂ 72
19-20	Laser Excitation Spectra of BrF(B-X) 74

21	Stern-Volmer fit for mix self-quenching in BrF $v'=5$	78
22	Stern-Volmer plot for argon quenching of BrF $v'=5$	81
23	Quenching of BrF(B) $v'=6$ by bromine	83
24	Stern-Volmer plot of oxygen quenching of BrF(B) $v'=2$	86
25	BrF(B-X) $v'=2$ total fluorescence waveform influenced by SF ₆	86
26	Comparison of experimental and theoretical BrF(B) $v'=5$ waveforms influenced by SF ₆	91
27	Vibrational Transfer Spectrum	103
28	Montroll-Shuler fit to the (6-9) band	106
29	Montroll-Shuler fit to the (5-2) band	106
30	Montroll-Shuler fit to the (4-3) band	107
31	Montroll-Shuler fit to the (3-3) band	107
32	Montroll-Shuler fit to the (2-2) band	108
33	Montroll-Shuler fit to the (1-6) band	108
34	Montroll-Shuler fit to the (0-6) band	109
35	Stern-Volmer plot of Montroll-Shuler fits to the (6-9) band.	111
36	Demonstration of Landau-Teller scaling	115
37	Vibrational thermalization of BrF(B) after initial excitation of $v'=5$	116
38	Vibrational thermalization of BrF(B) after initial excitation of $v'=3$	116
39	Montroll-Shuler comparison to rate equation result	141
40	Spectral Resolution of the McPherson 0.3m monochromator.	144
41	Spectral Resolution of the ISA HR-360 0.64m monochromator.	144
42	Relative spectral response to total fluorescence	147

List of Tables

<u>Table</u>		<u>Page</u>
I	Predicted $[\text{BrF(B)}]/[\text{O}_2(\text{b})]$ Ratios	57
II	$\text{O}_2(\text{b})$ Quenching by Diatomic Halogens	60
III	BrF(B) Electronic Quenching Rate Coefficients	80
IV	Computed Spectral Overlap Fractions	104
V	Fundamental Vibrational Transfer	112
VI	BrF(B) total vibrational transfer rate constants induced by oxygen	114
A.I	Vibrational Spectroscopic Constants for BrF(X)	130
A.II	Term Values for BrF(B)	131
A.III	Rotational Constants for BrF(X)	132
A.IV	Rotational Constants for the Vibrational levels of BrF(B)	133
A.V	Franck-Condon Factors of ^{79}BrF	134
A.VI	BrF(B) Radiative Lifetimes.	137
B.I	Input parameters for the rate matrix comparison	141
C.I	Observation Wavelengths used in the Vibrational Transfer Experiments	148

Notation

<u>Symbol</u>	<u>Description</u>
Fundamental constants and variables:	
c	speed of light
h	Planck's constant
k	Boltzmann's constant
T	temperature
t	time
t'	transformed time variable
μ	reduced mass
Spectroscopic symbols:	
$V(r)$	potential energy at internuclear separation r
r	internuclear separation
r_e	equilibrium internuclear separation
$(\sigma_g) (\pi_u) (\pi_g) (\sigma_u)$	electronic configuration symbols
$^2P_{1/2,3/2}$	atomic energy states
$^1\Sigma^+, ^3\Pi(0^+), ^1\Delta_g, ^1\Sigma_g^+$	molecular electronic energy states
ν	frequency
ν_p	frequency of an absorbed photon
ν_r	frequency of a radiated photon
λ	wavelength
T_e	total energy of an electronic state
T_v	total energy of a vibrational level
v	vibrational quantum number

J	rotational quantum number
,	electronically excited $B^3\Pi(0^+)$ state
"	ground electronic state $X^1\Sigma^+$
ω_e	fundamental vibrational frequency
$\omega_e x_e$	first anharmonic vibrational term
$\omega_e y_e$	second anharmonic vibrational term
$\omega_e z_e$	third anharmonic vibrational term
$B_e, \alpha_e, \gamma_e, B_v, D_v, H_v$	rotational constants
A_{11}	Einstein coefficient for spontaneous emission from level 1 to level 1
$\Delta\varepsilon$	energy difference
$q_{v',v''}$	Franck-Condon factor
S_J	rotational line strength factor
R_e	electronic dipole moment
$h(\lambda_{\text{obs}} - \lambda_{v',v''})$	spectral response function
λ_{obs}	observation wavelength
$\lambda_{v',v''}$	wavelength of $v'-v''$ bandhead
Kinetic symbols	
k^P	rate coefficient for photon excitation
k^{V-T}	rate coefficient for vibrational to translational energy transfer
k^{V-V}	rate coefficient for vibrational to vibrational energy transfer
k^{R-T}	rate coefficient for rotational to translational energy transfer
k^{EQ}	rate coefficient for electronic quenching

k^Q	total quenching rate coefficient
k^r	rate coefficient for photon radiation
k^{PD}	rate coefficient for predissociation
k_n	rate coefficient of equation (3.n)
$k^v(1,0)$	fundamental vibrational transfer rate coefficient
k^v	rate coefficient for total vibrational removal
$I(v')$	emission intensity from level v'
$N(v')$	population density in level v'
τ_r	radiative lifetime
τ_{CF}	collision free lifetime
τ_{eff}	effective lifetime
Γ_o	first order deactivation rate coefficient
Γ	total first order decay coefficient
[]	denotes concentration
z_n	population solution in Montroll-Shuler model
x_n	population solution including radiative and electronic quenching losses

Abstract

When Br_2 is combined with F atoms and discharged oxygen in a flow tube, $\text{BrF } B^3\Pi(0^+)$ is produced in a highly non-thermal distribution peaking at $v'=3$. The emission was linearly dependent on the $\text{O}_2(b^1\Sigma)$ concentration. The observed dependence of the BrF(B) emission on Br_2 and atomic oxygen is inconsistent with a steady state prediction of a sequential excitation mechanism, where BrF(X) is excited by successive collisions with singlet oxygen. The experimental data are consistent with a three body mechanism involving Br and F atoms.

Electronic quenching of BrF(B) by a number of collision partners (Br_2 , CO_2 , O_2 , N_2 , CF_4 , SF_6 , Ar) was examined for three vibrational levels using laser induced fluorescence (LIF) techniques. The rate coefficients ranged from $<6 \times 10^{-14} \text{ cm}^3/(\text{molecule} \cdot \text{s})$ as an upper limit for argon, to $(6.86 \pm .18) \times 10^{-11} \text{ cm}^3/(\text{molecule} \cdot \text{s})$ for Br_2 .

Vibrational transfer in BrF(B) , induced by the BrF production mix ($\text{CF}_4, \text{Br}_2, \text{F}$) was measured by observing the spectrally resolved LIF emission from each vibrational level after an initial excitation of BrF(B) $v'=5$. This vibrational transfer obeyed a simple theoretical prediction, the Montroll-Shuler model. A single fundamental rate coefficient $k^v(1,0) = (3.5 \pm .6) \times 10^{-12} \text{ cm}^3/(\text{molecule} \cdot \text{s})$ characterizes vibrational transfer.

COLLISIONAL DYNAMICS OF THE $B \pi(0)^+$ STATE

OF

BROMINE MONOFLUORIDE

I. Introduction

1.1 Overview

The collisional transfer of energy is a fundamental process of gas-phase chemistry. A complete understanding of this phenomena is of critical importance in fields as diverse as atmospheric chemistry and laser physics. In the latter, the transfer of energy between the excited states of small molecules, is the basis for an exciting and versatile class of high energy lasers. This class, the short wavelength chemical lasers (SWCLs), offer a number of advantages over more conventional chemical lasers (HF, DF) as well as other high energy laser device concepts such as Nd:glass and CO_2 lasers (Pines,1987).

SWCLs would operate on electronic transitions in gas-phase molecules. Through proper selection of the rotational-vibrational levels involved, these devices offer tunable output in the visible frequency range. Thus, SWCLs are promising for spectroscopic and chemical processing applications since the energies produced are orders of magnitude better than the best dye lasers. Visible output is very attractive for space based weapons applications since the size and thus the mass of targeting optics varies inversely with the square of the wavelength. Here tunability is also an

advantage since it enhances the problems involved with defending against such a weapon.

As chemical lasers, SWCLs are powered by a chemical reaction as opposed to an external excitation such as an electric discharge. Thus, SWCLs are potentially less massive than other high energy laser (HEL) concepts which require bulky electronic power supplies.

Research in SWCLs is focused on two primary areas: selection and evaluation of lasing molecules, and development of chemical excitation mechanisms.

1.2 Halogens and Interhalogens

Halogens and interhalogens are particularly attractive as SWCL media. In these molecules, the equilibrium nuclear separation in the electronically excited state, the $B^3\Pi(0^+)$ state, is greatly displaced from that of the ground state, the $X^1\Sigma_g^+$ state (see Figure 1). Therefore, any $B \rightarrow X$ transition, due to the Franck-Condon principle (Franck, 1925), will terminate on a high vibrational level of the ground state. Simply put, the Franck-Condon principle states that transitions between electronic levels take place on an extremely short timescale in comparison to internuclear vibrations. In a thermal distribution these high vibrational levels will be unpopulated, thus providing an initial population inversion for a laser.

The B-states of these molecules have long radiative lifetimes and generally low electronic quenching rates. These are both key factors in maintaining a population inversion.

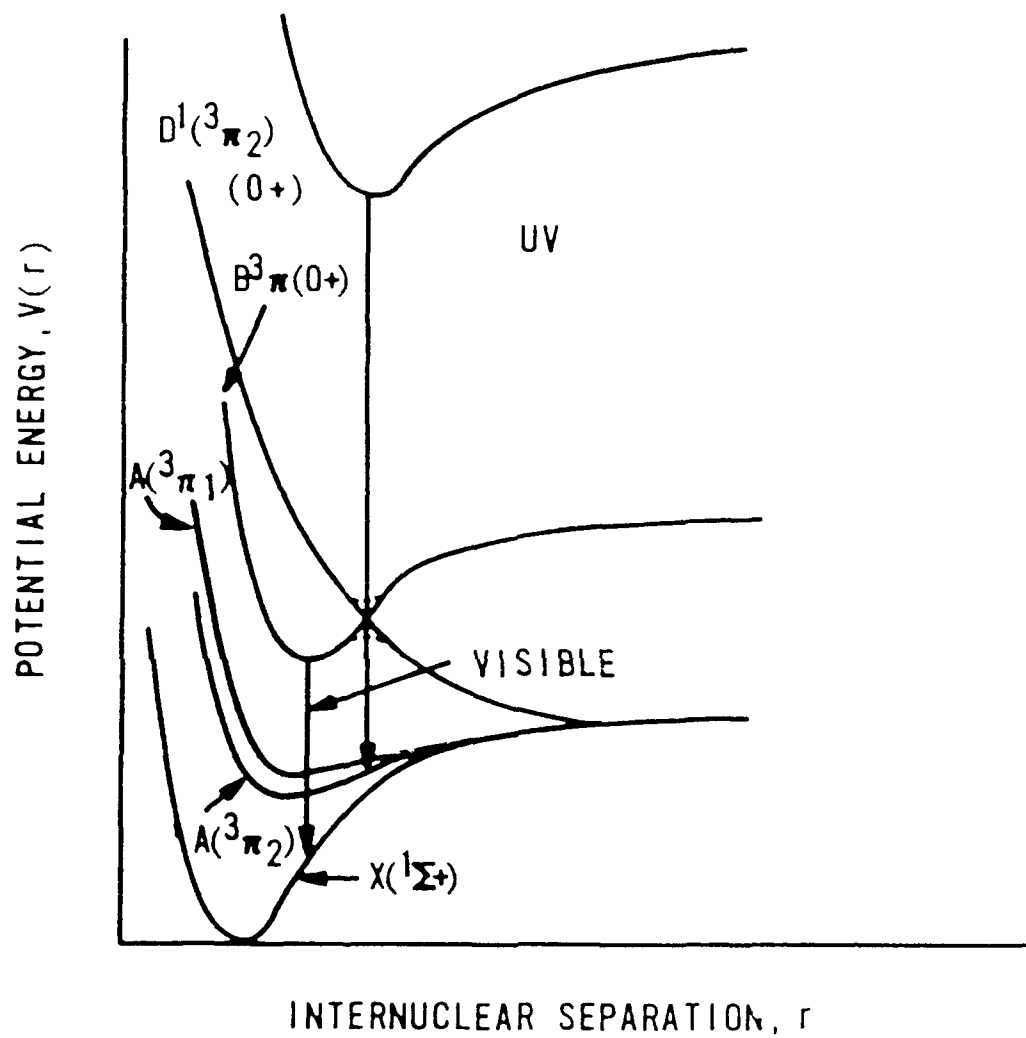


Figure 1. Typical Interhalogen Potential Energy Curves (Perram, 1986)

Viable chemical excitation schemes exist for a number of these molecules. An excellent example is the excitation of the IF (B) state by resonant energy transfer from metastable $O_2(^1\Delta_g)$ (Whitefield, 1983). $O_2(^1\Delta_g)$ has a radiative lifetime of 65 minutes due to a forbidden downward transition (Badger, 1965). This lifetime is inconceivably long for a laser candidate, but ideal for an energy production and storage reservoir.

In most of the interhalogen molecules, optical pumping is feasible (Davis, 1979:181). Thus the problems involved in lasing can be separated from those of the chemical excitation scheme. Lasing through optical excitation has been demonstrated for I_2 (Byer, 1972), Br_2 (Wodarczyk, 1977), and IF (Davis, 1983).

If the spectroscopic characteristics of a given molecular specie are acceptable, collisional energy transfer is the determining factor for lasing potential. Two primary forms, vibrational energy transfer, and electronic quenching are involved.

A chemical excitation is likely to deposit its energy across a range of B-state vibrational levels. For an efficient laser, these energy levels must swiftly thermalize through vibrational-vibrational (V-V) and vibrational-translational (V-T) processes so that lasing can proceed from a single, $v'=0$, excited state vibrational level. Thus the dependence of vibrational transfer rates on collision partner must be well understood.

Unfortunately some efficient vibrational transfer partners may also be efficient as electronic quenching agents. Electronic quenching is the collisional deactivation of electronically excited molecules. Electronic quenching and predissociation are the primary non-radiative energy loss

mechanisms for electronic energy. Thus an efficient electronic quencher steals energy from a lasing transition. The electronic quenching rates of potential laser medium and buffer gas molecules must thus be determined.

Of more general scientific interest is how vibrational energy transfer in the interhalogens obeys energy transfer models such as the Landau-Teller (Landau, 1936) and Schwartz, Slawsky and Herzfeld (SSH) theories (Schwartz, 1952). SSH theory uses time-dependent perturbation theory to describe vibrational transfer in a harmonic oscillator, where interactions are weak and restricted to single quantum vibrational transitions. In IF(B), V-T transfer scales with reduced mass as $\mu^{1/3}$ as predicted by SSH theory, whereas the rates for I₂(B) and BrCl(B) deviate significantly from this dependence. The vibrational spacing in IF(B) is relatively large (400 cm⁻¹) so that multi-quantum transitions are unlikely. In I₂(B) and BrCl(B), which do not follow SSH theory, the spacing is much smaller (128 and 200 cm⁻¹ respectively) (Perram, 1986). The probability for multi-quantum transfer is high when the vibrational transfer is this small, $\Delta\epsilon/kT \approx 1$. In BrF(B) the vibrational energy spacing (372 cm⁻¹) is close to that in IF(B). The vibrational transfer scaling in BrF(B) with collision partner reduced mass should be a compromise between that of IF(B) and BrCl(B).

1.3 Bromine Monofluoride (BrF)

The interhalogen BrF is a promising chemical laser candidate. The strongest BrF(B \rightarrow X) lasing transition would be (ν', ν'') = (0,8) at 766 nm (Clyne, 1972). This near visible output represents a considerable

improvement over the infrared outputs of existing chemical lasers. Like IF, BrF is thermochemically unstable and rapidly disproportionates via the reaction (Clyne, 1976):



Therefore, BrF must be produced and studied in a flow tube reactor. A flow tube allows access to that period of time where BrF exists. This can be a disadvantage since the chemistry of flow tube production controls the obtainable BrF population densities, limiting the ultimate gain of a potential laser. One possible advantage is that the molecule can be produced with vibrational excitation which can be utilized in production of the electrically excited state. This is the case with flow tube production of IF (Kessler, 1991).

The BrF(B-X) spectra was first probed by Durie in flame emission in 1951 (Durie, 1951) and in absorption by Broderon and Sicre in 1955 (Broderon, 1955). In 1972, Clyne et. al. used a novel method to obtain emission spectra (Clyne, 1972). They found that a bright orange-yellow flame characteristic of B→X emission is produced when Br₂, F atoms and the products of a microwave discharge of oxygen are mixed in a flow tube. This chemiluminescence was used for spectroscopic measurements, and although a three-body mechanism was proposed, no detailed study of the excitation channel was conducted.

In 1976, Clyne et.al. first used laser induced fluorescence to probe rotational structure of the vibrational bands (Clyne, 1976). They were able to then estimate the rotational constants for the BrF B and X states.

In this paper Clyne first calculated both the Rydberg-Klein-Rees (RKR) (Steinfeld, 1986:133) potential energy curves for the $B^3\Pi(0^+)$ and $X^1\Sigma^+$ electronic states as well as the Franck-Condon factors for the B-X system.

Clyne then produced a series of papers in which LIF was used to determine radiative lifetimes for both the stable and predissociated levels of the B-state (Clyne, 1978a-c) on a ro-vibrationally resolved basis. In a final paper Clyne and Liddy were able to revise their lifetime estimates upward due to better understanding of the effects of diffusion in their experimental apparatus (Clyne, 1980). Through this LIF work as well as further absorption (Coxon, 1979), emission (Coxon, 1981) and infrared laser diode spectroscopy (Takehisa, 1988) (Nakagawa, 1988), the body of BrF spectroscopic knowledge has been well developed. Coxon's emission study offers the latest estimates of the BrF(B) and BrF(X) rotational and vibrational constants. The spectroscopic constants and Franck-Condon factors of the BrF (B-X) system are presented in Appendix A.

In contrast, there is very little data concerning collisional energy transfer in BrF. In 1977, Clyne and McDermid first studied electronic quenching of BrF by the collision partners BrF, Br₂ and He (Clyne, 1977). A single transition, the P(21) line of the $(v',v'') = (6,0)$ band of ⁸¹BrF was examined. Results presented in chapter IV of this dissertation, as well as Clyne's later work (Clyne, 1980), cast doubt on the conclusions drawn in that paper. Clyne and Liddy examined both electronic quenching and vibrational transfer with a number of collision partners. In only one case, oxygen, was more than a single ro-vibrational level excited. No study of the variation of quenching and with vibrational level was attempted. The vibrational transfer was studied using only bandpass

filters to resolve the emission from a single vibrational level. The signal strength was too low to allow the use of a monochromator. This method, complemented with the use of long-pass filters in total fluorescence experiments, was used to determine their results. The measured vibrational rate constants were for total population removal from an initially populated vibrational level. No observation of the population evolution for the other vibrational levels was attempted. In summary, the collisional energy transfer data base for BrF is sparse.

1.4 Problem Statement

The potential of BrF as a chemical laser medium rests on the resolution of two distinct problem areas: Chemical excitation of the $B^3\Pi(0^+)$ state and collisional energy transfer within the B-state manifold. This dissertation will address these questions in two primary experimental phases.

In phase 1, discussed in chapter III, the excitation of BrF $B^3\Pi(0^+)$ by metastable singlet oxygen $O_2(a^1\Delta, b^1\Sigma)$ was examined under steady state conditions in a flow tube reactor. A three body mechanism was identified which depends directly on $O_2(b^1\Sigma)$, not $O_2(a^1\Delta)$. Production efficiencies and rates and their implications for laser development were determined. Previously unknown quenching rates on $O_2(b^1\Sigma)$ by Br_2 and Br were measured.

In phase 2, discussed in chapter IV, collisional energy transfer in BrF was studied using temporally resolved laser induced fluorescence techniques. Total fluorescence studies were used to determine electronic quenching rates on BrF (\bar{B}) for a variety of collision partners, and three initially excited vibrational levels.

Spectrally and temporally resolved LIF was employed to determine vibrational energy transfer rates in the B-state manifold. These rates indicate the time evolution of vibrational population. Vibrational transfer in the BrF(B) manifold induced by the production mix was found to obey a relatively simple energy transfer theory, the Montroll-Shuler model.

1.5 Organization

This chapter will be followed in Chapter II by a discussion of the background theory common to the two experimental phases of this dissertation. Chapter III will discuss the theory, experiments and results relevant to the chemiluminescent flow tube experiments examining singlet oxygen excitation of BrF(B). Chapter IV will do the same for the LIF experiments exploring collisional energy transfer in BrF (B). These two chapters are intended to be relatively self-contained for simplicity. Chapter V will present the overall conclusions of this dissertation and discuss the suitability of singlet oxygen excitation of BrF(B) in a chemical laser and BrF as a lasing molecule.

II. Background Theory

There are two experimental phases in this dissertation. Both the chemiluminescent flow tube studies of singlet oxygen excitation of BrF(B), and the laser induced fluorescence (LIF) studies of electronic quenching and vibrational energy transfer in BrF share a fundamental background. Although the means of excitation differ, in each case the emission from the B-state of BrF is observed. In the chemiluminescent flow tube experiment the excitation is accomplished through collisions with singlet oxygen and observed under steady-state conditions. In pulsed LIF the B-state is excited directly by a laser pulse and the time evolution of the fluorescence is then examined. Both phases share a theoretical background with respect to the spectroscopy and, to a lesser extent, the kinetics of BrF. This chapter will discuss those common points. Each of the experimental chapters will then explore those theoretical aspects particular to the experiment in greater detail.

2.1 Spectroscopy

Two particular aspects of spectroscopy, Hund's cases and predissociation, are especially significant both for BrF and the interhalogens as a class of molecules.

2.1.1 Hund's Cases. The halogen atoms all have a ground state electronic configuration with s^2p^5 outer shells. When two of these atoms form a diatomic molecule this produces an electronic configuration of

$(\sigma_g)^2(\pi_u)^4(\pi_g)^4(\sigma_u)^0$ for the valence electrons (see Figure 2). This document will employ the shorthand 2440 for this configuration with the '0' denoting the unfilled (σ_u) level. Since the outer shell is completely filled, this is a $^1\Sigma_g^+$ totally symmetric spin state. The immediate excited states for this class of molecule are formed when an electron is excited to the (σ_u) level in either a 2431 or 2341 configuration.

Hund specified the possible angular momentum coupling cases (Herzberg, 1950). In Hund's case (a), it is assumed that the interaction of the nuclear rotation with the spin and orbital electronic motion is very weak; however, the electronic motion, is very strongly coupled to the line joining the two nuclei. It is this coupling that produces the $^1\Sigma_g^+$ term symbol for the 2440 state. The excited 2431 state has a $(\sigma_g)^2(\pi_u)^4(\pi_g)^3(\sigma_u)^1$ electronic configuration. The term symbol is found by adding a σ_u electron to the $^2\Pi_g$ normal state. The spins add or cancel and the parity goes as $u \times g = u$ producing a $^{1,3}\Pi_u$ symbol. Similarly, the 2341 excited state has a $^{1,3}\Pi_g$ term symbol. The $^3\Pi$ states are split into three components, $^3\Pi(0)$, $^3\Pi(1)$, $^3\Pi(2)$, by the weak spin orbit interaction. Furthermore, the interaction between nuclear rotation and the orbital angular momentum L splits the electronic angular momentum $\Omega = 0$ state into two components in a splitting that is called Λ doubling. This splitting occurs for all cases where $\Lambda \neq 0$. It is only for $\Omega=0$ that this splitting is independent of the total angular momentum J . The two split cases are labeled by + and -, thus Hund's case (a) for the interhalogens produces the $^3\Pi_{u,g}(2,1,0+,0-)$, $^1\Pi_{u,g}(1)$ and $^1\Sigma_g^+(0)$ electronic states.

Hund's case (c) is the other angular momentum coupling case that

applies to the diatomic halogen and interhalogen molecules. In the heavier molecules, the interaction between L and the spin angular momentum S can be stronger than the interaction with the internuclear axis. Here only Ω is a good quantum number. The energy expressions are as in case (a); except that here the manifold of levels appears as distinct electronic states rather than a splitting of the electronic levels within a single state (see Figure 3). The halogen atoms have $^2P_{3/2,1/2}$ atomic states. In case (c) coupling, the addition of two $^2P_{3/2}$ atomic states yields ($3u, 2u, 2g, 1u, 1u, 1g, 0u-, 0u-, 0g+, 0g+$) states, while the addition of a $^2P_{1/2}$ atomic state with a $^2P_{3/2}$ atomic state yields ($2u, 2g, 1u, 1u, 1g, 1g, 0g+, 0g-, 0u+, 0u-$) states.

These states are generated according to the rules presented by Mulliken (Mulliken, 1932). If the two atoms have the same S , L , and J values, and J is half integral, the Hund's case (c) terms are generated by the rule:

$$\begin{aligned}
 &(2J)u, (2J-1)u, \dots, 0u-, \\
 &\quad (2J-1)g, \dots, 0g+, \\
 &\quad \dots \dots \dots \quad (2.1) \\
 &\quad \quad \quad 0g+
 \end{aligned}$$

For states with differing half integral J values the rule is:

$$\begin{aligned}
 &J_1+J_2, J_1+J_2-1, \dots, 0+, \\
 &\quad J_1+J_2-1, \dots, 0-, \\
 &\quad \dots \dots \dots \quad (2.2) \\
 &\quad J_1-J_2, \dots 0+ \text{ or } 0-
 \end{aligned}$$

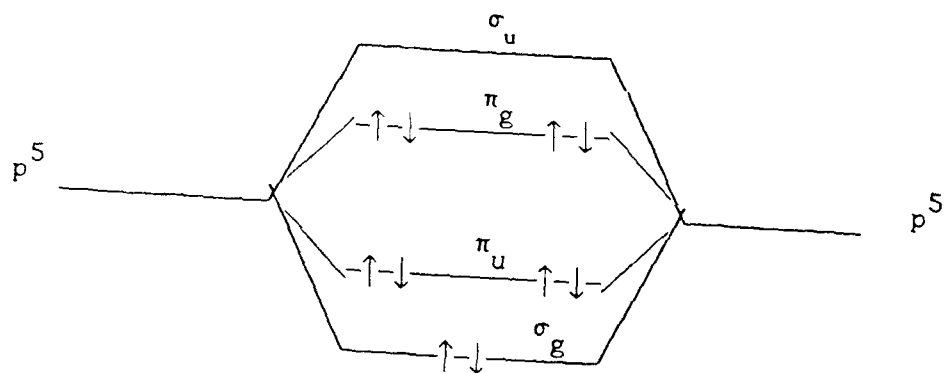


Figure 2. Ground state interhalogen electronic configuration.

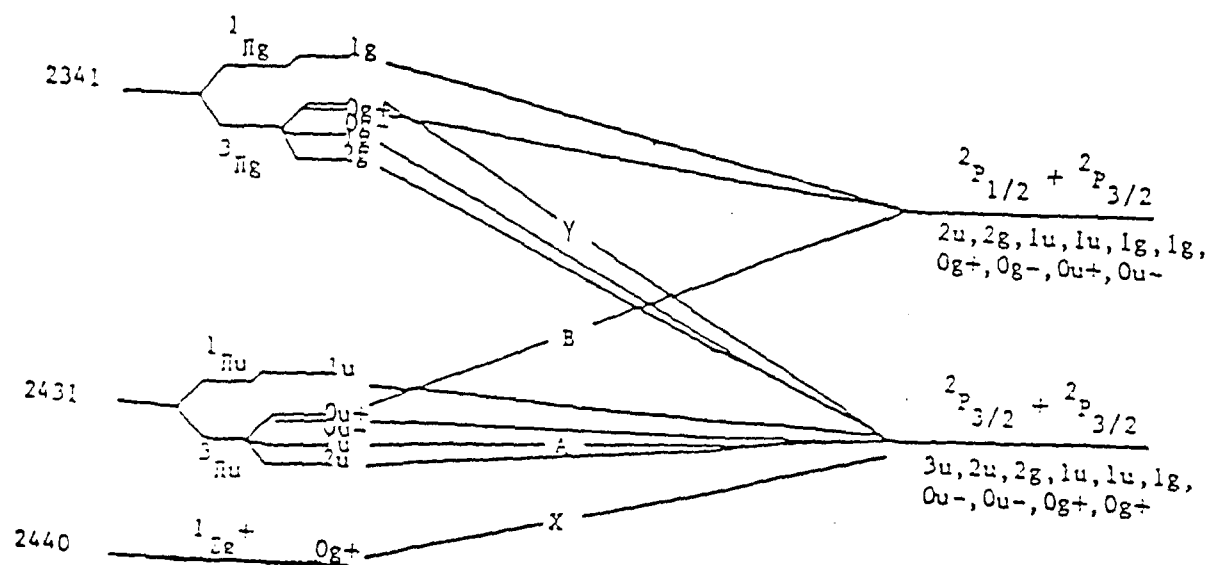


Figure 3. Hund's cases correlation diagram (Perram, 1986).

For this case, there will be equal numbers of 0^+ and 0^- states and each term occurs as both a u and a g.

For the interhalogens, no inversion symmetry exists; therefore the u,g labeling seen in Figure 3 does not apply. Clyne first noted that in BrF, the $B^3\Pi(0^+)$ excited state corresponded in the dissociation limit with an excited Br($^2P_{1/2}$) atom and a ground state F($^2P_{3/2}$) atom (Clyne, 1972). The $A^3\Pi(1)$ state is always lower in energy and dissociates into two ground state atoms. In Figure 3 note that the $B^3\Pi(0^+)$ state, arising from the 2431 electronic configuration, crosses the repulsive $Y(0^+)$ state, arising from the 2341 configuration. In general, potential energy curves for states of the same symmetry and angular momentum do not cross (see Figure 4). This perturbs the energy levels and allows for predissociation. This energy level perturbation produces a potential energy maximum between the B state and the separated atoms.

There are in fact five 0^+ states that correlate with a combination of $^2P + ^2P$ atoms. Two of these correlate with the atomic ground state atoms $^2P_{3/2} + ^2P_{3/2}$, one with each of the singly excited states $^2P_{3/2} + ^2P_{1/2}$, and one with the doubly excited state $^2P_{1/2} + ^2P_{1/2}$. The lowest in energy of these is the $X^1\Sigma_g^+$, and the second and third respectively are the $Y(0^+)$ and the $B^3\Pi(0^+)$ states.

2.1.2 Predissociation This phenomena occurs when the discrete energy states of the bound molecule overlap the continuous range of levels corresponding to dissociation into individual atoms. This overlap allows a radiationless transition from an excited molecular state into separated atoms. In Herzberg case I(c) predissociation, the excited $B^3\Pi(0^+)$ state

and the repulsive $Y(0^+)$ state curves meet at a point above the asymptote of the Y state curve (Figure 4). This asymptote corresponds to the separated atom state. This allows those B state molecules at a vibrational level higher than this point to cross over to the Y state and dissociate into two ground state atoms. The electronic excitation of the B state molecule is lost in a radiationless transition. Thus the term predissociation; the molecule can dissociate even though it has less internal energy than the interatomic bond. This $Y(0^+)—B^3\Pi(0^+)$ interaction is generally true for the interhalogens, thus the B states of these molecules are all to a certain degree unstable. This is quite significant, since the B state is the potential upper laser level for a number of these molecules. Predissociation can shorten the radiative lifetime, depleting the $B^3\Pi(0^+)$ population by a nonradiative process. This impacts on the ability of a potential interhalogen laser to maintain a population inversion and removes energy from the laser.

Clyne and McDermid suggest that the situation is not as clear cut for BrF (Clyne, 1978c). Unlike the interhalogens in general, they suggest that for BrF predissociation is Herzberg case I(b) for the $v' = 6, 7$ levels and rotational for $v' = 8$. In case I(b), the intersection point between the excited B and repulsive Y states is actually below the Y state asymptote forming a shallow potential well weakly binding the predissociating state. Here the predissociation limit has the energy of the asymptote of the Y state curve. Clyne and McDermid feel that this level structure is caused by the crossing of the predissociated curve by a shallow bound state. The nature of the state is not clear but they feel it could be another $^3\Pi(0^+)$ correlating with $Br(^2P_{3/2})$ and $F(^2P_{1/2})$ separated atoms. This state would

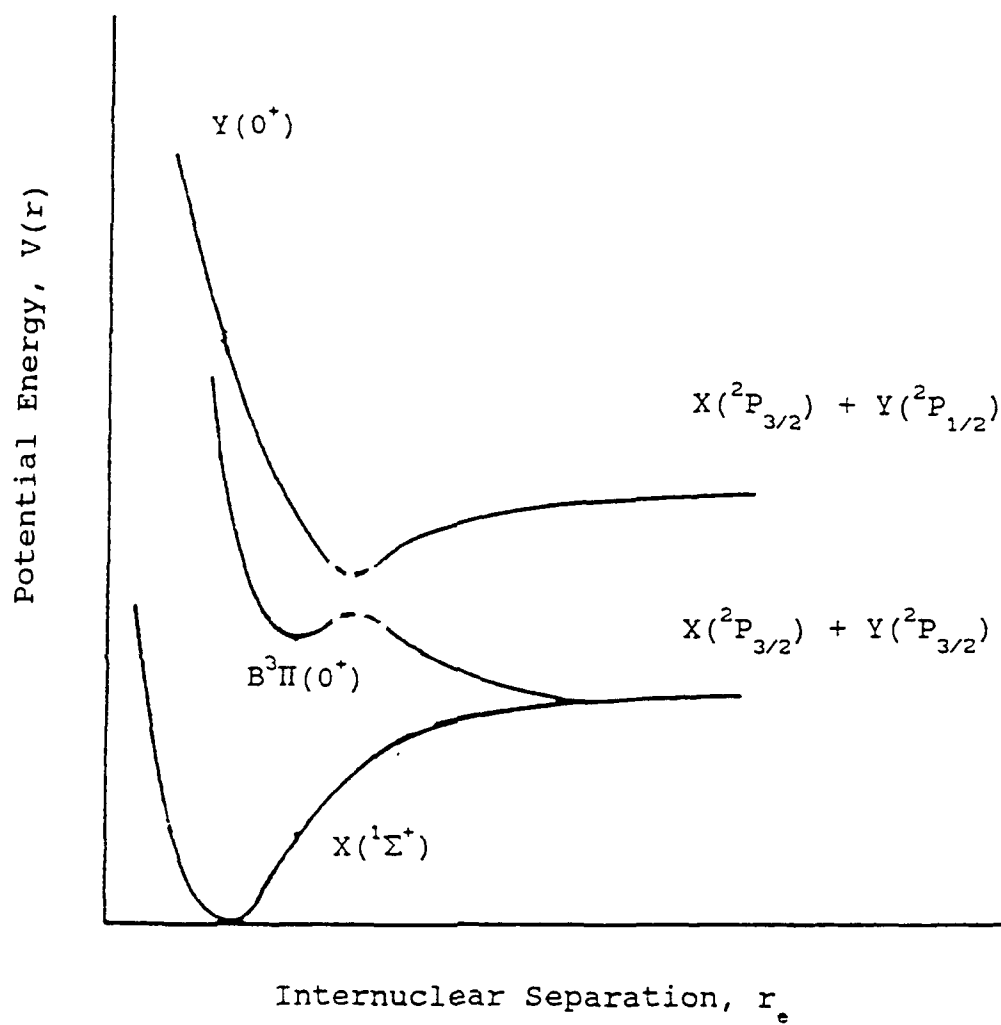


Figure 4. Herzberg Case I(c) predissociation.

have a large internuclear displacement, in comparison to the ground state, which would prohibit direct downward transitions. This state could then dissociate to ground state atoms via the repulsive $Y(0^+)$ state. They found that predissociation commences abruptly at the levels $v'J'=6,49$ and $v'J'=7,30$. The lifetime behavior of the $v'=8$ level is different. In this vibrational level there is a definite relationship between lifetime and rotational level J' . This suggests rotational predissociation in this vibrational level.

In rotational predissociation, the effective potential energy curve depends on rotational level:

$$V_J(r) = V_0(r) + \frac{h}{8\pi^2 c \mu r^2} J(J+1) \quad (2.3)$$

Where μ is the reduced mass, J is the rotational level and r is the internuclear separation. This variation in potential energy curve changes the point of intersection with the repulsive state. Thus the lifetime decreases with increasing J level, which is the case for the $v'=8$ level of BrF(B) .

2.2 Kinetics

The major goal of the proposed research is to probe and understand the energy transfer processes of the BrF molecule. These include collisional excitation of the $\text{BrF } B^3\Pi(0^+)$ electronic state, collisional deactivation of the excited state, and vibrational energy transfer. The discussion that follows describes in detail those processes that transfer

energy in the excited state. Once the B-state has been excited the same processes operate in both experiments. The discussion will begin with a review of LIF since the kinetics presentation is from the viewpoint of this technique.

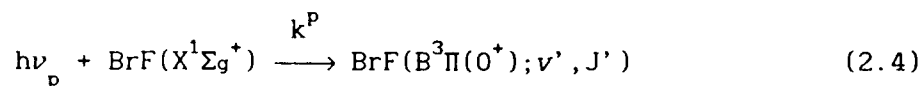
2.2.1 Laser Induced Fluorescence (LIF). The variety and sensitivity of spectroscopic techniques increased dramatically after the development of the laser in 1960. One of the simplest and most effective techniques is LIF. In LIF, a tunable laser is used to pump an excited state of a molecular or atomic species. When the excited atoms or molecules relax to lower energy states they spontaneously emit photons. These photons have energies equivalent to the spacing between the upper and lower levels of the transition. When the laser is tuned across its frequency range a number of excited energy levels are populated which then emit photons of various frequencies. By monitoring total fluorescence as the laser is tuned, a complete excitation spectrum can be generated. In this spectrum, analogous to an absorption spectra, the relative intensities of the spectral lines are characteristic of the ground state vibrational populations.

LIF has a number of advantages over conventional absorption or emission spectroscopy. Lasers provide very high powers in extremely narrow spectral linewidths. Thus very specific rotational and vibrational levels within the electronically excited state can be probed. Very short pulses down to the femtosecond range allow excellent temporal resolution which is vital when examining kinetic processes. This is done by monitoring the time evolution of intensity of the fluorescence emitted

from a level excited by the laser pulse. The time evolution is characteristic of the electronic and vibrational energy transfer processes. In general, a given fluorescence waveform is averaged over a large number of pulses (1000 or more), to reduce noise factors. In LIF, the intense laser photons can probe the excited states of species at very low concentrations where absorption spectroscopy is difficult.

LIF has already been used in the examinations of a number of the interhalogen molecules (Wolf, 1985) (Perram, 1986). Electronic quenching, radiative lifetimes and vibrational energy transfer in BrF will be probed using this technique. The collisional excitation studies will employ a conventional chemiluminescent flow tube described later in this document.

2.2.2 Energy Transfer In LIF the first step is the excitation of some upper level by laser photons, as seen in transition 1 in Figure 5. Using BrF as an example:



In the chemiluminescence experiments this state is prepared chemically. For example in both BrF (Clyne, 1972) and IF (Whitefield, 1983), the B-state is excited by resonant collisions with singlet oxygen.

In vibrational to translational (V-T) energy transfer, seen in transition 2, molecular vibrational energy is transferred to the kinetic energy of a bath gas molecule M.

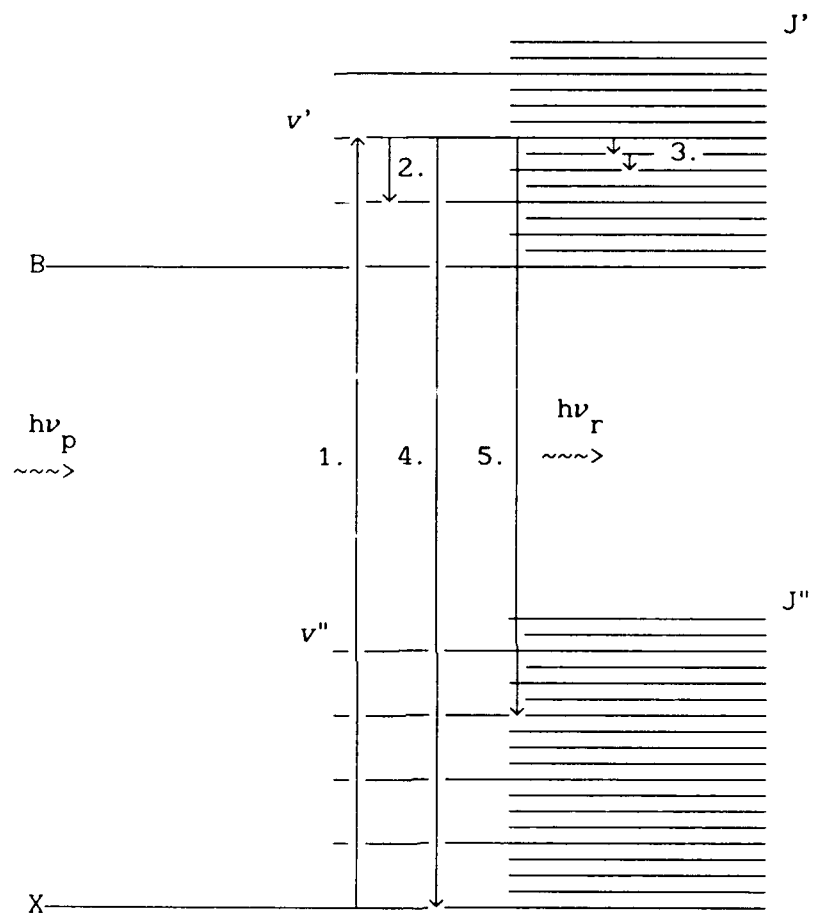
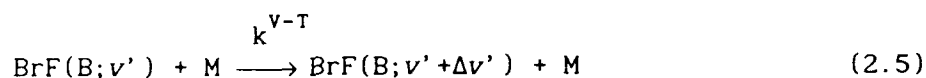
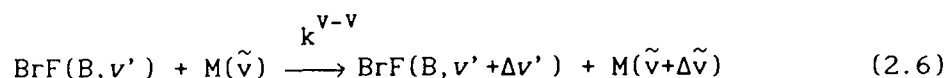


Figure 5. Energy transfer processes.

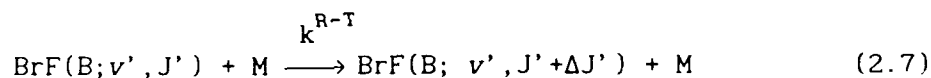


The same transition in Figure 5 could also represent vibrational to vibrational (V-V) energy transfer with a diatomic or polyatomic molecule.

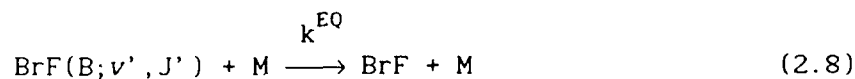


where $\tilde{\nu}$ denotes the vibrational level of the colliding molecule.

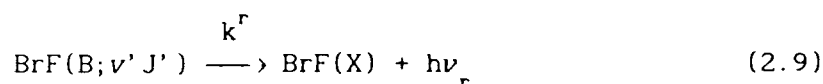
Rotational energy can also be transferred to the translational kinetic energy of a colliding molecule as seen in transition 3.



In electronic quenching, as seen in transition 4, collision with another molecule takes the BrF molecule to a lower electronic state.

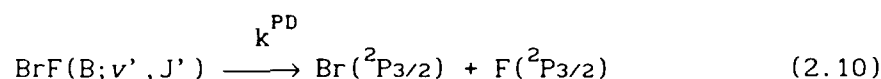


All of the above processes remove energy from the excited state non-radiatively. Thus these processes can drain the energy that would go into the radiative transition. Transition 5 describes a radiative transition in which a photon with an energy equivalent to the difference between initial and final levels is emitted:



where ν_r is the frequency of the emitted photon. The ground state vibrational level ν'' after this transition is determined by the Franck-Condon factor, $q_{\nu', \nu''} = \langle \nu' | \nu'' \rangle$ which is the overlap integral of the vibrational wave functions of the ν' and ν'' levels. Detection of these emitted photons is the diagnostic tool used in LIF.

Predissociation, discussed earlier, is a non-collisional process that dissociates the BrF molecules from the excited molecular state into ground state atoms without emitting photons.



Thus predissociation steals laser energy and shortens the effective lifetime.

At pressures less than 3 mtorr, low particle densities reduce the collision rate to the point that only collisionless processes, spontaneous emission and predissociation, are significant. The change in intensity of an emitted line is directly proportional to the change in population density of the upper level, thus:

$$\frac{dI(\nu', J')}{dt} \propto \frac{dN(\nu', J')}{dt} = - \frac{N(\nu', J')}{\tau_r(\nu', J')} - k^{\text{PD}} N(\nu', J') \quad (2.11)$$

Where $\tau_r(v', J')$ denotes the radiative lifetime of the (v', J') level. Thus the overall collision-free lifetime of a given v', J' state is given by:

$$\frac{1}{\tau_{CF}(v', J')} = \frac{1}{\tau_r(v', J')} + k^{PD} \quad (2.12)$$

2.3 Types of Spectra

Three different types of spectra were observed and recorded in this dissertation research. Emission spectra were observed in the singlet oxygen excitation studies (chapter 3). In these spectra the emission from the excited vibrational levels is observed by scanning the monochromator. In the specific cases observed in chapter III, the excitation is through microwave excitation, directly in the oxygen spectra, or by collision with the singlet oxygen in the case of BrF.

Laser excitation spectra were used in the chapter IV studies of collisional energy transfer to select pump transitions. As the laser is tuned in frequency total fluorescence peaks occur that are characteristic of the $v'' \rightarrow v'$ bands. Since the ground state is thermally populated strong bands arise only from ground stated $v'=0,1$.

Vibrational transfer spectra were used to select observation wavelengths in the vibrational energy transfer studies. Here the laser is fixed in wavelength and the resolved fluorescence is observed as the monochromator is tuned. This fluorescence is the $B \rightarrow X$ emission from the v' levels. This spectra shows the population in vibrational levels other than the initially excited level, showing how much transfer has occurred.

III. Singlet Oxygen Excitation of BrF B³Π(O⁺)

3.1 Introduction

A primary consideration for any potential chemical laser medium is the availability of chemical excitation schemes. The diatomic interhalogens have been studied extensively as potential visible chemical laser candidates (Davis, 1987). A favored approach for providing electronic excitation has been energy transfer from an energetic metastable specie such as the singlet states of O₂ or NF (Perram, 1990). While excitation of IF B³Π(O⁺) by energy transfer has been studied extensively, the most recent examination being the 1989 study by Piper (Piper, 1989) and the 1991 results of Kessler (Kessler, 1991), corresponding studies for BrF have largely not been accomplished.

A bright orange-yellow flame is produced when Br₂, F and the effluents of a microwave discharge of oxygen are mixed in a flow tube apparatus (Clyne, 1972). This emission proves conclusively that singlet oxygen does excite the BrF(B) state. In this chapter the rates and mechanism for excitation of the B³Π(O⁺) state of bromine monofluoride by energy transfer from the metastable O₂(b¹Σ_g⁺) are reported. The results distinguish between two classes of excitation mechanisms: 1. A three-body recombination involving fluorine and bromine atoms or 2. Sequential energy transfer involving a vibrationally or electronically excited BrF intermediate state.

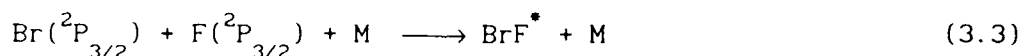
3.2 Background Theory

The formation of BrF(B) in the presence of singlet oxygen has been suggested to proceed from a three-body recombination process, but no extensive kinetic studies have been performed (Clyne, 1972). In all such experiments, no BrF emission was observed unless F, Br and singlet oxygen were all present. Note that bromine atoms will be formed from Br₂ mixed with discharged oxygen due to the presence of atomic oxygen:

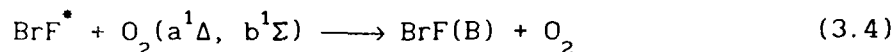


These reactions possess nearly gas kinetic rate coefficients (Clyne, 1971) and thus the oxygen atoms will be rapidly converted quantitatively to bromine atoms provided $[\text{Br}_2] > [\text{O}]/2$.

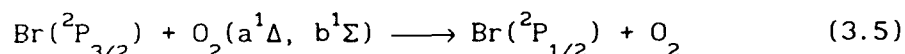
Recombination of ground state $^2\text{P}_{3/2}$ halogen atoms



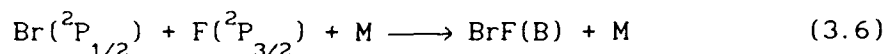
could produce either highly vibrationally excited ground state, BrF(X, $v'' > 0$), or electronically excited BrF $^3\Pi(2,1,0^-)$. The location of these intermediate electronic states is uncertain (Coxon, 1975). These possible intermediate states are denoted collectively as BrF^{*}. The specie M represents any possible collision partner, predominantly O₂(X) in the current experiments. Excitation to BrF(B) could then proceed by energy transfer:



Three-body recombination could also proceed with an excited bromine atom, $\text{Br}(^2\text{P}_{1/2})$, produced from energy transfer:



This process is resonant and very efficient for $\text{O}_2(a)$ and iodine atoms (Derwent, 1972), but largely unexplored for bromine atoms. Since the $\text{B}^3\Pi(0^+)$ state of BrF correlates with $\text{Br}(^2\text{P}_{1/2}) + \text{F}(^2\text{P}_{3/2})$ separated atoms, the B-state could be formed directly from recombination:



The spin-orbit splitting in atomic fluorine is 404 cm^{-1} and production of BrF(B) from $\text{F}(^2\text{P}_{1/2}) + \text{Br}(^2\text{P}_{3/2})$ is energetically inaccessible (Clyne, 1972).

Another class of excitation mechanisms may be considered by examining the potential energy curves for BrF and energy levels for molecular oxygen as shown in Figure 6 (Coxon, 1981). The available energy of $\text{O}_2(b^1\Sigma, v=0)$, $13,121 \text{ cm}^{-1}$, or $\text{O}_2(a^1\Delta, v=0)$, $7,882 \text{ cm}^{-1}$ (Herzberg, 1950), is insufficient to excited $\text{BrF(B, } v'=0)$ at $18,116 \text{ cm}^{-1}$ (Coxon, 1981) in a single

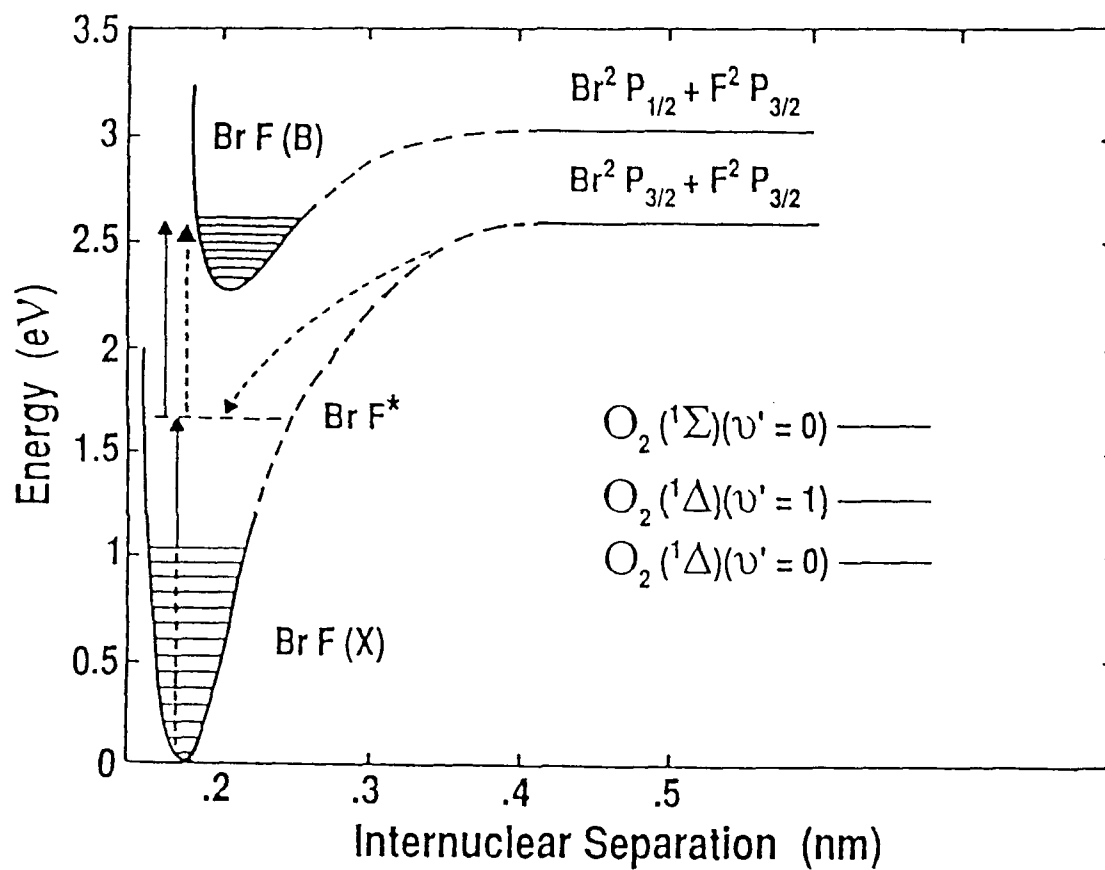


Figure 6. Potential energy curves for BrF and energy levels for molecular oxygen (Coxon, 1981). Two BrF(B) excitation mechanisms are shown: (---) recombination and (—) sequential excitation. The repulsive O^+ state causing predissociation in BrF(B) is not shown.

collision. However, a two-step excitation process again involving some excited BrF intermediate, BrF^* , is possible:

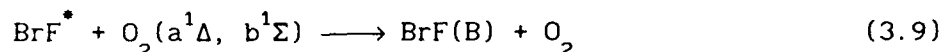
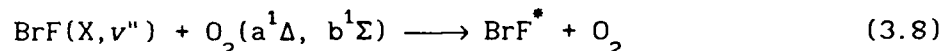


Figure 6 illustrated this process with $\text{O}_2(\text{b})$ as the first step and $\text{O}_2(\text{a})$ as the second step. Unless considerable vibrational relaxation occurred within the intermediate BrF^* , two $\text{O}_2(\text{b})$ collisions would lead to population of predissociated states. Two $\text{O}_2(\text{a})$ collisions are not sufficiently energetic to populate $\text{BrF}(\text{B})$ without utilizing possible vibrational excitation of $\text{BrF}(\text{X})$ from reaction (3.7).

All of these processes have been studied, and recently reviewed (Davis, 1989a.), for singlet oxygen excitation of $\text{IF } \text{B}^3\Pi(0^+)$.

Whitefield et al observed two distinct chemiluminescence zones when F and I_2 were injected into a flow of discharged oxygen (Whitefield, 1983). A strong $\text{IF}(\text{B-X})$ emission near the I_2 injector was followed by a much weaker emission that filled the flow volume. The initial, bright emission was attributed to a two step, sequential excitation mechanism similar to reactions (3.7-3.9). The weaker emission was attributed to three-body recombination. The characteristic yellow emission from $\text{I}_2(\text{B-X})$ observed in chemical oxygen-iodine lasers (COIL) also exhibits these two distinct emission regions. Some of the most intense $\text{IF}(\text{B})$ emissions have been observed when vibrational excitation of $\text{IF}(\text{X}, \nu'')$ from the reaction, $\text{F} + \text{I}_2 \longrightarrow \text{IF}(\text{X}, \nu'' > 0) + \text{I}$, is utilized in an excitation mechanism probably

involving two $O_2(a^1\Delta)$ and $IF A'(^3\Pi_2)$ as the intermediate (Davis, 1989b).

The research described in this chapter will distinguish between the recombination and sequential excitation mechanisms by examining the dependence of the $BrF(B)$ and $O_2(b)$ emission intensity on Br_2 , O , F , and buffer gas partial pressures. In doing so, the rates for deactivation of $O_2(b)$ by BrF reagents (CF_4 , Br_2 and Br) and the rate of production of $BrF(B)$ will be determined.

3.3 Experiment

The experiments were performed in a typical flow tube apparatus as shown schematically in Figure 7. The flow tube was a 8 cm diameter, 60 cm long Pyrex tube equipped with a 6.4 mm diameter injector tube and two 5 cm diameter observation windows. The exit plane of the injector tube was simply a single, 4 mm diameter hole with no rake assembly for enhanced mixing. Side ports of 1.2 cm diameter were available for additional gas flows. A 1 mm thick teflon insert matched to the flow tube geometry was used to reduce $O_2(b)$ wall deactivation rates. The system was pumped by a Sargent Welch 1000 l/min vacuum pump through a liquid nitrogen cold trap to provide a linear flow velocity in the 8 cm tube of 1 m/s at a typical total pressure of 3 torr. The cold trap was required to protect the vacuum pump from the halogen reagents. The system leak rate was less than 1.3 mtorr/min. Total gas pressures were recorded with an MKS model 390 10 torr capacitance manometer. Gas flows for O_2 and CO_2 were controlled by Sierra Instruments model 840 2000 sccm flow controllers. Gas flows for

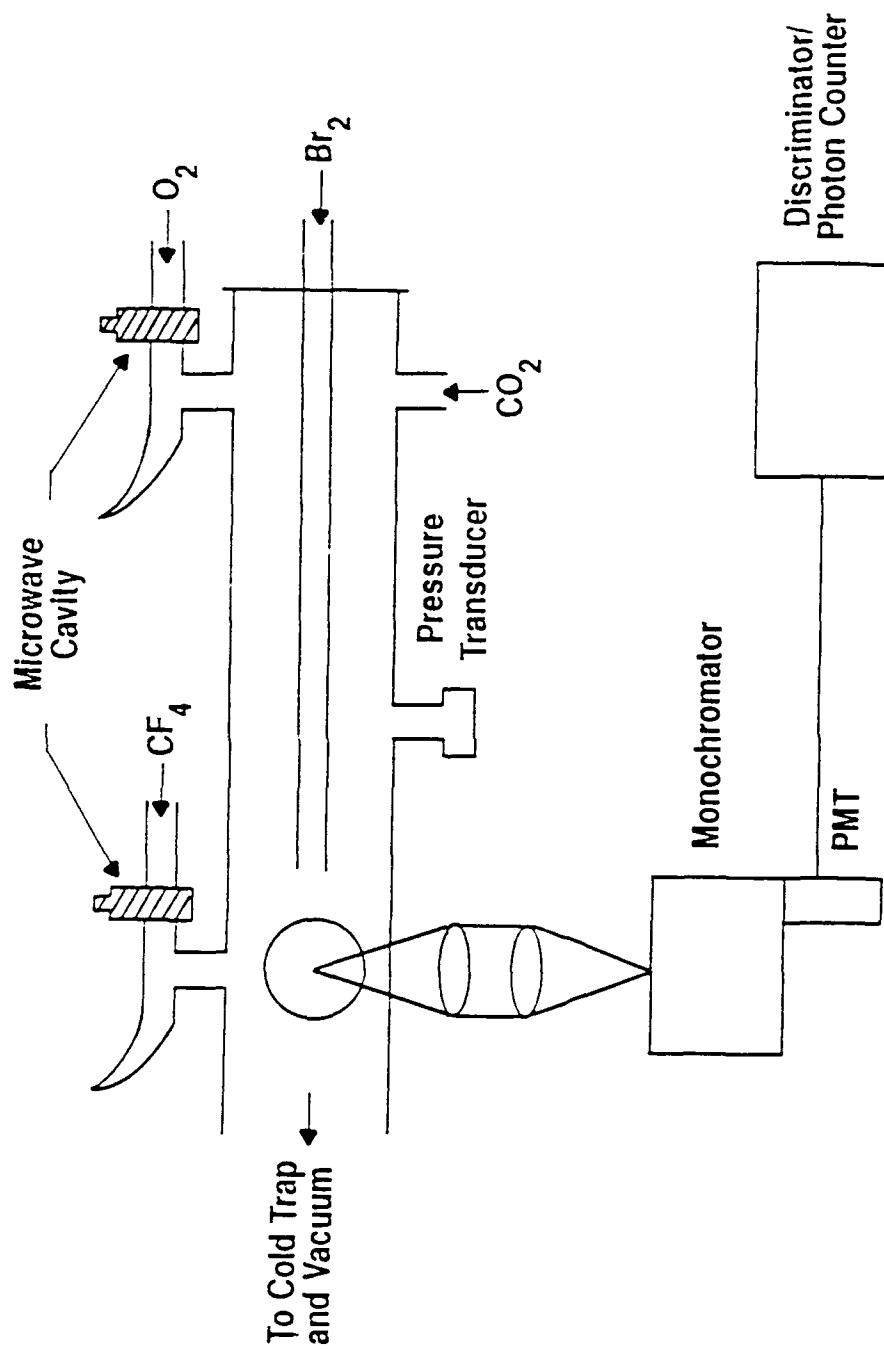


Figure 7. Chemiluminescent flow tube apparatus.

CF_4 and Br_2 were controlled by Nupro S-series metering valves. These valves were calibrated for absolute flow rate just prior to any quantitative experiments by observing the rate of pressure rise in the known flow tube volume of 3.28 l.

Ultra high purity oxygen (Airco 99.999%) was passed through an alumina tube inside an Opthos 2450 MHz, 100 watt microwave cavity at 600-1000 sccm and 2.3-3.8 torr at about 30 cm from the point of injection into the flow tube. While the absolute concentrations of $\text{O}_2(\text{a}^1\Delta)$, $\text{O}_2(\text{b}^1\Sigma)$, and $\text{O}(\text{P})$ were not determined in the present apparatus, such a discharge typically produces 2-5% $\text{O}_2(\text{a})$, $10^{-3} - 10^{-2}\%$ $\text{O}_2(\text{b})$ and $10^{-4}\%$ O (Derwent, 1972). The $\text{O}_2(\text{b})$ concentration is actually driven by the steady-state balance between $\text{O}_2(\text{a})$ pooling and $\text{O}_2(\text{b})$ quenching and wall deactivation, as described in equations (3.10)-(3.14). For an $\text{O}_2(\text{a})$ concentration of 5×10^{15} molecules/cm³, and the observed $\text{O}_2(\text{b})$ first-order deactivation rate coefficient of about 10 s^{-1} , this yields an $\text{O}_2(\text{b})$ concentration of 7×10^{13} molecules/cm³. The concentration of oxygen atoms produced by the discharge could be reduced by recombination on a HgO coating. This coating was formed downstream of the cavity by flowing the oxygen past a Hg reservoir during discharge (Arnold, 1968).

Fluorine atoms were produced from a CF_4 (Matheson 99.7%) flow of about 190 sccm in a second, identical microwave discharge. Such a discharge typically produces 1.9 - 4.7 % fluorine atoms (Kolb, 1972). For the strongest $\text{BrF}(\text{B})$ signals the fluorine atoms were injected transverse to the oxygen flow at the observation window. For the determination of the three-body recombination rate coefficient discussed in section 3.4.2, the fluorine atoms were delivered through the 6.4 mm injector tube. The

CF₄ discharge was located within 15 cm of the flow tube and a Wood's horn was used to eliminate discharge emission from the flow tube. The typical atomic fluorine concentration delivered to the flow tube is estimated at 4×10^{14} atoms/cm³.

The flow of molecular bromine was controlled by the following handling system. Liquid bromine (Spectrum Chemical, 99.5%) was transferred to one of two bulbs and distilled by repeated freeze/thaw cycles. The vapor pressure of bromine in an ice bath at 273K is 65 torr (Samsonov, 1968). This pressure was used to drive a low flow rate (0.08 - 1.8 sccm) of Br₂ to the 6.4 mm injector tube through the metering valve. This provided a molecular bromine concentration in the flow tube of 0.1 - 5×10^{14} molecules/cm³. During the three-body rate determination experiments the bromine was delivered through one of the side ports at the upstream end of the flow tube. In either case the bromine was fully mixed with the oxygen flow prior to injection of fluorine atoms. This allowed for complete reaction with any oxygen atoms via equations (3.1)-(3.2).

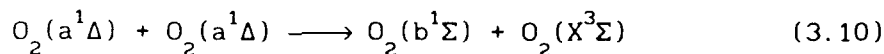
The emission detection system consisted of a McPherson 0.3 meter monochromator with a 1200 groove/mm grating blazed at 500 nm, an RCA C31034A-02 GaAs photomultiplier tube cooled to -30C, and a PARC model 1121 amplifier-discriminator and model 1112 photon counter/processor. A f=75 mm, 4 cm diameter pyrex lens was used to collect the chemiluminescence and a second f= 150 mm, 6.5 cm pyrex lens was used to focus the radiation on the monochromator entrance slit. A f=12.6 cm, 7.5 cm diameter silver mirror was placed 1.5 cm from the second flow tube window and increased the observed emission signals by about 30 %. Spectra were recorded on a

strip chart recorder. The relative spectral response of this detection system was determined using a 1270 K blackbody source.

3.4 Results

3.4.1. Quenching of $O_2(b)$. The first set of experiments was designed to assess the deactivation of $O_2(b)$ by BrF reagents. In a clean reactor with the teflon insert and only a flow of discharged O_2 , a strong $O_2\ b^1\Sigma_g^+ - X^3\Sigma_g^-$ (0,0) emission band was observed near $\lambda = 762$ nm and with 0.05 nm resolution the rotational spectrum of Figure 8 was obtained. The best spectroscopic description of this band is reported from atmospheric absorption experiments (Babcock, 1948). The spectrum exhibits a unique four branch (P^P, P^Q, R^R, R^Q) rotational structure described by Hund's case b coupling for a magnetic dipole transition (Babcock, 1948). The spectrum of Figure 8 is characterized by a rotational temperature of $T = 295 \pm 14$ °K.

The rate for quenching of $O_2(b)$ by various collision partners can be determined under steady-state conditions by observing the $O_2(b-X)$ (0,0) emission intensity as a function of quencher gas pressure. $O_2(b)$ is produced from energy pooling:



with a rate coefficient of $k_{10} = 2.7 \times 10^{-17}$ cm³/(molecule·s) (Lilenfeld, 1984). Balancing this production, quenching and wall collisions deactivate $O_2(b)$:

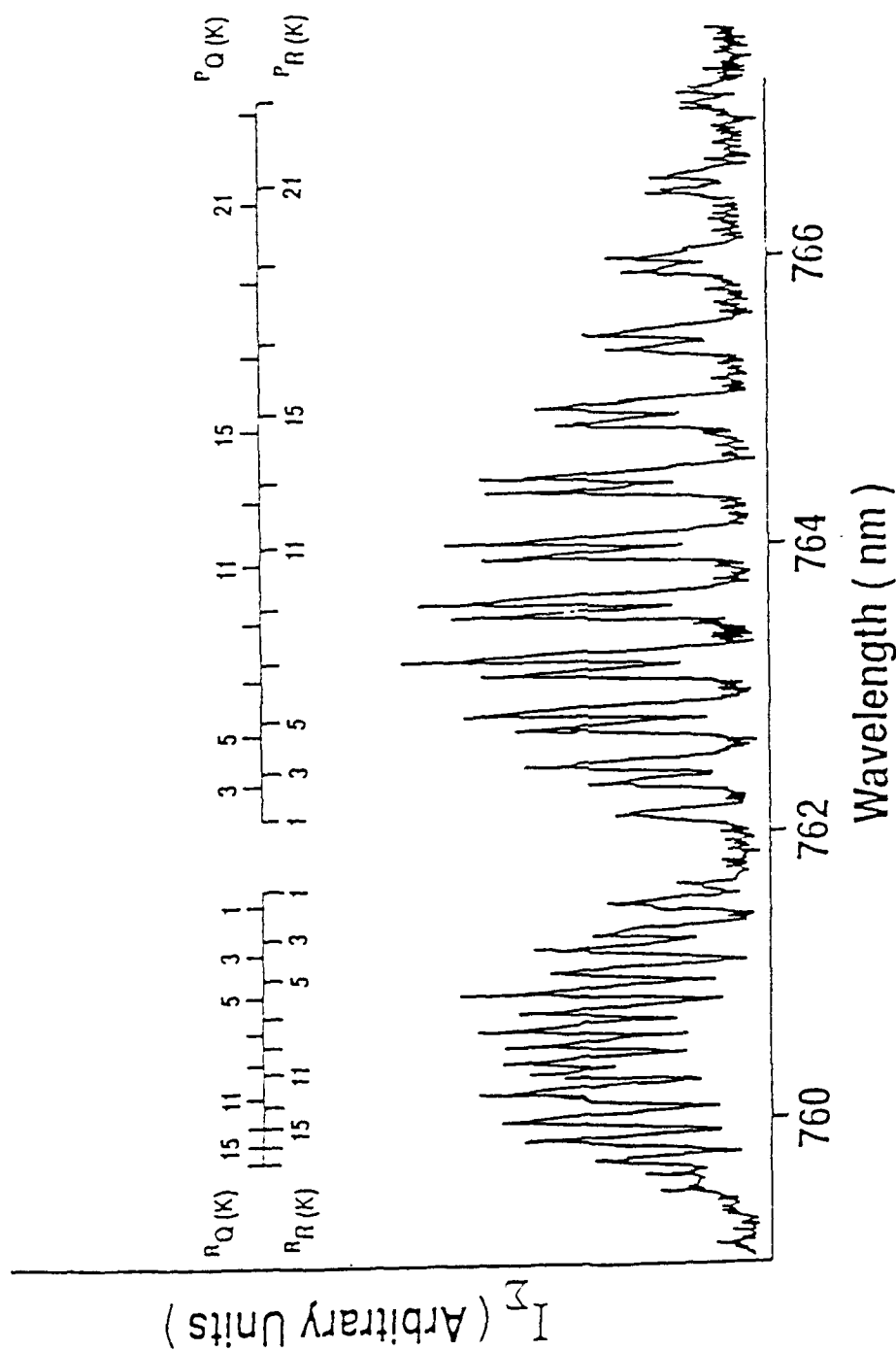
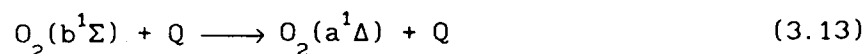
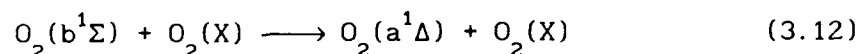
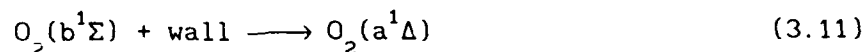


Figure 8. Emission spectrum for O_2 $b^1\Sigma_g^+ \rightarrow X^3\Sigma_g^-(0,0)$ band at 0.05 nm resolution. The observed lines are assigned to the four branches according to the total angular momentum excluding spin, K'' . The two R-branches head near $K''=29$ and $\lambda=759.4$ nm.



where Q is the quenching specie to be studied. A steady-state analysis of reactions (3.10)-(3.13), assuming constant $[O_2(a)]$, provides a dependence of $O_2(b-X)$ emission intensity, I, as a function of quencher concentration, [Q], of (Becker, 1971)

$$I(Q=0)/I(Q) = 1 + k_{13}[Q]/\Gamma_o \quad (3.14)$$

where

k_n = rate coefficient for reaction (3.n)

$\Gamma_o = k_{11} + k_{12}[O_2]$ = pseudo first order $O_2(b)$ deactivation

rate coefficient

k_{13}^Q = rate coefficient for reaction (3.13) with quencher specie Q

Figure 9 shows the linear dependence on quencher concentration as predicted by equation (3.14) for CO_2 and CF_4 . Using the well known quenching rate coefficient for CO_2 of $k_{13}^{CO_2} = 3 \times 10^{-13} \text{ cm}^3/(\text{molecule}\cdot\text{s})$ (Singh, 1985b), the first order deactivation rate coefficient is determined for this apparatus under the specified conditions of Figure 9 as $\Gamma_o = 20 \text{ s}^{-1}$. This rate coefficient significantly increased when the flow tube had been exposed to halogen gases or the atmosphere.

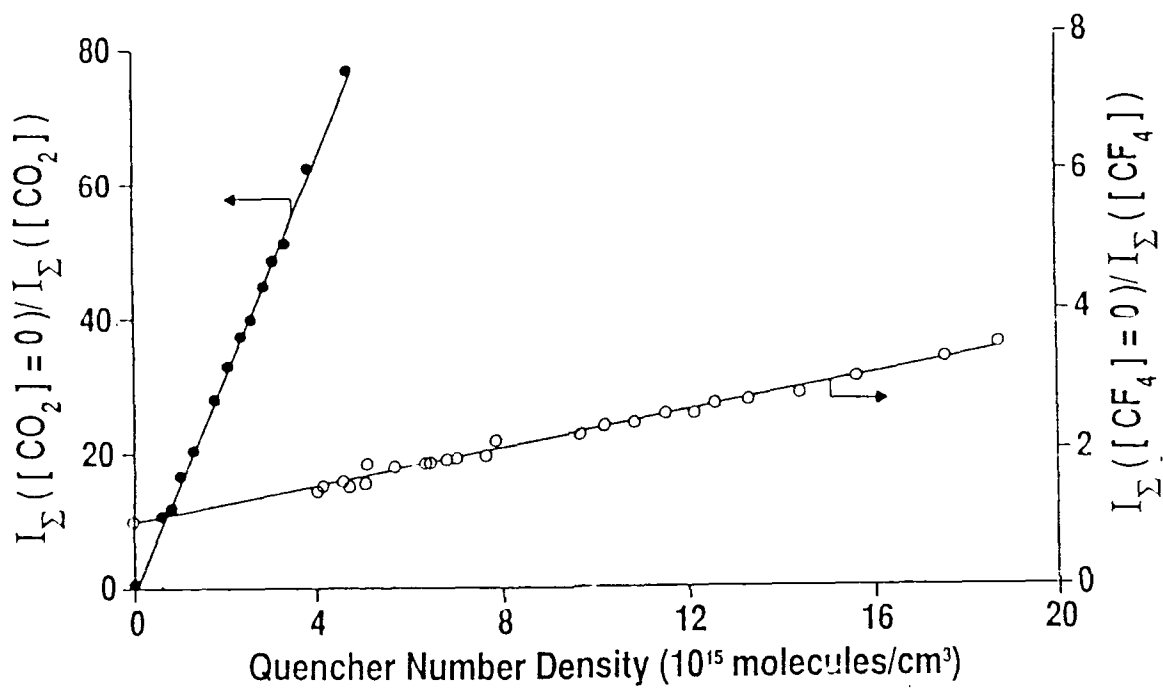


Figure 9. Stern-Volmer plot for quenching of $O_2(b^1\Sigma)$ by CO_2 (●) and CF_4 (○). The first-order decay rate for both plots is $\Gamma_0 = 20 \text{ s}^{-1}$.

The rate coefficient for quenching by other species was determined relative to the CO_2 quenching rate coefficient using this approach. The relative slopes of the CO_2 and CF_4 data of Figure 9 provide a CF_4 quenching rate of $2.7 \times 10^{-15} \text{ cm}^3/(\text{molecule} \cdot \text{s})$, in very close agreement to a previous measurement (Davidson, 1977). The statistical error in this measurement is small (3%), and the primary source of error is in the CO_2 reference rate coefficient (~30%).

The quenching of $\text{O}_2(b)$ by the addition of molecular bromine is more complex and shown in Figure 10. Two distinct quenching regions are observed with a sharp transition at $[\text{Br}_2] = 2 \times 10^{13} \text{ molecules/cm}^3$. Recall, for $[\text{Br}_2] < [\text{O}]/2$, no molecular bromine will survive the region where Br_2 and the discharged oxygen are mixed due to the reactions (3.1)-(3.2). Adding one bromine molecule removes two oxygen atoms and produces two bromine atoms. Thus, for low bromine pressures, twice the difference in atomic bromine and oxygen quenching rates, $2(k_{13}^{\text{Br}} - k_{13}^{\text{O}}) = (2.8 \pm 0.6) \times 10^{-11} \text{ cm}^3/(\text{molecule} \cdot \text{s})$, is observed. This statistical error bound is based on the reproducibility of six rate coefficient measurements. However, systematic errors associated with the flow rate calibration are estimated at 50%. The atomic oxygen quenching rate coefficient is known to be slow, $k_{13}^{\text{O}} = 8 \times 10^{-14} \text{ cm}^3/(\text{molecule} \cdot \text{s})$ (Slanger, 1979), yielding a bromine atom quenching rate of $k_{13}^{\text{Br}} = (1.4 \pm 0.3) \times 10^{-11} \text{ cm}^3/(\text{molecule} \cdot \text{s})$. At the higher bromine pressures, a much slower rate coefficient of $k_{13}^{\text{Br}_2} = (9.7 \pm 0.5) \times 10^{-13} \text{ cm}^3/(\text{molecule} \cdot \text{s})$ is observed

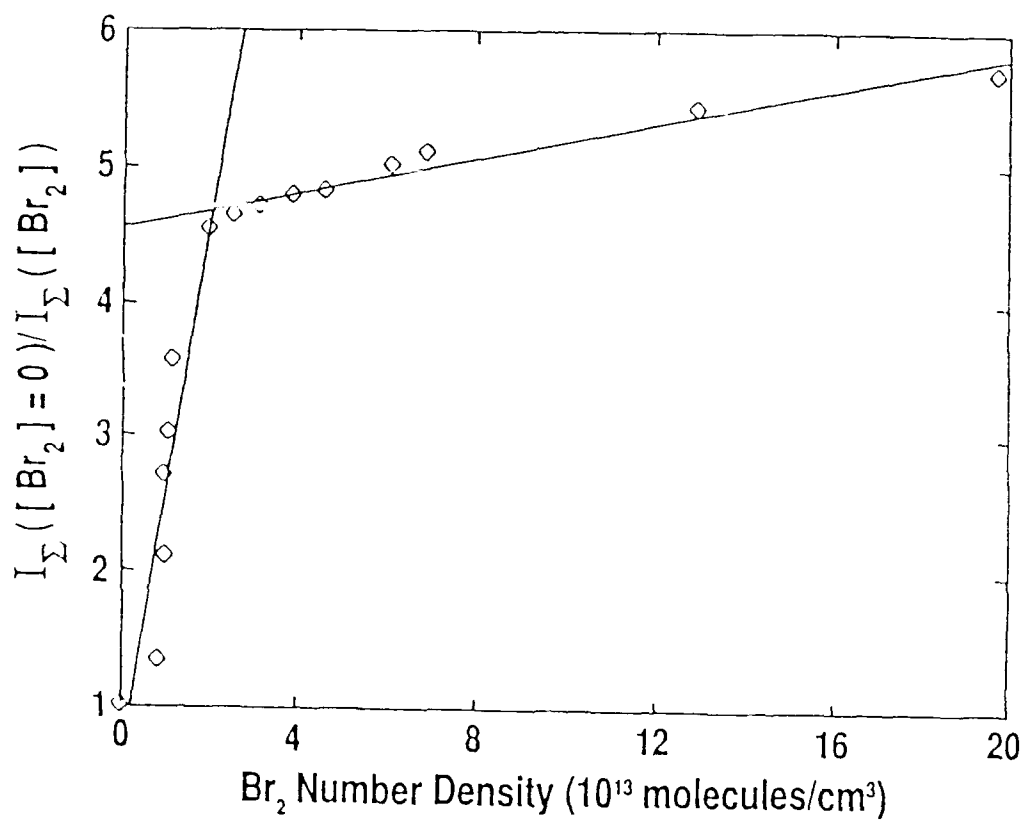


Figure 10. Stern-Volmer plot for quenching of $O_2(b^1\Sigma)$ by the addition of molecular bromine. The pseudo first-order rate coefficient at $[O_2] = 9.76 \times 10^{16}$ molecules/cm³ and without a HgO coating is $\Gamma_o = 150 \text{ s}^{-1}$.

and attributed to quenching of $O_2(b)$ by Br_2 . This observation also provides a determination of oxygen atom concentration, $[O] \approx 4 \times 10^{13}$ atoms/cm³.

3.4.2 Chemiluminescence Spectrum. A strong $BrF(B-X)$ chemiluminescence signal is obtained only when both the oxygen and CF_4 discharges are active and only for low Br_2 concentrations, $[Br_2] < 5 \times 10^{14}$ molecules/cm³. The injection of fluorine atoms at the observation window and transverse to the oxygen flow is convenient because an approximately vertical flame is observed which matches the monochromator slit geometry. In addition, little opportunity for fluorine atom losses at wall surfaces is encountered with this geometry. The flame persists for about 5 cm and exhibits about a 30 degree curvature due to the oxygen flow. The imaging system spatially integrates over about half of this length, aiding in a steady-state kinetic analysis. A low resolution $BrF(B-X)$ chemiluminescence spectrum obtained under these conditions is shown in Figure 11.

Several vibrational progressions from $v'=0-5$ are clearly observed in the spectrum. When the spectral response of the detection system was accounted for, the non-thermal vibrational distribution shown in Figure 12 was obtained. The large error bounds for the population in $v'=3$ and 5 are due to the strong overlap of vibrational bands at the short wavelength end of the spectrum. The $O_2(b-X)$ (0,0) band with the two prominent rotational branches is also indicated in Figure 11. The ratio of radiative lifetimes is low, $\tau_r^{BrF(B)} / \tau_r^{O_2(b)} = 5 \times 10^{-6}$, and the resulting concentration ratio is $[BrF(B)]/[O_2(b)] \approx 5 \times 10^{-4}$.

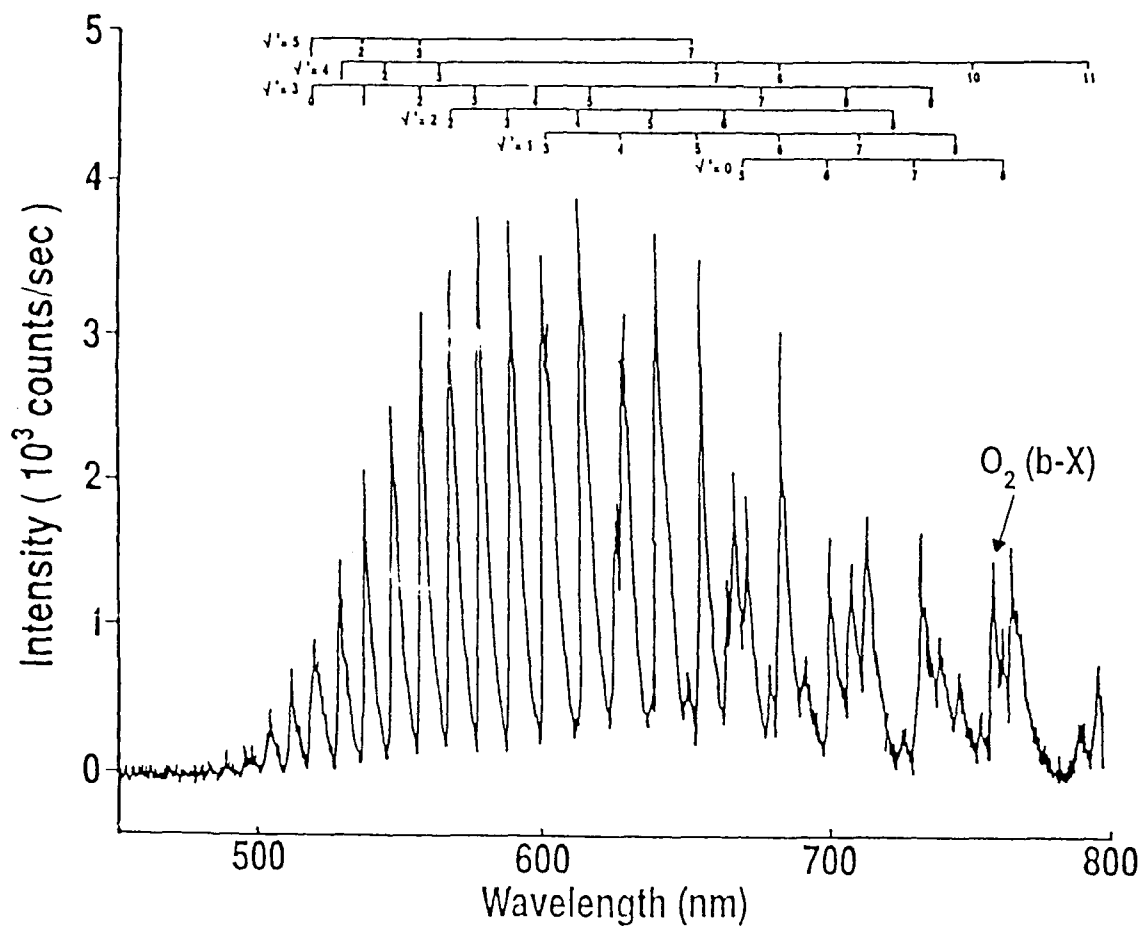


Figure 11. Chemiluminescence spectrum of $BrF\ B^3\Pi(0^+) - X^1\Sigma(0^+)$ produced from the injection of Br_2 and F into a flow of discharged oxygen. v' progressions are indicated by labeling the band head for each (v', v'') transition. Monochromator resolution is 1.2 nm.

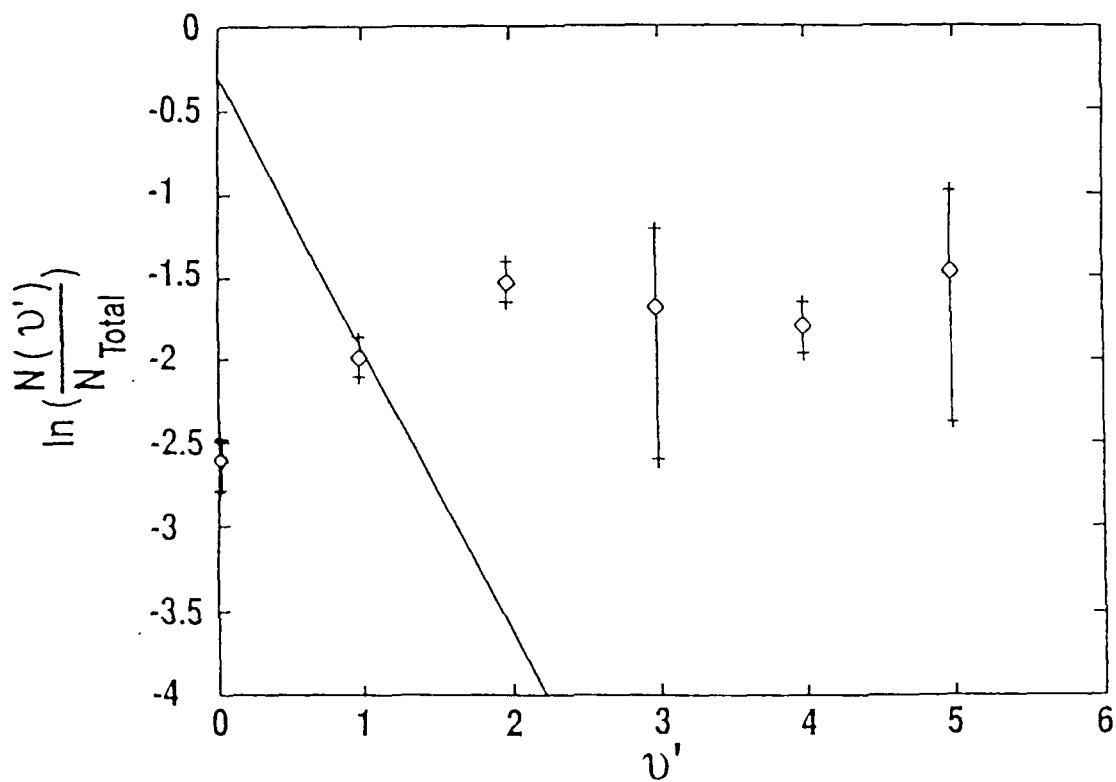


Figure 12. Relative vibrational population distribution for BrF(B) obtained from the spectrum of Figure 11. The total flow tube pressure is 3.52 torr. BrF(B) vibrational states above $v'=6$ are highly predissociated. A thermal vibrational distribution at 300K is also indicated (—).

The spatial extent of the chemiluminescence was best examined with the fluorine atoms delivered through the tube injector. The BrF(B-X) total fluorescence, observed with the monochromator at zero order, as a function of axial distance from the tube injector is shown in Figure 13. Spatial resolution in the flow direction is achieved from the image of the monochromator slit, but limited by the spatial extent of the flame along the viewing axis. The spatial resolution is estimated to be ≤ 6 mm, which yields a resolvable flow time of ≤ 7 ms. After a time due to mixing (≈ 30 ms), the emission decays exponentially with a lifetime of $\tau = 65 \pm 4$ ms. The decay rate was observed to increase linearly with total oxygen concentration. No significant deviation from a first order decay is evident. No secondary emission region is noted in the current apparatus.

3.4.3 Excitation Mechanism. The studies of the excitation mechanism focused on two issues: 1. the role of $O_2(b^1\Sigma_g^+)$ as an energy transfer partner, and 2. discrimination between the recombination and sequential energy transfer mechanisms.

No BrF(B-X) emission was observed in the absence of $O_2(a,b)$ and the energetics illustrated in Figure 6 require at least one energy transfer event involving singlet oxygen. While $O_2(a)$ is the prominent energetic species in the system the results of section 3.4.2 show that sufficient $O_2(b)$ is present to account for the observed BrF(B-X) emission intensity. In order to assess the role of $O_2(b)$ as an energy transfer partner, a method for decoupling the steady state $O_2(b)$ concentration from the $O_2(a)$ pooling process is required. This was accomplished by the use of a selective quencher of $O_2(b^1\Sigma)$ was used. CO_2 is a moderately fast quencher

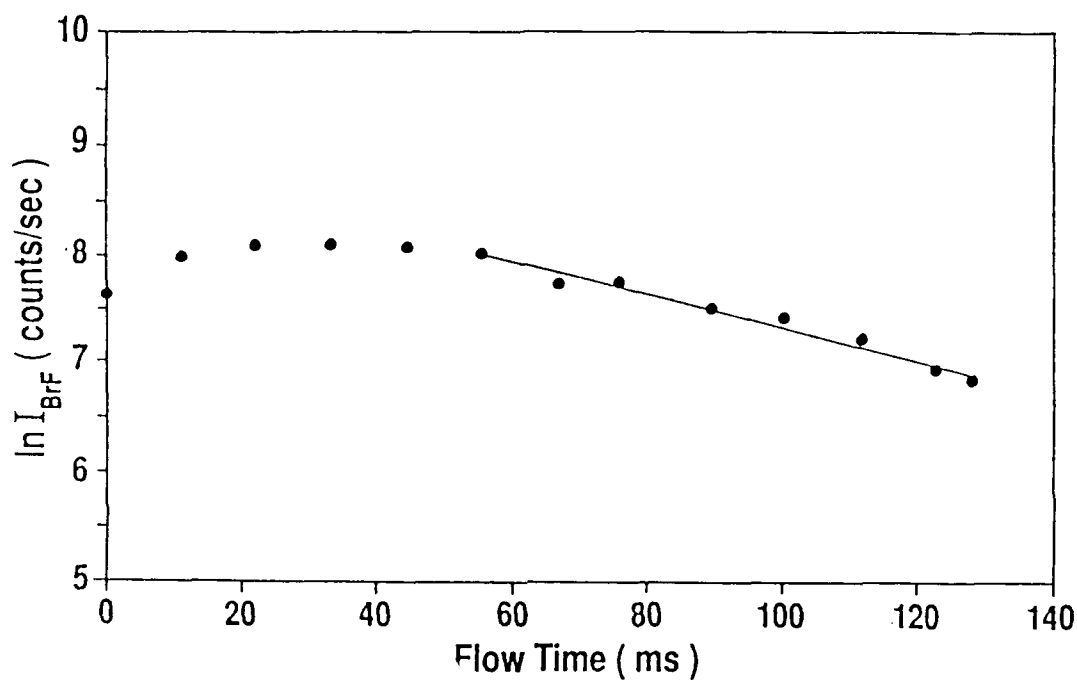


Figure 13. Spatially resolved, spectrally unresolved BrF(B) emission intensity, I_{BrF} , as a function of flow time (axial distance). Fluorine atoms are delivered through the movable injector. The bulk flow velocity is 0.895 m/s at $[\text{O}_2] = 9.7 \times 10^{17}$ molecules/cm³. An exponential fit to the data (—) provides $\tau = 65 \pm 4$ ms.

of $O_2(b)$, $k_{13}^{CO_2} = 3 \times 10^{-13} \text{ cm}^3/(\text{molecule} \cdot \text{s})$, and given our pseudo first-order deactivation rate for $O_2(b)$ of about $\Gamma_o = 10^3 \text{ s}^{-1}$ in the $O_2/Br_2/F$ flow, the addition of $3.5 \times 10^{15} \text{ molecules/cm}^3$ of CO_2 is sufficient to reduce the steady-state $O_2(b)$ concentration by a factor of two. The $O_2(a)$ was not monitored in the current experiments, but should be unaffected by this CO_2 addition, as its quenching rate by CO_2 is many orders of magnitude smaller, $5.8 \times 10^{-18} \text{ cm}^3/(\text{molecule} \cdot \text{s})$ (Singh, 1985a). Thus, the addition of CO_2 to the $O_2/Br_2/F$ flow should provide a clear description of the dependence of $BrF(B)$ production on $O_2(b)$. This technique has previously been applied to $O_2(b)/IF(B)$ excitation studies (Davis, 1989a).

A nearly linear dependence of $BrF(B)$ emission intensity on $O_2(b)$ concentration is shown in Figure 14. This provides strong evidence that at least one $O_2(b)$ collision is involved in a rate determining step for the production of $BrF(B)$. Further discussion of this data including the small observed curvature is presented in section 3.5.

The dependence of the $BrF(B)$ and $O_2(b)$ emission intensities as a function of Br_2 concentration shown in Figure 15a also provides information on the excitation mechanism. The $BrF(B)$ emission is strongly maximized at a bromine concentration of $[Br_2]_{opt} = 2 \times 10^{13} \text{ molecules/cm}^3$. This corresponds to half the atomic oxygen concentration, as determined from Figure 10. Indeed, this optimal Br_2 concentration was dependent on oxygen atoms, as demonstrated by the application of the HgO coating to remove O . The optimal Br_2 concentration was not dependent on CF_4 flow rate, indicating no relationship to fluorine atom concentration.

The sequential excitation mechanism of reactions (3.7-3.9) would predict a peak BrF(B) signal when the ground state concentration of BrF(X) produced from reaction (3.7) is maximized. This would occur when all the atomic fluorine is converted to BrF(X) at $[\text{Br}_2] = [\text{F}] \cong 4 \times 10^{14}$ molecules/cm³, which is a Br₂ concentration 20 times higher than observed. In fact, at the optimal $[\text{Br}_2] = [\text{O}]/2$, no molecular bromine remains to produce BrF(X), and a minimum BrF(B) signal would be predicted.

The three-body excitation mechanism, reactions (3.3-3.4), would predict a peak BrF(B) signal when the concentration product $[\text{Br}] [\text{F}] [\text{O}_2(\text{b})]$ is maximized. This assumes the BrF* removal is dominated by O₂(X) quenching, see equation (3.19). When $[\text{Br}_2] < [\text{O}]/2$, the addition of molecular bromine produces additional atomic bromine from reactions (3.1)-(3.2) without affecting the concentration of atomic fluorine, and the BrF(B) signal rises. After all the atomic oxygen is consumed, reaction (3.7) produces atomic bromine, but at the expense of atomic fluorine. The product of atomic bromine and fluorine will exhibit a maximum when about half of the initial fluorine atoms have reacted with Br₂. However, the approach to this maximum is gradual, and the quenching of O₂(b) shown in Figure 15a is relatively rapid. Thus, the $[\text{Br}] [\text{F}] [\text{O}_2(\text{b})]$ product will produce a peak BrF(B) signal near $[\text{Br}_2] = [\text{O}]/2$, as observed.

The data of Figure 15a are recast in terms of the quenching analysis of equation (3.14) in Figure 15b. The quenching of O₂(b) is linear. The O₂(b) first order decay rate in the presence of discharged CF₄ was determined by the CO₂ quenching technique as $\Gamma_0 = 740 \text{ s}^{-1}$. This yields an O₂(b) quenching rate for the addition of Br₂ of $(3.2 \pm 2.2) \times 10^{-11}$

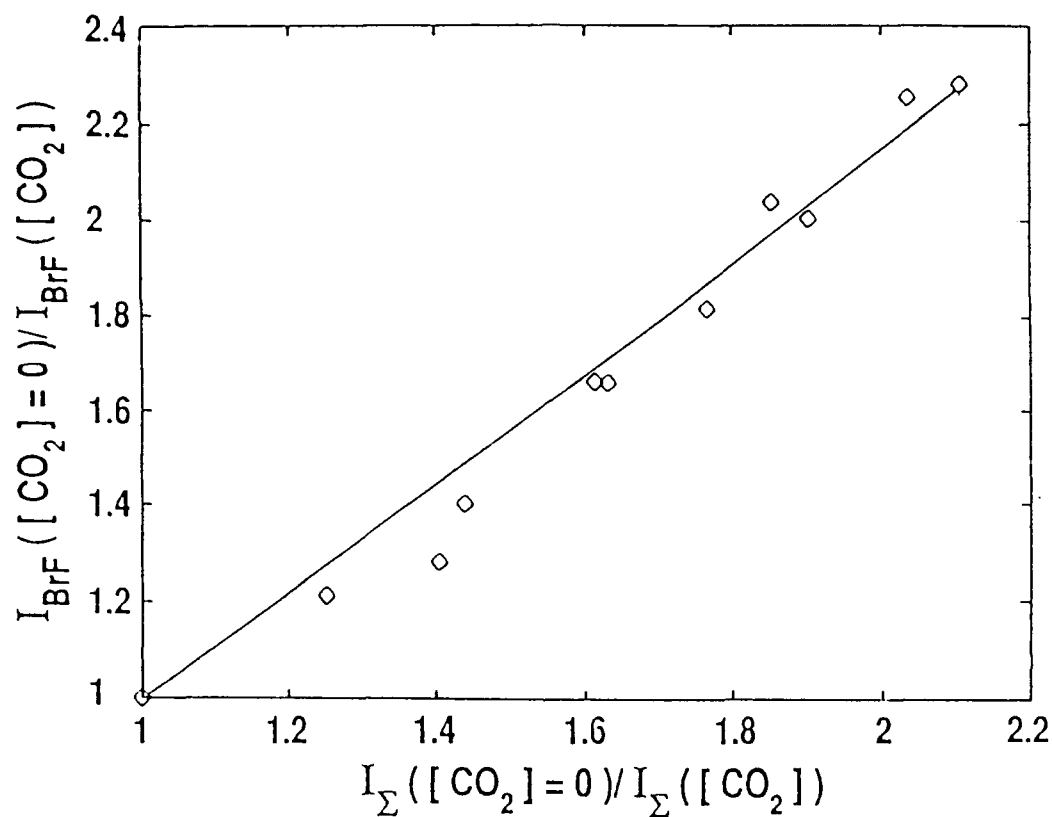


Figure 14. Relationship between BrF(B) intensity, I_{BrF} , and $O_2(b)$ intensity, I_{Σ} , when the selective quencher CO_2 is added. The BrF(B-X) (0,8) band is used to monitor the BrF(B) intensity. The steady-state kinetic analysis of equation (3.19) is also provided (—), showing a slight curvature due to CO_2 quenching of BrF(B).

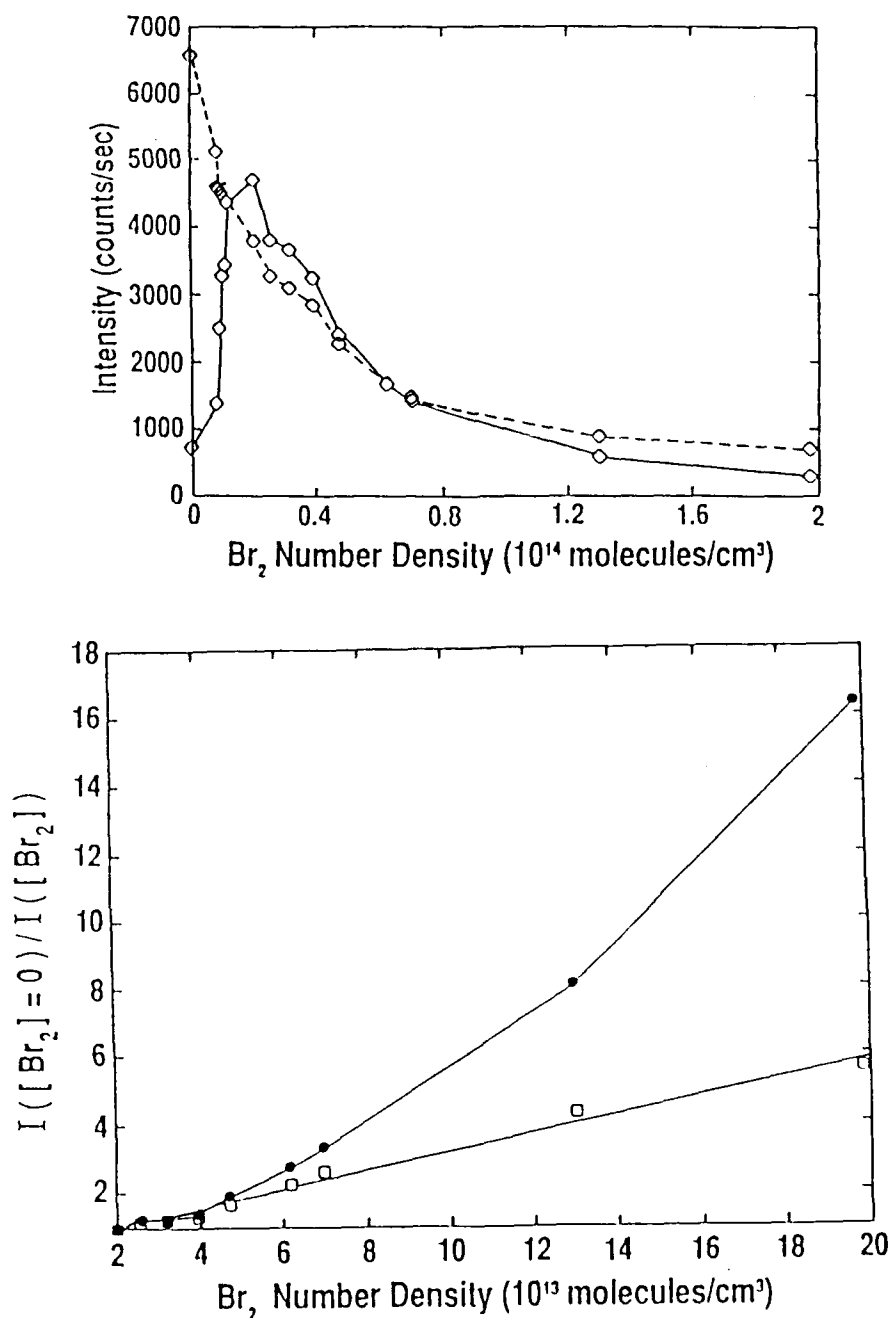


Figure 15. (a) BrF(B) (—) and O₂(b) (---) emission intensities as a function of molecular bromine concentration. (b) Same data as Figure 15a, presented as a Stern-Volmer plot: (●) BrF(B) and (□) O₂(b) emission intensities. The pseudo first-order rate coefficient as measured from a CO₂ quenching plot with the CF₄ discharge on and no HgO coating is $\Gamma_o = 740 \text{ s}^{-1}$.

$\text{cm}^3/(\text{molecule}\cdot\text{s})$. The primary result of adding Br_2 beyond $[\text{O}]/2$ is to produce $\text{Br} + \text{BrF}$ from reaction (3.7). If this quenching is attributed to these products, then the observed quenching rate compares well with the above determined rate coefficient for quenching by atomic bromine of $(1.4 \pm 0.3) \times 10^{-11} \text{ cm}^3/(\text{molecule}\cdot\text{s})$. The difference in these two rates might be attributed to BrF quenching, but the given error bounds do not preclude a negligible BrF quenching rate coefficient.

In contrast, the decay of BrF(B) emission accelerates as the molecular bromine concentration approaches the initial fluorine atom concentration. This is observed in the curvature of the BrF(B) plot of Figure 15b. The three-body recombination mechanism would predict this rapid decrease in BrF(B) signal as all the atomic fluorine is removed by reaction (3.7).

The sequential excitation mechanism would predict a BrF(B) decay at the same rate as the $\text{O}_2(\text{b})$ decay. In this mechanism, and under conditions where BrF(X) has been maximized by complete reaction of Br_2 with F , the addition of molecular bromine should simply quench $\text{O}_2(\text{b})$ with the rate coefficient of $k_{13}^{\text{Br}_2} = 9.7 \times 10^{-13} \text{ cm}^3/(\text{molecule}\cdot\text{s})$. The observed $\text{O}_2(\text{b})$ decay is much too fast for simple Br_2 quenching.

Finally, the relationship between the BrF(B) and $\text{O}_2(\text{b})$ emission intensities when the oxygen atom concentration is varied is shown in Figure 16. These data were obtained by applying a variable HgO coating downstream of the O_2 discharge as discussed above. The O_2 , Br_2 and CF_4 flow rates are held constant. Data were acquired both during the application of the HgO coating (decreasing oxygen atoms) and after the Hg reservoir was sealed off (increasing oxygen atoms) over a period of 30-60

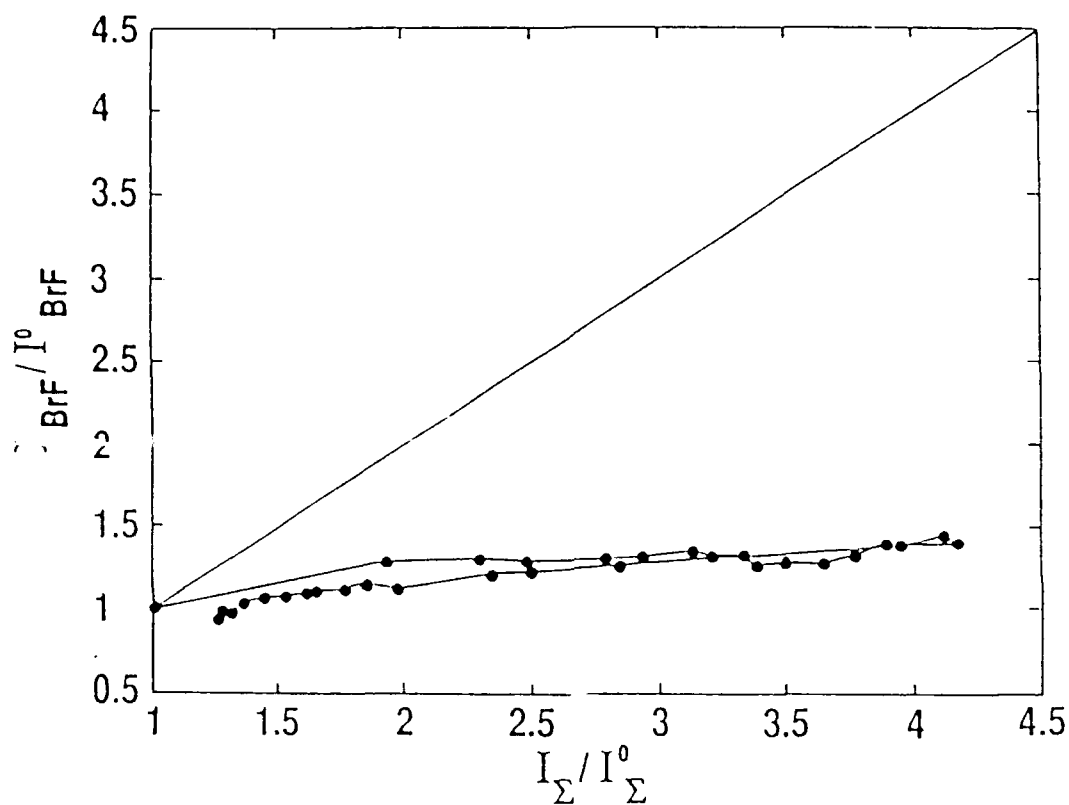


Figure 16. Relationship between the BrF(B) emission intensity, I_{BrF} , and $O_2(b)$ intensity, I_{Σ} , when the oxygen atom concentration is varied. A line of slope one is shown for discussion purposes. The data (●) are connected sequentially in time by the solid line. The reference intensities, I_{Σ}^0 and I_{BrF}^0 , are obtained prior to the application of the HgO coating.

minutes. No significant difference in the signals is observed with these two approaches. The $O_2(b)$ signal is strongly affected by the presence of atomic oxygen, but the BrF(B) emission intensity is observed to be roughly independent of $[O]$.

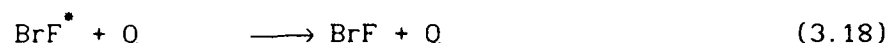
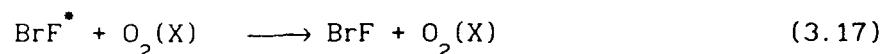
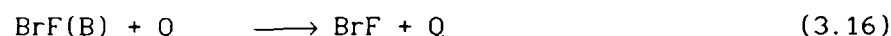
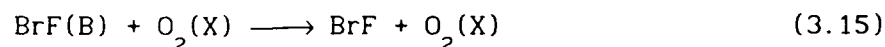
The data of Figure 16 do not exhibit the same first order dependence of $[BrF(B)]$ on $[O_2(b)]$ shown in the CO_2 selective quenching data of Figure 14. The addition of oxygen atoms increases the number of bromine atoms produced from reactions (3.1)-(3.2) and decreases the residual molecular bromine concentration. There are two effects of changing the atomic and molecular bromine concentrations: 1. quenching of $O_2(b)$ by atomic bromine and 2. the rate of BrF production either from reaction (3.3) or reaction (3.7). The rapid quenching of $O_2(b)$ by atomic bromine linearly decreases the BrF(B) emission. The relationship between $[BrF(B)]$ and $[O_2(b)]$ accounting only for the atomic bromine quenching is indicated in Figure 16 by the solid line.

Removal of atomic oxygen increases the residual Br_2 available for reaction (3.7) to produce BrF, and thus, the sequential excitation mechanism would further benefit from less atomic oxygen and the slope of Figure 16 should be greater than 1.0. This is clearly not consistent with the observations. Reducing $[O]$ results in less atomic fluorine and bromine, required to drive the three-body recombination reaction (3). This counters the increased $O_2(b)$ concentration and thus, a slope of less than 1.0 would be predicted. Indeed, the steady-state kinetic analysis presented in section 3.5.1 predicts a slope of nearly zero, in close agreement to the observations of Figure 16.

3.5 Discussion

Five principal results indicate a three-body recombination mechanism is responsible for the BrF(B) emission observed in these studies: 1. the BrF(B) emission is optimized at very low molecular bromine concentrations, $[\text{Br}_2] = [\text{O}]/2$, independent of atomic fluorine flow rate, 2. the BrF(B) emission intensity is linearly dependent on $\text{O}_2(\text{b})$ concentration when all other conditions remain constant, 3. the BrF(B) emission intensity does not increase as oxygen atoms are removed from the flow despite a significant increase in $[\text{O}_2(\text{b})]$, 4. the rate of decay for BrF(B) emission increases dramatically as the molecular bromine concentration approaches the atomic fluorine concentration, and 5. the emission requires the simultaneous presence of Br, F and $\text{O}_2(\text{b}^1\Sigma)$. While it is difficult to conclusively prove a given mechanism, these results are inconsistent with the predictions of the sequential excitation mechanism of reactions (3.7)-(3.9). All of the reported observations do agree both qualitatively and quantitatively with the predictions from the steady-state analysis of the three-body excitation mechanism, as shown below.

3.5.1 Steady-State Kinetic Analysis. A steady-state analysis ($d[\text{BrF}^{\bullet}]/dt = d[\text{BrF(B)}]/dt = 0$) of the three-body excitation mechanism of reactions (3.3)-(3.4) should include quenching of BrF^{\bullet} and BrF(B) by $\text{O}_2(\text{X})$ and quencher Q:



This analysis predicts a BrF(B) concentration given by:

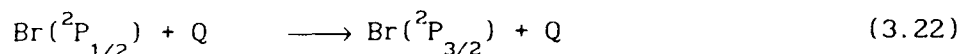
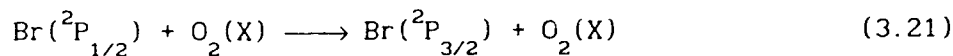
$$[\text{BrF(B)}] = \frac{k_3 k_4 [\text{F}] [\text{Br}] [\text{O}_2(\text{b})] [\text{O}_2(\text{X})]}{\{k_4 [\text{O}_2(\text{b})] + k_{18} [\text{Q}] + k_{17} [\text{O}_2(\text{X})]\} \{k_{15} \text{O}_2[(\text{X})] + k_{16} [\text{Q}] + 1/\tau_r\}} \quad (3.19)$$

where the rate coefficient k_n corresponds to the reaction given in equation (3.n). The radiative lifetime of BrF(B) has been measured as a function of vibrational level as, $55.5 \leq \tau_r \leq 64.2 \mu\text{s}$ for $3 \leq v' \leq 7$ (Clyne, 1980). Three-body recombination due to the added quencher Q has been neglected. The active singlet oxygen specie is taken as $\text{O}_2(\text{b}^1\Sigma)$ from the results of Figure 14.

A slightly different result is obtained if $\text{Br}(\text{}^2\text{P}_{1/2})$ is involved in the recombination process through reactions (3.5-3.6):

$$[\text{BrF(B)}] = \frac{k_5 k_6 [\text{F}] [\text{Br}] [\text{O}_2(\text{b})] [\text{O}_2(\text{X})]}{\{k_6 [\text{F}] + k_{22} [\text{Q}] + k_{21} \text{O}_2[(\text{X})]\} \{k_{15} [\text{O}_2(\text{X})] + k_{16} [\text{Q}] + 1/\tau_r\}} \quad (3.20)$$

The intermediate, $\text{Br}(\text{}^2\text{P}_{1/2})$, is assumed to be in steady-state and the quenching of excited bromine atoms is described by the following reactions:



The same kind of analysis for the sequential excitation mechanism of reactions (3.7)-(3.9) yields:

$$[\text{BrF}(\text{B})] = \frac{k_8 k_9 [\text{BrF}] [\text{O}_2(\text{b})] [\text{O}_2(\text{a})]}{\{k_9 [\text{O}_2(\text{a})] + k_{17} [\text{Q}] + k_{18} [\text{O}_2(\text{X})]\} \{k_{15} \text{O}_2[(\text{X})] + k_{16} [\text{Q}] + 1/\tau_r\}} \quad (3.23)$$

Equation (3.23) assumes one $\text{O}_2(\text{b})$ followed by one $\text{O}_2(\text{a})$ interaction, as shown by the solid arrows in the energy level diagram of Figure 6.

In all cases, the $[\text{Br}]$, $[\text{F}]$, and $[\text{BrF}]$ depend on $[\text{Br}_2]$ and $[\text{O}]$ according to equations (3.24)-(3.26):

$$[\text{F}] = \begin{cases} [\text{F}]_0 & [\text{Br}_2] < [\text{O}]/2 \\ [\text{F}]_0 - ([\text{Br}_2] - [\text{O}]/2) & [\text{F}]_0 + [\text{O}]/2 > [\text{Br}_2] > [\text{O}]/2 \\ 0 & [\text{Br}_2] > [\text{F}]_0 + [\text{O}]/2 \end{cases} \quad (3.24)$$

$$[\text{Br}] = \begin{cases} 2 [\text{Br}_2] & [\text{Br}_2] < [\text{O}]/2 \\ [\text{Br}_2] + [\text{O}]/2 & [\text{F}]_0 + [\text{O}]/2 > [\text{Br}_2] > [\text{O}]/2 \\ [\text{O}] + [\text{F}]_0 & [\text{Br}_2] > [\text{F}]_0 + [\text{O}]/2 \end{cases} \quad (3.25)$$

$$[\text{BrF}] = [\text{F}]_0 - [\text{F}] \quad (3.26)$$

The concentrations for the reagents $[\text{Br}_2]$, $[\text{O}]$, and $[\text{F}]_0$ are initial values before reaction. The concentration for products, $[\text{F}]$, $[\text{Br}]$, and

[BrF] are evaluated after the fast production reactions, but prior to BrF(B) excitation. For low $[\text{Br}_2]$, all the molecular bromine is converted to two bromine atoms from the reaction with atomic oxygen, equations (3.1-3.2), and the atomic fluorine is unaffected. When $[\text{Br}_2]$ exceeds $[\text{O}]/2$, the remaining molecular bromine reacts with atomic fluorine via equation (3.7) to produce Br and BrF. Atomic fluorine recombination is very slow (Ultee, 1977) at $T=300^\circ\text{K}$ and the reduction in fluorine atoms must appear as BrF.

The linear dependence of BrF(B) on $\text{O}_2(\text{b})$ shown in Figure 14 clearly indicates at least one $\text{O}_2(\text{b})$ collision is involved in the excitation mechanism. Two $\text{O}_2(\text{b})$ collisions could yield a linear dependence only if kinetic removal from the intermediate BrF^* state were controlled by the excitation step to BrF(B). Due to the preponderance of $\text{O}_2(\text{X})$ over $\text{O}_2(\text{b})$, this could be achieved only if the excitation process were rapid and the quenching of BrF^* by $\text{O}_2(\text{X})$ were slow. The ratio of the rate coefficients for these two processes would need to be greater than 10^4 to achieve this result. In addition, two $\text{O}_2(\text{b})$ collisions could provide as much as $26,000\text{ cm}^{-1}$, which accesses repulsive BrF electronic states. Therefore, a single $\text{O}_2(\text{b})$ interaction is favored.

A slight positive curvature is evident in Figure 14. This cannot be explained by the secondary dependence on $\text{O}_2(\text{b})$ in the denominator of equation (3.19), as this leads to a negative curvature. More likely is the effect of CO_2 quenching on BrF(B). A prediction of the data based on equation (3.19) with CO_2 quenching of BrF(B) at a rate coefficient on the order of $1 \times 10^{-12}\text{ cm}^3/(\text{molecule}\cdot\text{s})$ is also shown in Figure 14 and is sufficient to explain the observed curvature.

The absolute value of the slope observed in the atomic oxygen data of Figure 16 can also be predicted from the steady-state analysis of the three-body recombination mechanism, equations (3.19) and (3.24)-(3.26). The slope is evaluated by normalizing the observed BrF(B) intensity to the intensity before application of the HgO coating, yielding:

$$\frac{[\text{BrF(B)}]}{[\text{BrF(B)}]_0} = \{1 + \Delta[\text{O}]/2[\text{F}]_0\} \{1 + \Delta[\text{O}]/2[\text{O}]_0\} [\text{O}_2(\text{b})]/[\text{O}_2(\text{b})]_0 \quad (3.27)$$

where

$[\text{BrF(B)}]_0$ = the BrF(B) concentration before application of the HgO coating

$[\text{O}_2(\text{b})]_0$ = the $\text{O}_2(\text{b}^1\Sigma)$ concentration before application of the HgO coating

$\Delta[\text{O}] = [\text{O}] - [\text{O}]_0$, the change in atomic oxygen concentration during application of HgO coating

The change in atomic oxygen concentration is not directly observed, but can be inferred from the effect of atomic bromine quenching on the observed $\text{O}_2(\text{b})$ signal predicted from equation (3.14). Changes in oxygen atom concentration affects Br and BrF concentrations according to equations (3.24)-(3.26). Thus, the atomic oxygen concentration for a given $\text{O}_2(\text{b})$ signal is given by equation (3.28):

$$\Delta[\text{O}] = \{1 - [\text{O}_2(\text{b})]/[\text{O}_2(\text{b})]_0\} \Gamma_0 / (k_{13}^{\text{Br}} - k_{13}^{\text{BrF}}) \quad (3.28)$$

The atomic fluorine concentration is an order of magnitude larger than atomic oxygen and the first factor in the right hand side of equation (3.27) may be neglected. The observed slope is about 0.15, which provides $(k_{13}^{\text{Br}} - k_{13}^{\text{BrF}}) = 1.6 \times 10^{-11} \text{ cm}^3/(\text{molecule} \cdot \text{s})$, for an estimated $\Gamma_o = 10^3$. This is clearly consistent with the observed $\text{O}_2(\text{b})$ quenching by atomic bromine, $k_{13}^{\text{Br}} = 1.4 \times 10^{-11} \text{ cm}^3/(\text{molecule} \cdot \text{s})$ and a negligible BrF quenching rate coefficient.

Finally, the observed ratio for $[\text{BrF(B)}]/[\text{O}_2(\text{b})] = 5 \times 10^{-4}$ can be compared to the predictions of equations (3.19)-(3.20) and (3.23). All of the rate coefficients required to evaluate the predicted concentration ratios are not known, but lower bounds for the rates in the denominator can be estimated to provide upper bounds for $[\text{BrF(B)}]/[\text{O}_2(\text{b})]$. The BrF(B) lifetime is assumed equal to the radiative lifetime, $\tau_r \approx 60 \mu\text{s}$ (Clyne, 1980). For the recombination mechanisms, it is assumed that the BrF^* or $\text{Br}({}^2\text{P}_{1/2})$ intermediate removal is dominated by $\text{O}_2(\text{X})$ quenching, as suggested by Figure 14. For the sequential excitation, the favorable case that BrF^* removal is dominated by excitation to BrF(B) is assumed. The value for the three-body recombination rate coefficient is $k = 7 \times 10^{-31} \text{ cm}^6/(\text{molecule}^2 \cdot \text{s})$, as described below. Using the atomic concentrations $[\text{F}] = 4 \times 10^{14}$ and $[\text{Br}] = 4 \times 10^{13} \text{ atoms/cm}^3$ at the peak BrF(B) signal and a BrF concentration equal to the molecular bromine concentration, leads to the predicted concentration ratios given in Table I.

The rate coefficient for removal of $\text{Br}({}^2\text{P}_{1/2})$ by ground state oxygen has been recently measured as, $k = 1.5 \times 10^{-15} \text{ cm}^3/(\text{molecule} \cdot \text{s})$ (Taatzjes, 1991). If the excitation rate for reaction (3.5) is assumed equal to the quenching rate for $\text{O}_2(\text{b})$ by atomic bromine, then the

Table I
Predicted $[\text{BrF(B)}]/[\text{O}_2(\text{b})]$ Ratios

<u>Excitation Mechanism</u>	<u>$[\text{BrF(B)}]/[\text{O}_2(\text{b})]$</u> (Upper Bound)	<u>Equation</u>
$\text{Br}(^2\text{P}_{3/2}) + \text{F} + \text{M}$	$5 \times 10^{-7} (k_4/k_{17})$	(3.19)
$\text{Br}(^2\text{P}_{1/2}) + \text{F} + \text{M}$	$2 \times 10^{-7} (k_5/k_{21})$	(3.20)
$\text{BrF(X)} + \text{O}_2(\text{a,b})$	$9 \times 10^8 (k_8)$	(3.23)
Experimentally Observed	5×10^{-4}	

upper bound for the concentration ratio is $[\text{BrF(B)}]/[\text{O}_2(\text{b})] < 2 \times 10^{-3}$. This is above the measured concentration ratio, thus it is possible that excitation proceeds through excited bromine atoms.

The mechanism involving recombination of ground state atoms would require a relatively rapid excitation from BrF^\bullet to BrF(B) via reaction (3.4) to match the observed $[\text{BrF(B)}]/[\text{O}_2(\text{b})]$ ratio. The relative value for the rate coefficient for excitation to quenching would need to be $k_4/k_{17} > 10^3$. This does not violate the assumption that BrF^\bullet removal is dominated by quenching since, $[\text{O}_2(\text{b})]/[\text{O}_2(\text{X})] \cong 10^4$. The quenching of BrF^\bullet might be quite inefficient if the intermediate was vibrationally excited $\text{BrF(X}, \nu'' > 0)$. Many vibrational quanta would need to be

deactivated in a multistep process to drop the energy of BrF^{\bullet} below the level where $\text{O}_2(\text{b})$ could access $\text{BrF}(\text{B})$.

The prediction for the sequential excitation mechanism would require the rate limiting step of the excitation to have a rate coefficient greater than $5 \times 10^{-13} \text{ cm}^3/(\text{molecules} \cdot \text{s})$. This is a reasonable rate coefficient and this mechanism cannot be ruled out on the basis of this observation.

3.5.2 BrF(B) Excitation Rate. In section 3.3.2, the $\text{BrF}(\text{B})$ emission was observed to decay exponentially with a lifetime of $\tau = 65 \pm 4 \text{ ms}$ at an oxygen concentration of $[\text{O}_2(\text{X})] = 9.7 \times 10^{16} \text{ molecules/cm}^3$. Equation (3.19) indicates the $\text{BrF}(\text{B})$ signal will decay as the limiting reagent, atomic bromine, is removed by the three-body recombination of reaction (3.3). For a large excess of fluorine atoms, the atomic bromine would indeed decay exponentially. Evaluating the rate coefficient from equation (3.29) with $[\text{F}] = 2.2 \times 10^{14} \text{ atoms/cm}^3$:

$$1/\tau = k_3 [\text{F}] [\text{O}_2(\text{X})] \quad (3.29)$$

provides $k_3 \approx 7 \times 10^{-31} \text{ cm}^6/(\text{molecule}^2 \cdot \text{s})$. This is the limiting rate coefficient for the production of $\text{BrF}(\text{B})$ in the current experiments.

3.5.3 Energetics of the Excitation Mechanism. The vibrational distribution for $\text{BrF}(\text{B})$ observed to peak at $v'=3$ in Figure 12 is clearly not nascent, as considerable vibrational relaxation could occur at 3 torr total pressure within the $\approx 60 \mu\text{s}$ $\text{BrF}(\text{B})$ radiative lifetime. It does

however indicate that excitation to BrF(B) likely occurs near the potential maximum caused by the repulsive curve crossing. If all of the energy available in the $O_2(b^1\Sigma)$ energy transfer collision were transferred to BrF, then a BrF^* intermediate near $BrF(X, v''=10)$ would be indicated. This is too low for an intermediate electronic state of BrF. It is possible that $O_2(b)$ is deactivated to $O_2(a^1\Delta)$ in the energy transfer collision. The product of $O_2(b)$ quenching is often $O_2(a)$ (Singh, 1985b). In this case, energetics would demand an intermediate near 1.5 - 1.7 eV, as indicated in Figure 6. The only report of an intermediate electronic state of BrF is for the $^3\Pi(1)$ state at $T_e = 16,870 \text{ cm}^{-1}$ (Broderson, 1955). However, this spectroscopic assignment has been questioned (Coxon, 1975). Further investigation, both spectroscopic and kinetic, of the intermediate BrF^* is clearly needed.

3.5.4 Singlet Oxygen Quenching Studies. The quenching of $O_2(b^1\Sigma)$ by molecular bromine exhibits a rate coefficient intermediate between the rate coefficients for I_2 and Cl_2 (Perram, 1988), as presented in Table II. Quenching of $O_2(b)$ by diatomic halogens can lead to population of the $A^3\Pi(1_u)$ state or possibly dissociated atoms (Aviles, 1980). Table II shows that the A-state is accessible from the energy of one $O_2(b)$ collision only for I_2 and Br_2 . Thus, the observed Br_2 quenching rate appears to agree with previous studies of other halogen molecules.

The quenching of $O_2(b^1\Sigma)$ by atomic bromine is relatively fast, $k_{13}^{Br} = (1.4 \pm 0.3) \times 10^{-11} \text{ cm}^3/(\text{molecule} \cdot \text{s})$, which suggests the possibility of resonant energy transfer. Indeed, the spin-orbit splitting in atomic bromine is 3685 cm^{-1} and the energy difference between $O_2(b^1\Sigma, v=0)$ and

Table II
O₂(b) Quenching by Diatomic Halogens

Quencher	k_Q (cm ³ /(molecule·s))	T_e A ³ Π(1 _u) (cm ⁻¹)
I ₂	2.0 × 10 ⁻¹¹	11,888 (ref 29)
Br ₂	9.7 × 10 ⁻¹³	13,814 (ref 29)
Cl ₂	< 2 × 10 ⁻¹⁵	17,440 (ref 45)

O₂(a¹Δ, v=1) is 3753 cm⁻¹. Thus, the energy transfer would be within 68 cm⁻¹ of resonance. While the production of Br(²P_{1/2}) from this quenching is plausible, no effort to detect the excited bromine atoms was undertaken in the current experiments.

3.5.5 Potential for a BrF(B-X) Chemical Laser. The spectroscopic properties of BrF B³Π(0⁺) are ideal for chemical laser development. The B-state exhibits a large shift in equilibrium internuclear separation so that the most probable transition from v'=0 terminates on v''=8 with a low thermal population. The radiative lifetime is roughly 60 μs (Clyne, 1980), which is long enough to maintain an inversion during any mixing region, but short enough to provide a reasonable cross section for stimulated emission. The B³Π(0⁺) state is stable with respect to predissociation to vibrational level v'=6 (Clyne, 1980). The collisional

dynamics, quenching and vibrational energy transfer, of the B-state have been examined in the investigations discussed in the next chapter.

Excitation of BrF(B) by an efficient, sequential energy transfer mechanism would be ideal for laser development. The three-body recombination mechanism is less favorable. Typically, excitation rates of 10^{19} molecules/(cm³·s) are required to reach threshold in visible chemical lasers (Perram, 1990). It is unlikely that a three-body mechanism can achieve such rates at the low pressures typically encountered in the supersonic cavities of chemical lasers. This does not eliminate BrF(B) as a lasant candidate; however, as other excitation schemes might be identified.

3.6 Conclusions

The kinetics of the BrF B³Π(0⁺) chemiluminescence produced from Br₂ and F injected into a flow of discharged oxygen have been studied. The most intense flame is produced at low molecular bromine flow rates and persists for 15 - 65 ms in the flow direction. The BrF(B) is produced in a highly non-thermal vibrational distribution that peaks at $v' \approx 3$. The BrF(B) emission depends linearly on O₂(b¹Σ) concentration. The dependence of BrF(B) emission intensity on molecular bromine and atomic oxygen concentration is inconsistent with the steady-state predictions of a sequential energy transfer mechanism involving a two collisions with singlet oxygen. All the experimental data are consistent with a three-body recombination mechanism, most likely involving ground state halogen atoms. The rate coefficients reported for the deactivation of O₂(b) by Br₂ and Br are consistent with the same processes for other

halogens. An estimate for the rate coefficient applicable to the three-body recombination of fluorine and bromine atoms in the presence of molecular oxygen of $7 \times 10^{-31} \text{ cm}^6/(\text{molecule}^2 \cdot \text{s})$ is reported. The excitation process is inferred to be relatively efficient from the observed concentration ratio $[\text{BrF(B)}]/[\text{O}_2(\text{b})] = 5 \times 10^{-4}$.

IV. Collisional Energy Transfer in BrF B³Π(0⁺)

4.1 Introduction

In any chemical laser, the chemical excitation mechanism will excite a number of vibrational levels in the excited state manifold. In the specific case of singlet oxygen excitation of BrF B³Π(0⁺), the post-excitation vibrational distribution in the B-state manifold is strongly non-thermal peaking at $v'=3$. Similarly in IF(B), singlet oxygen excitation also produces a non-thermal vibrational distribution, in this case peaking at $v' \approx 6$ (Whitefield, 1983). In an efficient laser, the bulk of the excited state population should be in a single vibrational level. Thus most of the excitation energy would feed the lasing transition. In a chemical laser, efficient vibrational energy transfer is required to relax the excited state population down to primarily $v'=0$. This relaxation is caused by collisional energy transfer from the lasing molecules to other gas phase molecules in the laser media. A good example for a BrF laser is the CF₄ precursor used to produce fluorine atoms. Vibrational energy transfer rates must be determined in a potential chemical laser actual operating conditions. If the naturally occurring vibrational transfer is slow, a buffer gas can be added to induce rapid thermalization. This chapter examines the vibrational energy transfer in BrF induced by the BrF production mix. This transfer was found to obey a relatively simple energy transfer theory, the Montroll-Shuler model (Montroll, 1957), which will greatly simplify any further examinations of BrF.

One major problem associated with both added and background gases is electronic quenching. This collisional energy transfer takes a lasing molecule to a lower electronic state non-radiatively, removing energy from the laser. This could drastically lower laser efficiency and in extreme cases prevent laser operation. Accordingly electronic quenching of BrF by a number of collision partners has been studied using laser induced fluorescence (LIF). The electronic quenching rate coefficients ranged from 10^{-14} – 10^{-11} cm³/(molecule·s).

4.2 Experimental Arrangement

4.2.1 BrF Production. The first step in the study of BrF is the production of this unstable molecule. Both of the laser induced fluorescence studies discussed in this chapter utilize the reaction:



as the source of ground-state BrF molecules. Bemand and Clyne (Bemand, 1976) found that this reaction has a rate coefficient of $(2.2 \pm 1.1) \times 10^{-10}$ cm³/(molecule·s), which is essentially gas kinetic. In other words, every collision between a fluorine atom and a bromine molecule produces a BrF(X) molecule. These ground state molecules are then excited directly to the B-state by the laser.

Due to its instability, BrF must be produced and studied in a flowing system. A schematic diagram of the experimental apparatus used in both the electronic quenching and vibrational energy transfer studies is shown in Figure 17. The electronic quenching studies at times required the

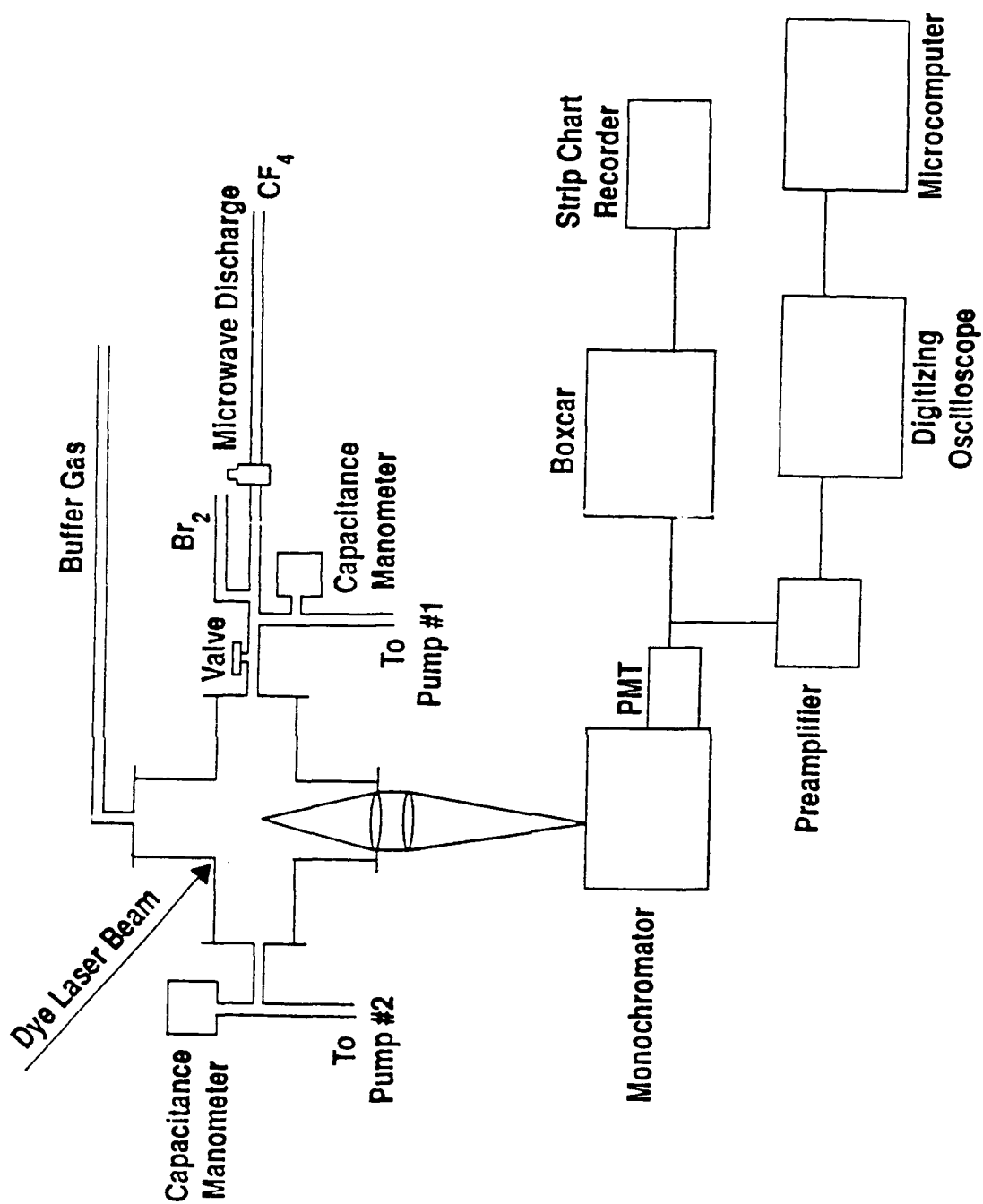


Figure 17. Experimental LIF Apparatus.

addition of large amounts of buffer gases. Therefore, to avoid affecting the BrF production, this took place at a relatively high pressure (760 mtorr). Precise amounts of the BrF mix were delivered through a ball valve into the fluorescence chamber where buffer gases were added. This chamber was constructed from a stainless steel six-way cross. Each leg had a diameter of 7.2 cm while the total length along each axis was 20 cm. The BrF mix flow is along one axis. This flow exits to a Sargent Welsh model 1376 35 l/min mechanical pump. The pressure in the chamber is monitored at the exit point by a MKS model 390, 1 torr capacitance manometer. The laser probe beam passes through the second axis. Brewster windows sealed to 1/2" tubing are mounted on the ends of the chamber to reduce reflection losses. A 7.2 cm diameter observation window seals one leg of the final axis. A 1/2" Cajon Ultratorr connector on the remaining leg is used to deliver buffer gas flows.

The fluorescence chamber leak rate was measured at 1.04 mtorr/hr. Buffer gas flows were controlled by a Granville-Phillips series 203 variable leak valve. All other gas flows were controlled with Nupro S-series metering valves.

Fluorine atoms were produced by passing CF_4 gas (Airco 99.7%) through an alumina tube inside an Opthos 2450 MHz, 100 watt microwave discharge. This was both safer and more convenient than using fluorine gas as the F-atom source, as was done in some other studies (Bemand, 1976) (Clyne 1976) (Clyne, 1980). The discharge operated at a CF_4 pressure of 760 mtorr, which maximized BrF production. At this pressure F-atom production was approximately 1%. This was determined by the amount of Br_2 required to maximize the BrF signal. Pressures in the discharge were

monitored by an MKS model 122a 10 torr capacitance manometer. As in the chapter III study, liquid bromine (Spectrum Chemical, 99.5%) was distilled by repeated freeze-thaw cycles. During actual experiments the Br_2 storage bulb was immersed in an ice bath. This assured a constant bromine head pressure of 63 torr (Samsonov, 1968). The bromine and CF_4 /F-atom flows mixed immediately downstream of the microwave discharge. Typical Br_2 partial pressures were 5-10 mtorr. BrF production is essentially immediate through reaction (4.1). The bulk of the mix then flows directly into a separate Sargent-Welsh model 1462 25 ℓ/min mechanical pump. This pump was required to isolate the BrF production from the fluorescence chamber.

Varying levels of BrF mix flows could be delivered directly into the fluorescence chamber through a ball valve. This system was very flexible, providing a wide range (5-700mtorr) of mix pressures. This is a considerable advantage over the fixed pinhole technique employed by Clyne (Clyne, 1978c). Buffer gases were delivered directly to the fluorescence chamber. This allowed experiments with small precise concentrations of collision partner gases. The Buffer gases were all 99.999% pure (Airco) with the exception of oxygen (99.994% Airco) and CO_2 (99.9%).

4.2.2 Excitation System. Both the electronic quenching and vibrational energy transfer studies utilized pulsed LIF as the primary experimental technique. Laser excitation was provided by a Spectra-Physics model PDL-3 pulsed dye laser pumped by a Quanta-Ray DCR-3 pulsed Nd:YAG laser. The tripled output of the Nd:YAG laser was used to pump Exciton Coumarin 500 dye at a pulse rate of 20 hz. The tuning range

of this dye was sufficient to access all of the pump transitions used in these studies. During the first phase of the research examining electronic quenching the dye laser produced pulse energies of 1 mJ at a pulsewidth of 10 ns. The laser was then upgraded with a preamplifier and a transversely pumping optics for the amplifier before the vibrational transfer studies. These improvements increased pulse energies by a factor of 10. This was critical, for these spectrally resolved studies where the signal strength was low. This pulse energy is a dramatic improvement over the 10 μ J pulse energies employed in earlier BrF kinetic studies (Clyne, 1980).

4.2.3. Detection System. In the total fluorescence studies of electronic quenching the emission from the fluorescence chamber was collected by a 5 cm diameter, 10cm focal length, lens and then focused by a 5cm diameter, 15cm focal length, lens directly into a room temperature RCA C31034 photomultiplier tube (PMT). Two LP 6300 angstrom, colored glass, long pass filters were used to block any scattered laser light from the chamber. In time resolved studies, the output from this tube was input to a LeCroy 9450 350MHz digitizing oscilloscope. This device, triggered by the pump laser, was used to take at least a 1000 shot average for each waveform. The digitized result was then transferred to a Zenith 248 microcomputer for final processing. Total fluorescence was also used in generating laser excitation spectra. Here the output of the PMT was input to a Princeton Applied Research Corp. (PARC) model 160 boxcar integrator also triggered by the pump laser. Its output then drove a

strip chart recorder to generate continuous spectra as the dye laser was tuned in wavelength.

In the spectrally resolved studies, a 25 cm focal length lens focuses the chamber emission through the entrance slit of an Instruments SA model HR60 .64 m monochromator with 1200 groove/mm grating blazed at 1 micron. The same PMT was mounted on the exit slit of this device. The signals were much lower in these studies so a PARC model 115 preamplifier was used to amplify the PMT output before delivery to the LeCroy 9450 for lifetime studies. In order to choose examination wavelengths in the vibrational transfer study, the monochromator was scanned in wavelength with the laser excitation wavelength fixed at an absorption line. The output from the boxcar integrator generated a vibrational transfer spectrum indicating the vibrational populations after pumping a single excited state vibrational level.

4.3 Electronic Quenching

Electronic quenching is the collisional loss of electronic excitation energy. In BrF, electronic quenching returns a B-state molecule to a lower electronic state, depopulating what would be the upper laser level. Furthermore, interpretations of the spectrally resolved observations that yield vibrational transfer rates, must consider electronic quenching effects. Thus it is critical, from both the global perspective of laser potential and the more restricted goal of examining vibrational transfer, that electronic quenching in BrF(B) be well understood.

4.3.1 Background Theory. Quenching by a single species M , is described by:

$$\frac{dN_i}{dt} = -\sum_1 A_{i1} N_i - k^{EQ} N_i M = -\Gamma N_i \quad (4.2)$$

Where: N_i = The population of the i th level

A_{i1} = the Einstein coefficient of spontaneous emission

k^{EQ} = the rate coefficient for electronic quenching

M = The concentration of collision partners

Γ = a total first order decay constant that takes into account both radiative and electronic quenching depopulation of the excited state.

Electronic quenching is studied in pulsed LIF by monitoring the decay of total fluorescence with time. There are two limiting cases of electronic quenching rate coefficients. In a thermalized vibrational distribution, when the V-T rates are faster than the quenching rate, then a Stern-Volmer analysis of the spectrally unresolved data will provide the total electronic quenching rate for the collision species M, k^{EQ} . At low pressures and high electronic quenching rates, vibrational transfer is slow so that the bulk of the B-state population is quenched directly from the initial vibrational level. In this case the vibrational dependent electronic quenching rate coefficient $k^{EQ}(v')$ can be determined. Mathematically a Stern-Volmer analysis involves integrating equation (4.2) with respect to time:

$$\frac{I}{I_0} = \frac{N_i}{N_i(t=0)} = e^{-t\Gamma} \quad (4.3)$$

thus:

$$\ln(I/I_0) = -\Gamma t \quad (4.4)$$

The total decay rate Γ , is just the negative slope of the $\ln(I/I_0)$ versus time plot. Figure 18 shows the effects of electronic quenching of BrF(B) on both linear and logarithmic scales. In the Stern-Volmer analysis, this decay rate is then plotted versus the pressure of the quenching species M. The slope of the line best fitting the data points in this graph, provides the electronic quenching rate coefficient k^{EQ} and the zero pressure intercept is $1/\tau_{CF}$ the collision free lifetime.

$$\Gamma = \frac{1}{\tau_{eff}} = \frac{1}{\tau_{CF}} + k^{EQ} M \quad (4.5)$$

where τ_{eff} is the effective lifetime and:

$$1/\tau_{CF} = 1/\tau_r + k^{PD} = \sum_i A_{i1} + k^{PD} \quad (4.6)$$

Of course for those vibrational levels where predissociation is not a factor the collision free lifetime equals the radiative lifetime.

4.3.2 Experimental Results. This section will describe in detail the experiments and the results involved in the determination of electronic quenching rates on BrF(B).

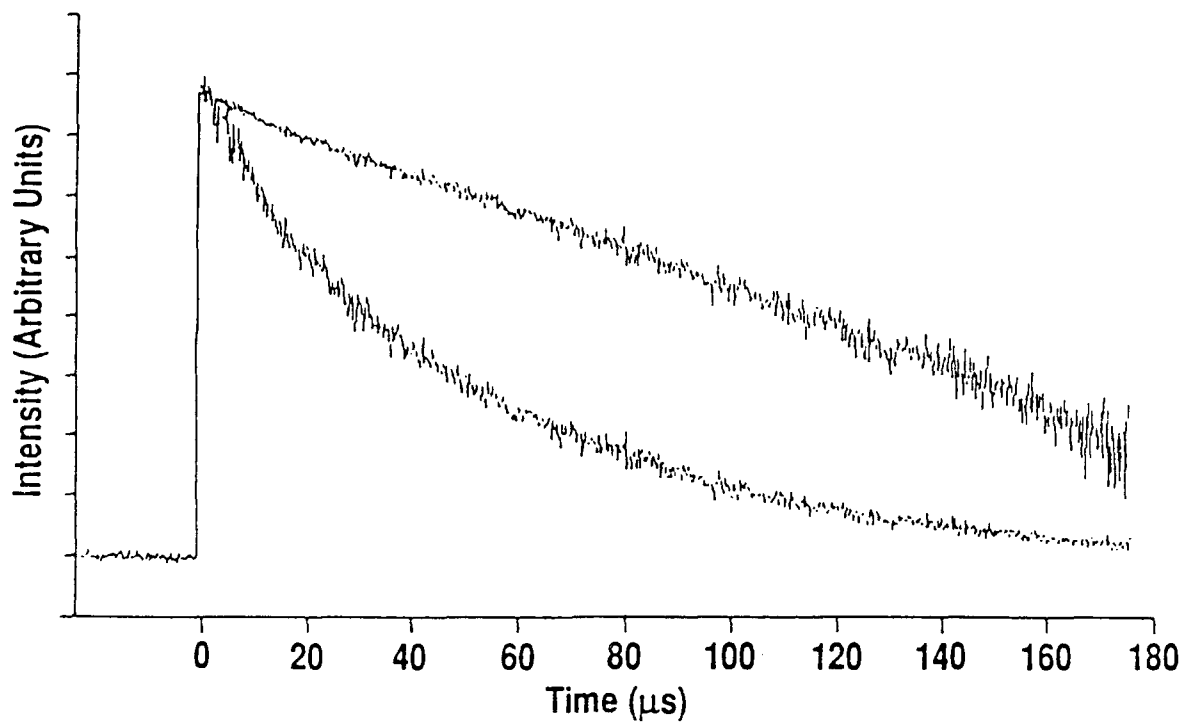


Figure 18. Fluorescence decay of BrF(B) $v'=5$, with 1 mtorr of CO₂ at a mix pressure of 14 mtorr. The intensity axis is plotted in both linear and logarithmic scales.

4.3.2.1 Laser Excitation Spectra. The first step in the use of laser induced fluorescence spectroscopy is the identification of the proper laser excitation wavelength. It is critical in these total fluorescence experiments that only a single B-state vibrational level is populated. If not, the detected fluorescence would be a blend of different bands, rendering logarithmic curve fits to the time evolution data meaningless. Figure 19 shows the laser excitation spectrum generated by tuning the dye laser through the entire response curve of Coumarin 500 dye. The use of the boxcar integrator triggered by the Nd:YAG pump laser provides a continuous response from the pulsed excitation. The boxcar integrator gate was set for 40 μ s in duration starting 16 μ s after the laser excitation pulse. This delay was set to eliminate any contributions from molecular bromine, whose effective lifetime is $\approx 3 \mu$ s near dissociation. At excitation wavelengths longer than 510.7 nm, the dissociation limit for bromine (McAfee, 1976), this might otherwise have been a problem. Figure 19. shows how coumarin 500 dye allowed access to a excitation transitions ranging from $v''=0 \rightarrow v'=2$ to $v''=0 \rightarrow v'=7$. The resolution of this spectrum was limited by the dye excitation laser linewidth (0.07 cm^{-1}) and the response speed of the boxcar integrator.

The individual bands were then examined with the scanning speed of the excitation laser reduced by a factor of 10. An excellent example is the 5030-5070 \AA high resolution scan of the $(v',v'')=5,0$ band shown in Figure 20. This spectrum shows excellent rotational resolution. The individual rotational lines in this band were easily resolved and identified using a combination differences analysis (Herzberg,

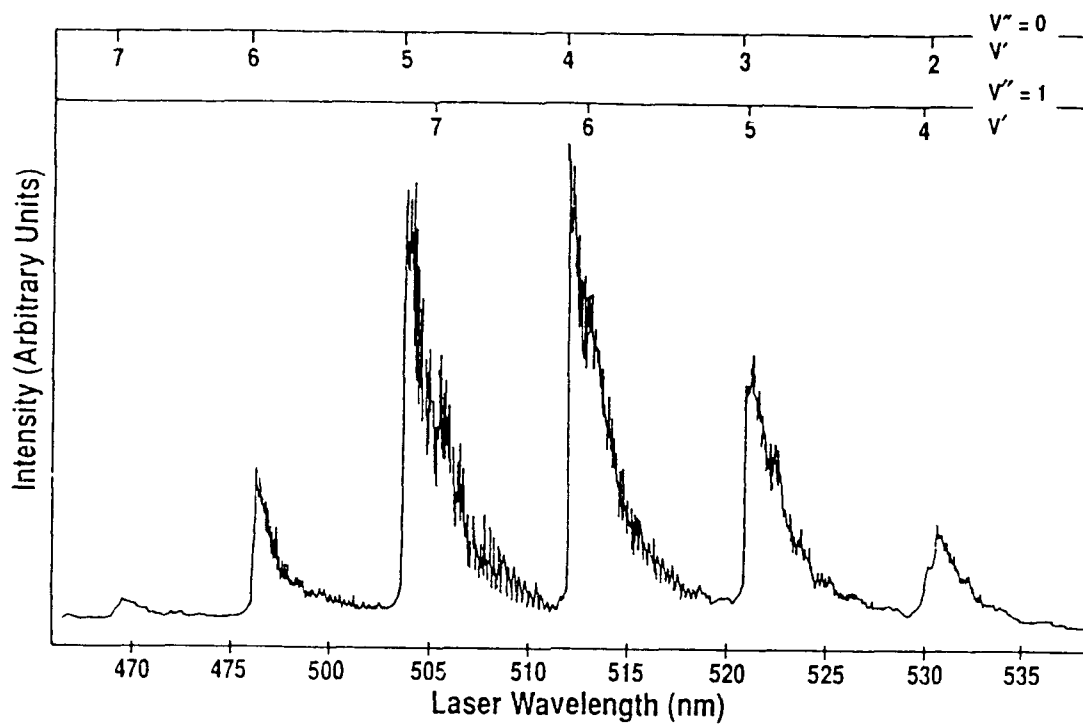


Figure 19. Laser excitation spectrum of the BrF(B-X) system generated with coumarin 500 laser dye at a mix pressure of 64 mtorr.

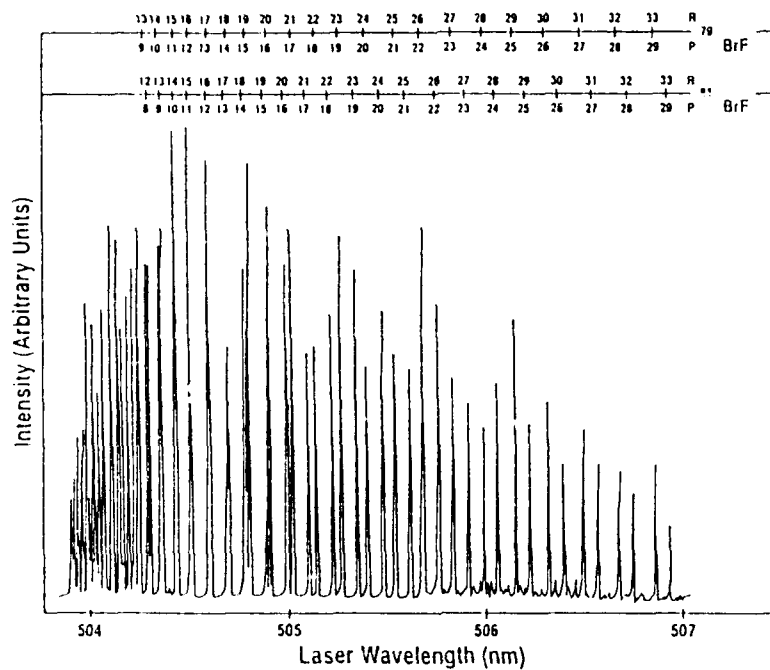


Figure 20. High resolution laser excitation spectrum of the $(v', v'')=5,0$ band of the BrF(B-X) system at a mix pressure of 62 mtorr.

1950:175-185). This band is overlapped by the $(v',v'')=7,1$ band at excitation wavelengths longer than 5056 Å. The relative intensities of the two bands differed greatly simplifying the discrimination between these two features. In the $(v',v'')=(5,0)$ band, the P(J) and R(J+4) lines for each isotope overlap almost exactly. Therefore sets of doublets generated from the two BrF isotopes, rather than sets of four lines when the two branches can be distinguished, are seen in this spectrum. Near the bandhead even the lines from the two isotopes begin to overlap.

This high resolution spectrum was used to choose the wavelength of the excitation transition for use in the electronic quenching and vibrational transfer studies in BrF $v'=5$. The chosen transition, at an air wavelength of 5044.3 Å, had a powerful resonance due to four overlapping lines the R(15) and P(11) lines in ^{79}BrF and the R(14) and P(10) lines in ^{81}BrF .

A similar analysis was used to identify the transitions in the $(v',v'')=(6,0)$ band. The P(21) line of ^{81}BrF , at an air wavelength of 4978.4 Å was chosen as the excitation transition for the electronic quenching studies of this band. This was the line employed by Clyne in his electronic quenching work (Clyne, 1977), allowing direct comparisons between his results and those of this dissertation.

In both the $(v',v'')=(4,0)$ and the $(v',v'')=(3,0)$ bands there are strong overlapping bands complicating the identification of discreet pump state populating a single v' level. The $(v',v'')=(2,0)$ band is overlapped by the $(v',v'')=4,1$ band; however, the relative intensities and placement of the rotational line simplified their identification. The P(27) line of

^{81}BrF at an air wavelength of 5331.3 Å was chosen as the excitation transition for all of the $\text{BrF } v'=2$ electronic quenching studies.

4.3.2.2 Electronic Quenching Experimental Procedures.

Electronic quenching rate coefficients for a variety of collision partners have been experimentally determined using the Stern-Volmer technique described in section 4.3.1. Each fluorescence decay waveform was averaged for a 1000 shots over a 200 μs period at a temporal resolution of .25 μs . This yielded an examination range of 180 μs after the excitation pulse. Pre-trigger information was recorded to determine the proper 'zero' baseline. This is a critical factor in taking exponential fits to raw data. In most circumstances this time setting allowed a drop of three e-folds from the initial intensity. This large intensity range increased confidence in the fits to the exponential fluorescence decay waveforms.

In some initial experiments a downward curvature was observed in the Stern-Volmer plots for buffer gases with low electronic quenching rates. This is symptomatic of an increase in lifetime with the initial increase in pressure. This was caused by excited state molecules diffusing from the observation region before electronic quenching occurs, resulting in an artificial reduction in signal from long lived states. The fluorescence collection lens in the experimental arrangement is focused on the laser axis, maximizing signal at the cost of a small observation region. Diffusion is slowed as the pressure increases, allowing better detection of long-lived states and thus a net increase in lifetime. There was a related problem in Clyne's early examinations of BrF(B) radiative

lifetimes (Clyne, 1978a-c). In this work, the observation window was only 17 mm from the laser axis. Deactivation of long lived states at the observation window lead to an underestimate of radiative lifetimes. In a later set of measurements the window was 37 mm from the laser axis leading to an $\approx 30\%$ increase measured radiative lifetime (Clyne, 1980). This was not the problem in the current work since the observation window was 9 cm from the laser axis.

To test whether the diffusion loss due to collection optics was the problem, a variable iris was placed between the focusing lens and the photomultiplier tube. As the iris was closed, restricting the field of view, the measured lifetime decreased, verifying that diffusion was the culprit. Two possible solutions were considered. The first was to replace the collection lens so that the focus was no longer exactly on the laser axis. Unfortunately, this method would also reduce signal strength, an unacceptable trade-off. The second solution was to increase chamber pressure, slowing diffusion, without affecting the electronic quenching rate. In the initial experiments it was found that the argon electronic quenching rate on BrF(B) was very low ($k^{EQ} < 10^{-13} \text{ cm}^3/(\text{molecule}\cdot\text{s})$). It was found that a 200 mtorr argon background could correct the diffusion problem without affecting electronic quenching rates. This background was used in all subsequent electronic quenching experiments.

4.3.2.3 Mix Self Quenching. The first electronic quenching rate coefficient determined by a Stern-Volmer analysis was the self quenching rate for the BrF production mix. Figure 21 shows the

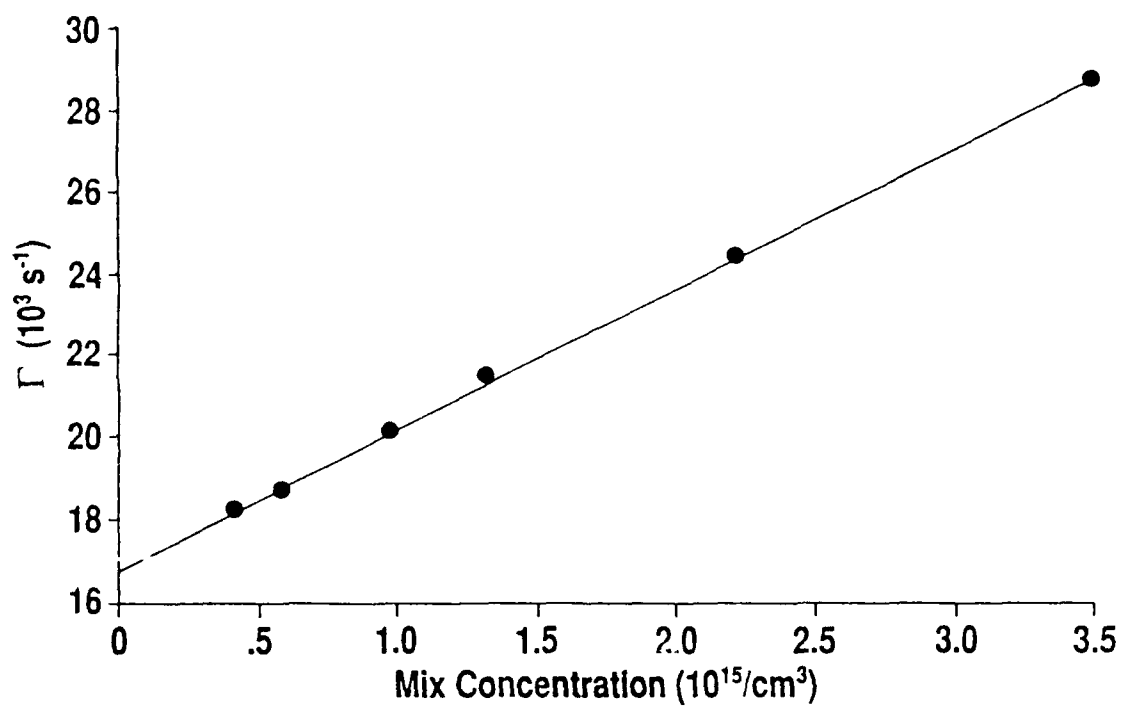


Figure 21. Stern-Volmer fit for mix self-quenching in the BrF $v'=5$ level.

Stern-Volmer fit which provided a rate coefficient of $k_{\text{MIX}}^{\text{EQ}} = (3.43 \pm 0.03) \times 10^{-12} \text{ cm}^3/(\text{molecule} \cdot \text{s})$. The quoted error is the standard deviation in the slope of the linear-least-squares fit to the Stern-Volmer data. The zero pressure intercept of this line yields a radiative lifetime for $v'=5$ of $\tau_r = (59.6 \pm 4) \mu\text{s}$ which matches Clyne's most recent estimate of $58.9 \mu\text{s}$ almost exactly (Clyne, 1980). This correspondence verified that the addition of the argon background did indeed solve the diffusion problem. Electronic quenching rate coefficients were then determined for a wide range of collision partners at three different v' levels each. Table III. summarizes these rates. The quoted errors are the standard deviations in the slopes of the Stern-Volmer plots.

4.3.2.4 Argon Quenching. Argon quenching waveforms were examined at argon pressures ranging up to 700 mtorr, the effective high pressure limit of the experimental arrangement. The BrF mix partial pressure was 8.7 mtorr implying a BrF partial pressure of $\approx .087$ mtorr. Over the range of added argon pressure, there were no significant decreases in BrF(B) lifetimes (see Figure 22). Considering the range of added pressure and estimating the minimum observable change in Γ of 1000 s^{-1} , an upper limit for argon electronic quenching rate coefficient is $k_{\text{Ar}}^{\text{EQ}}(v'=5) = 6 \times 10^{-14} \text{ cm}^3/(\text{molecule} \cdot \text{s})$, which is slightly lower than the $10^{-13} \text{ cm}^3/(\text{molecule} \cdot \text{s})$ upper bound reported by Clyne (Clyne, 1980). Due to the inability to measure more than an upper bound for the argon quenching rate, plans to examine electronic quenching by the other noble gases were dropped.

Table III

BrF(B) Electronic Quenching Rate Coefficients

Species	BrF(B) ν'	k^{EQ} cm ³ /(molecule·s)
Argon	5	$< 6 \times 10^{-14}$
Bromine	6	$(5.42 \pm .12) \times 10^{-11}$
	5	$(6.86 \pm .18) \times 10^{-11}$
	2	$(3.15 \pm .12) \times 10^{-11}$
CF ₄	6	$(1.73 \pm .06) \times 10^{-12}$
	5	$(2.07 \pm .05) \times 10^{-12}$
	2	$(2.31 \pm .06) \times 10^{-12}$
CO ₂	6	$(6.11 \pm .22) \times 10^{-11}$
	5	$(5.05 \pm .12) \times 10^{-11}$
	2	$(6.32 \pm .15) \times 10^{-11}$
N ₂	6	$(3.49 \pm .15) \times 10^{-12}$
	5	$(3.59 \pm .06) \times 10^{-12}$
	2	$(3.71 \pm .09) \times 10^{-12}$
SF ₆	2	$< 8 \times 10^{-14}$

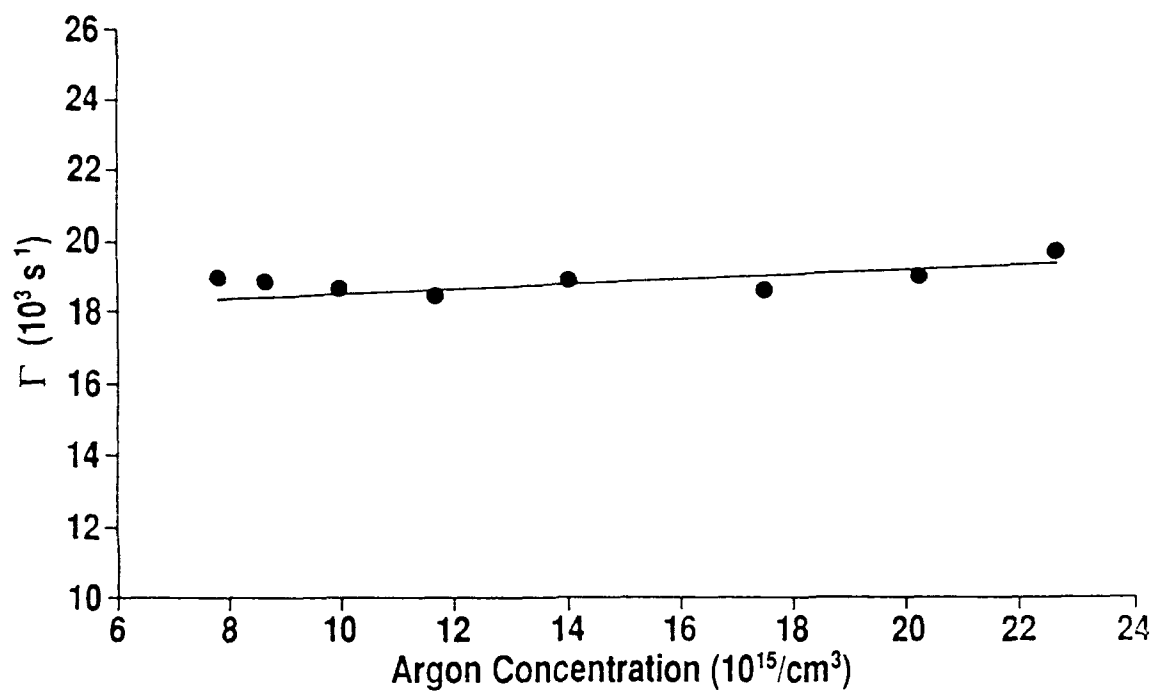


Figure 22. Stern-Volmer Plot for Argon quenching of BrF $v'=5$ at a mix pressure of 8.7 mtorr.

4.3.2.5 Bromine Quenching. These experiments required a slight modification in the basic experimental arrangement described in Figure 17. Here a small portion of the bromine is split off prior to the metering valve delivering Br_2 to the BrF production region. This bromine is passed through a separate metering valve and delivered to the fluorescence chamber as the buffer gas. Due to the high head pressure in the bromine storage reservoir this does not affect conditions in the BrF production region.

In each set of experiments the mix pressure chosen was that which provided the minimum utilizable emission strength. The rate coefficients provided by these fits are $k_{\text{Br}_2}^{\text{EQ}}(v'=2) = (3.15 \pm .12) \times 10^{-11} \text{ cm}^3/(\text{molecule} \cdot \text{s})$, $k_{\text{Br}_2}^{\text{EQ}}(v'=5) = (6.86 \pm .18) \times 10^{-11} \text{ cm}^3/(\text{molecule} \cdot \text{s})$ and $k_{\text{Br}_2}^{\text{EQ}}(v'=6) = (5.42 \pm .12) \times 10^{-11} \text{ cm}^3/(\text{molecule} \cdot \text{s})$. The differences between the $v'=5$ and $v'=6$ rate coefficients are within systematic error (Appendix D). The larger gap between these and the $v'=2$ rate constant must be attributed to a vibrationally dependent electronic quenching.

The fluorescence waveforms for $v'=5$ and $v'=6$ both show a fast decay on a short time scale (see Figure 23), which was not considered in the exponential fits and Stern-Volmer analysis used to determine the quoted quenching rate coefficients. This feature was present in all $v'=6$ experiments regardless of buffer gas. In $v'=5$ it is only observed in Br_2 quenching. A Stern-Volmer analysis, utilizing exponential fits to this short-term decay, provided quenching rate coefficients of $k_{\text{Br}_2}^{\text{EQ}}(v'=5 \text{ short}) = (1.58 \pm .02) \times 10^{-10} \text{ cm}^3/(\text{molecule} \cdot \text{s})$ and $k_{\text{Br}_2}^{\text{EQ}}(v'=6 \text{ short}) = (1.21 \pm .05) \times 10^{-10} \text{ cm}^3/(\text{molecule} \cdot \text{s})$. A possible explanation for this short time decay is discussed in detail in section 4.3.3.

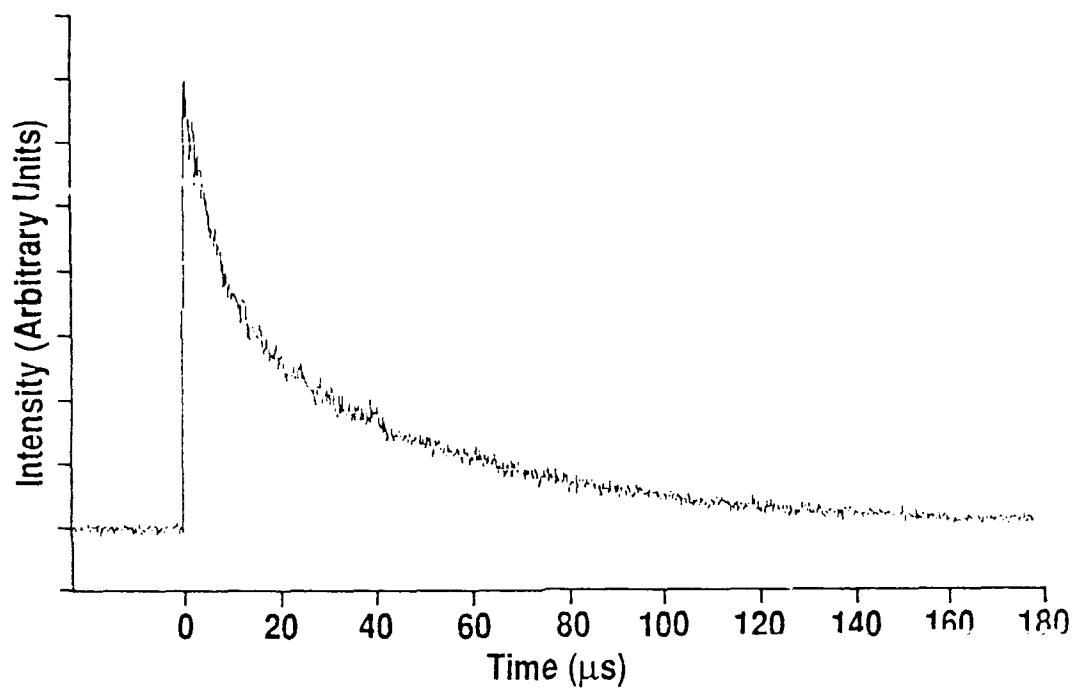


Figure 23. Quenching of $\text{BrF(B)} \nu'=6$ by 2.1 mtorr of Br_2 at a mix pressure of 46 mtorr.

4.3.2.6 CF₄, CO₂ and N₂ Quenching. The Stern-Volmer analyses of the quenching of BrF(B) by each of these buffer gases were quite straightforward. The electronic quenching rate coefficients derived from this effort are given in Table III. There were no signs of vibrationally dependent quenching from any of these species. In each case, the quenching rate coefficients from the BrF(B) $v'=6$, $v'=5$, and $v'=2$ were within systematic error.

A short term decay was present in the $v'=6$ data for all three gases. A Stern-Volmer analysis of this decay for CO₂ and N₂ provided rate coefficients of $(4.6 \pm 2) \times 10^{-11} \text{ cm}^3/(\text{molecule} \cdot \text{s})$ and $(3.3 \pm 4) \times 10^{-12} \text{ cm}^3/(\text{molecule} \cdot \text{s})$ respectively. These values are close to those found in the long period decay. This suggests that the only effect of added buffer gases on the short time decay is through the changing baseline of the long period decay. In the case of CF₄, the short-term data was too noisy for a linear Stern-Volmer fit.

4.3.2.7 Oxygen Quenching. The quenching behavior of molecular oxygen on BrF(B) is unique among the collision partners examined in this study. The measured rate coefficients for O₂ quenching of BrF(B) have different values in different pressure regimes. The initial addition of oxygen quenches BrF(B) quite rapidly. The linear fits in the Stern-Volmer analyses for levels $v'=5$ and $v'=2$ are quite good, providing rate coefficients of $k_{02}^{\text{EQ}}(v'=2) = (2.40 \pm 13) \times 10^{-11} \text{ cm}^3/(\text{molecule} \cdot \text{s})$ and $k_{02}^{\text{EQ}}(v'=5) = (2.87 \pm 12) \times 10^{-11} \text{ cm}^3/(\text{molecule} \cdot \text{s})$. Due to the apparently rapid quenching, the added O₂ pressure in these initial experiments reached only ≈ 20 mtorr. It was only in the $v'=6$ quenching data that the unusual

behavior of oxygen quenching of BrF(B) became apparent. The Stern-Volmer plot for this data shows curvature even at low added oxygen pressures. Data was then taken at a much higher range of pressures. Figure 24 shows how after an initial high quenching rate region at low pressure, the Stern-Volmer plot becomes linear at a much lower quenching rate at high oxygen pressures. Using this second linear region to derive a rate coefficient yields a dramatically slower rate $k_{O_2}^{EQ}(v'=2 \text{ high pressure}) = (5.37 \pm .46) \times 10^{-12} \text{ cm}^3/(\text{molecule} \cdot \text{s})$. Several mechanisms for this unusual behavior are discussed in section 4.3.3.

4.3.2.8 SF₆ Quenching. The total fluorescence waveforms of BrF(B- λ) emission intensity do not decay as a single exponential with the addition of SF₆. Instead, as SF₆ is added, an initial peak appears at 17 μs after the initial excitation in the $v'=5$ data. In $v'=2$, the hump is much less dramatic and occurs much sooner after the initial excitation (see Figure 25). The decay after this feature is essentially exponential. This $v'=2$ data was examined for pressure dependence. There was essentially no change in Γ for added SF₆ pressures up to 346 mtorr. As with the argon data, this was used to determine an upper limit on the SF₆ rate coefficient of $k_{SF_6}^{EQ}(v'=2) < 8 \times 10^{-14} \text{ cm}^3/(\text{molecule} \cdot \text{s})$

This behavior can be explained by noting that the emissions from $v'=1,0$ are detected most efficiently (see Appendix C). Rapid vibrational transfer into these levels would appear as an increase in the total fluorescence intensity. This explanation is examined in detail in section 4.3.3.

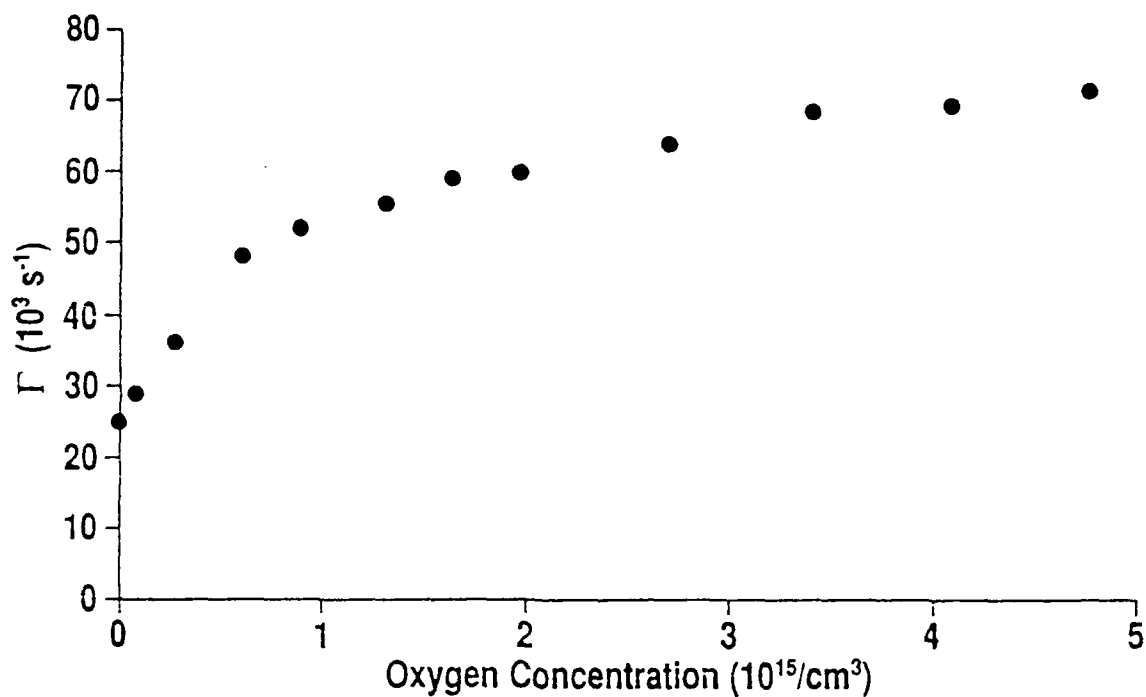


Figure 24. Stern-Volmer plot of O_2 quenching of $\text{BrF(B)} \nu'=2$ at a mix pressure of 54 mtorr.

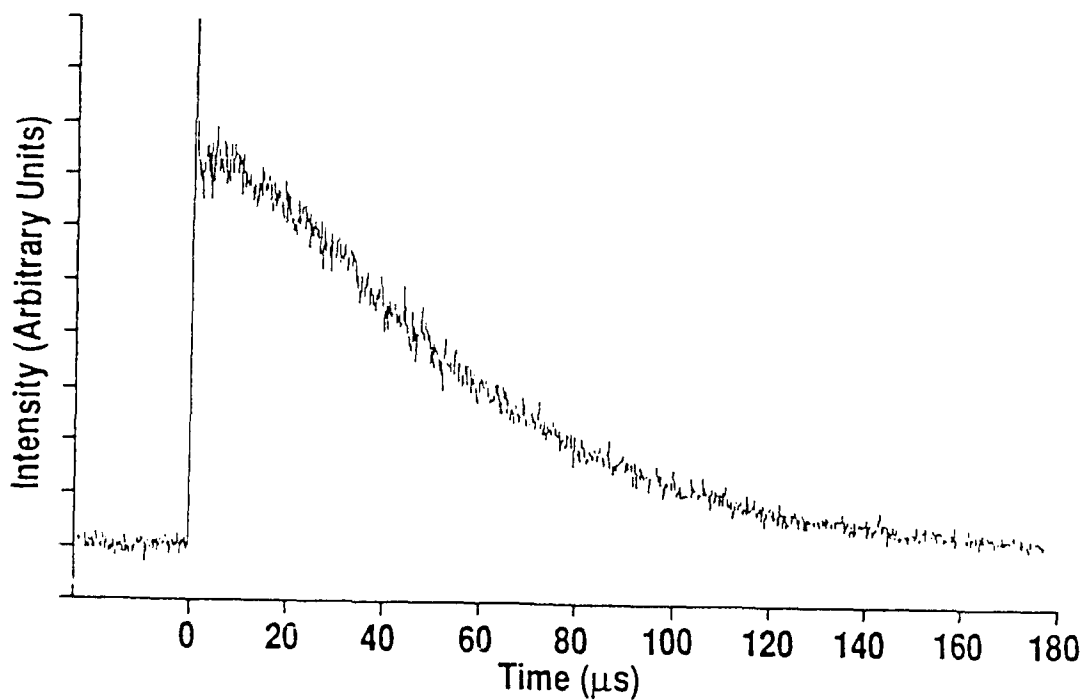


Figure 25. $\text{BrF(B-X)} \nu'=2$ total fluorescence waveform influenced by 168 mtorr of SF_6 at a mix pressure of 47 mtorr.

4.3.3 Discussion of Electronic Quenching Results

4.3.3.1 Bromine Quenching. The fluorescence decay waveforms for bromine quenching of BrF(B) show two exponential decay regions, a rapid short-term decay followed at longer times by a more gradual loss. These two decay regions are caused by different fundamental processes that both appear in total fluorescence waveforms. The slower decay is surely electronic quenching while the short term decay is most likely caused by population transfer to a predissociated energy level. In BrF(B) $v'=6$, predissociation commences abruptly at $J'=49$ (Clyne, 1980). The initially populated level in the quenching studies in $v'=6$ was $J'=20$. This level is quite close in energy, only 400 cm^{-1} , to the predissociated level. It was chosen since Clyne's examination of Br₂ quenching of BrF(B) also used this particular level (Clyne, 1977). The quoted rate coefficient, $k_{\text{Br}_2}^{\text{EQ}} = (1.50 \pm 0.23) \times 10^{-10} \text{ cm}^3/(\text{molecule} \cdot \text{s})$ is almost within error of the rate coefficient found, in the current research, for the short term decay $k_{\text{Br}_2}^{\text{EQ}} = (1.21 \pm 0.05) \times 10^{-10} \text{ cm}^3/(\text{molecule} \cdot \text{s})$. His fluorescence decay waveforms were measured on only a 50 μs time scale. Perhaps this is why he failed to observe the slower decay characteristic of BrF(B) electronic quenching. In a later paper (Clyne, 1980), Clyne discounts his interpretation of Br₂ quenching rates as mistaken due to predissociation effects, and never returns to examining quenching by this molecule.

Stern-Volmer plots generated by fits to the long and short time features in the $v'=6$ waveforms show significantly different $[\text{Br}_2]=0$ intercepts ($\Gamma=52,000\text{ s}^{-1}$ versus $\Gamma=20,000\text{ s}^{-1}$). On the other hand, in the

$v'=5$ data the intercepts are much closer ($\Gamma=28,000 \text{ s}^{-1}$ versus $\Gamma=18,000 \text{ s}^{-1}$). This is significant; in $v'=6$ the short term decay is present in the waveforms even without added bromine, whereas in the $v'=5$ data this decay is only evident with added bromine. The decay is always present in $v'=6$ regardless of buffer gas. It is only present in $v'=5$ when bromine is the collision partner.

Population transfer to predissociated energy levels can account for this behavior. In $v'=6$ the BrF mix $\text{CF}_4:\text{BrF}:\text{Br}_2$, is sufficient to induce rotational ladder climbing from the initially populated J' level through the slight energy gap to the predissociated levels. In $v'=5$, the mix is not sufficient to induce a direct ro-vibrational transition to a predissociated rotational level in $v'=6$. Thus there is no short time feature in this level until bromine is added. This hypothesis explains why, with other buffer gases, the rate coefficient of the short term feature is that of the long term decay. In both sets of waveforms the longer time decay is generated after vibrational transfer to lower vibrational levels where predissociation is not a factor. The other gases only affect the short time feature by changing the long-period decay rate. Br_2 appears especially efficient, perhaps due to its high mass and angular momentum, in inducing rotational energy transfer.

The rate coefficients for Br_2 quenching are near gas kinetic. There are two possible mechanisms for this high rate. The first is resonant electronic exchange, in which an electronic state in the collision partner is excited while quenching BrF to an intermediate electronic state or to some vibrational level in the ground state. In BrCl(B) mix self quenching, where electronic energy exchange with $\text{Cl}_2(\text{X})$ is effective, the

quenching rates vary by three orders of magnitude with vibrational level (Perram, 1986). In the current BrF studies, only a slight vibrational dependence was observed. The product of this exchange is $\text{Br}_2(\text{B})$; however, no $\text{Br}_2(\text{B-X})$ emission was observed for $v'=5,6$, where the excitation energy is above the Br_2 dissociation limit. This would indicate that the quenching method is not electronic energy exchange. This is not conclusive since the Br_2 emission would be faint.

The second quenching mechanism is energy transfer to the vibrational modes of ground electronic state Br_2 . The $\text{Br}_2(\text{X})$ dissociation limit, $16,000 \text{ cm}^{-1}$, allows sufficient vibrational energy for transfer from either a $\text{BrF}(\text{B} \rightarrow \text{A})$ or $\text{BrF}(\text{B} \rightarrow \text{X})$, high v'' level, transition.

The high Br_2 electronic quenching rate on $\text{BrF}(\text{B})$ has an important implication for a $\text{BrF}(\text{B} \rightarrow \text{X})$ transition chemical laser. Whatever the production scheme for fluorine atoms, it should be higher than the initial Br_2 population. It is important that little free bromine survive the BrF production process lest Br_2 quenching become the dominant energy loss mechanism in the laser.

4.3.3.2 CO_2 Quenching. The fluorescence decay waveforms and Stern-Volmer plots for CO_2 quenching of $\text{BrF}(\text{B})$ showed no unusual features. The quenching rate coefficients are quite large, $\approx 6 \times 10^{-11} \text{ cm}^3/(\text{molecule} \cdot \text{s})$, similar to those of bromine. The most likely explanation for this rapid quenching is an $\text{E} \rightarrow \text{V}$ collisional energy transfer. BrF would be quenched to either the 'A' electronic state or to a high ground state v'' of $\text{BrF}(\text{X})$, exciting vibrational modes in CO_2 . Highly excited vibrational modes with energies ranging up to $13,000 \text{ cm}^{-1}$

have been observed (Herzberg, 1945:275). Electronic excitation of CO_2 is not a possibility given the high energy, $45,000 \text{ cm}^{-1}$ of its first electronically excited state (Herzberg, 1966:503), far higher than the energy of BrF(B) . It is interesting to note that in ICl(B) , the only other instance of CO_2 quenching of an interhalogen in the literature, the quenching rate coefficient was also quite high $3 \times 10^{-11} \text{ cm}^3/(\text{molecule} \cdot \text{s})$ (Steinfeld, 1984).

No evidence of CO_2 induced BrF(B) vibrational transfer was observed. This is not surprising since, due to the extremely high quenching rate, the total amount of added CO_2 was less than 25 mtorr.

4.3.3.3 SF_6 Quenching. The fluorescence decay waveforms observed when SF_6 is added to BrF(B) are an obvious and dramatic instance of vibrational transfer appearing in total fluorescence observations. This is usually an indication of non-uniform spectral response to emission from the various upper state vibrational levels. The photomultiplier tube used in this study, an RCA C31034, has an essentially flat spectral response through the visible range out to 8800 \AA . As can be seen in Appendix C, a nonlinear spectral response is generated when the effects of the 8800 \AA long wavelength cutoff are combined with the 6300 \AA long pass filter used to block scattered laser light. Basically more of the emission bands originating from the lowest v' levels fall into this $6300\text{--}8800 \text{ \AA}$ window, thus total fluorescence observations will show a stronger response to emission from these levels.

Figure 26 shows the results of this effect in a BrF(B) $v'=5$ waveform. The initial rise in this curve is caused by vibrational

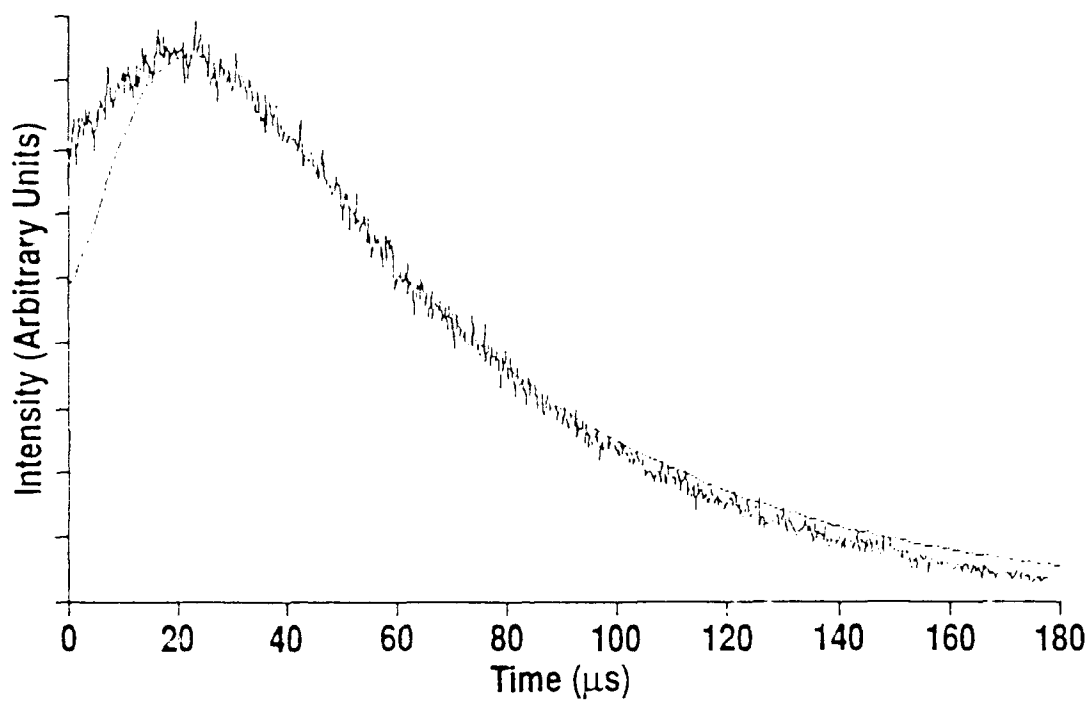


Figure 26. Comparison of experimental and theoretical BrF(B) $v'=5$ waveforms influenced by 148 mtorr of SF₆ at a mix pressure of 23 mtorr.

transfer to level $v'=1,0$. After this point the vibrational population has thermalized and the decay driven by radiative and electronic quenching effects. A Stern-Volmer analysis of this decay in $v'=2$ provided an upper limit for the electronic quenching rate coefficient. The experimental data in Figure 26 is overlaid by a calculated waveform generated using the Montroll-Shuler model of vibrational energy transfer (Montroll, 1957), which is discussed in detail in section 4.4. The calculation took into account the vibrational transfer from all $\text{BrF}(\text{B}) v'$ levels after initial excitation of $v'=5$ and is weighted by the effective spectral response (Appendix C). As can be seen in Figure 26, the curves are quite similar when a fundamental vibrational transfer rate coefficient of $k(1,0) = 1.8 \times 10^{-11} \text{ cm}^3/(\text{molecule} \cdot \text{s})$ is used. The excellent fit after the peak is due mostly to radiative lifetime. The short time divergence between the two waveforms is due to either 1. inaccuracies in the calculated spectral response, or 2. the effects of multi-quantum transfer. The Montroll-Shuler model only considers vibrational transfer between adjacent levels. Although the interpretation of vibrational transfer in this total fluorescence data is quite convoluted, the fundamental vibrational transfer rate coefficient induced by SF_6 is certainly on the order of $10^{-11} \text{ cm}^3/(\text{molecule} \cdot \text{s})$.

4.3.3.4 Oxygen Quenching. The Stern-Volmer plots for the quenching of $\text{BrF}(\text{B})$ by O_2 are nonlinear. At low pressure they show a linear rise characteristic of a large quenching rate coefficient, $(2.4 \pm 1.3) \times 10^{-11} \text{ cm}^3/(\text{molecule} \cdot \text{s})$. Then in $v'=2$, at an added O_2 pressure of ≈ 20 mtorr the data shows a dramatic bend, becoming linear at a lower

quenching rate coefficient $(5.37 \pm .46) \times 10^{-12} \text{ cm}^3/(\text{molecule} \cdot \text{s})$ for the high O_2 pressure data ($\leq 150 \text{ mtorr}$). In $v'=6$ there is some curvature even at low pressures followed by a major bend at approximately 20 mtorr as in $v'=2$. It is at this same pressure that a short time decay feature appears in the $v'=2$ fluorescence decay waveforms. This feature appears on a short time scale ($< 20 \mu\text{s}$), showing only slight narrowing with added buffer gas. The exponential fits that were used in the Stern-Volmer analysis, were drawn from the long time decay that is always present.

Two explanations for these unusual results will be explored:

1. Vibrational transfer and spectral response.
2. Vibrationally dependent quenching rates.

In Clyne's study of electronic quenching of BrF(B) by O_2 , waveforms similar in behavior to those in the current study were observed (Clyne, 1980). The initial rapid decay was attributed to vibrational transfer from the initially pumped state, while the slower decay was attributed to electronic quenching of a thermalized distribution. The waveform was believed to be the result of poor detector spectral response to the emissions from the lowest vibrational levels. This explanation is not supported in the current work where the detection system was most efficient in detecting emission from the lowest levels as was seen in the SF_6 study. Clyne's Stern-Volmer plot from the long time data does not show curvature; however, the lowest pressure on that plot was 100 mtorr, which is in the linear region of the current data. The resulting rate coefficient $k_{\text{O}_2}^{\text{EQ}}(\text{thermal}) = (2.6 \pm 0.6) \times 10^{-12} \text{ cm}^3/(\text{molecule} \cdot \text{s})$ is on the same

order as the rate coefficient derived in the current work for high pressure $5 \times 10^{-12} \text{ cm}^3/(\text{molecule} \cdot \text{s})$. It is possible if the current study had examined oxygen quenching at even higher pressures the final asymptotic rate coefficient would match Clyne's value.

If the electronic quenching rate for the lower v' levels was much lower than for the initially populated level, then two decay regions would be evident on the fluorescence decay waveforms. This could be caused by resonant electronic energy exchange from $\text{BrF}(B \rightarrow A, X v'')$ to $\text{O}_2(X \rightarrow a)$. This was postulated in oxygen quenching of $\text{IF}(B)$ (Wolf, 1985). The highest vibrational levels in $\text{IF}(B)$ have sufficient energy to excite $\text{O}_2(a)$, but the lowest ones do not. Thus immediately after excitation there is rapid decay through electronic energy exchange, then as the population transfers to lower vibrational levels a slower electronic quenching is observed.

This explanation does not fully account for the observed behavior in $\text{BrF}(B)$. The fluorescence decay waveforms and Stern-Volmer plots from $v'=2$ and $v'=6$ are quite similar. At such different pump levels, vibrationally dependent quenching should be apparent in the data and was not. In the $\text{IF}(B)$ work, fits to the long time decay data did not produce a curved Stern-Volmer plot. This could result from fitting to different decay regions in the fluorescence data.

At this time, the best, if inadequate, explanation for the J_2 quenching results is a combination of the effects of vibrationally dependent quenching and data fits to separate decay regions. Exact measurements of the energy of the $\text{BrF}(A)$ state are needed to discover if resonant electronic energy transfer from $\text{BrF}(B \rightarrow X)$ to $\text{O}_2(X \rightarrow a)$ is a viable

explanation. Future studies of O_2 induced vibrational transfer may offer valuable clues for a more definitive explanation of the quenching behavior. If quenching rates are dependent on vibrational level, vibrational transfer in the B-state will strongly influence the fluorescence decay waveforms.

4.3.3.5 Energy Channels. An electronically excited BrF(B) molecule can be deactivated to either the BrF(A) or BrF(X) states. The BrF(B) $v'=0-6$ levels are imbedded in the potential energy curve of the BrF(X) ground state. Thus deactivation to the ground state can occur at a wide range of transferred energy. Three channels exist for this energy transfer. Usually, the most efficient is resonant electronic energy exchange. This mechanism, discussed earlier for Br_2 , is an E-E process where the collision partner is excited electronically. Only in two of the examined collision partners, bromine and oxygen, is the electronic energy in the BrF(B) state sufficient to populate the first electronically excited state. This mechanism may be a factor in the large bromine quenching rate coefficient and the anomalous O_2 Stern-Volmer results. The quenching of interhalogens by halogens is usually rapid as evidenced by the $3.9 \times 10^{-10} \text{ cm}^3/(\text{molecule}\cdot\text{s})$ rate constant for I_2 quenching of IF(B) (Wolf, 1985).

E-V transfer is usually not as efficient. The electronic energy is transferred into the vibrational modes of the partner. In BrF(B-X) transitions to high v'' levels the energy gap can be small minimizing the required energy transfer. This process can be involved with any multi-atomic collision partner.

In contrast, in argon, an atomic species, E-T transfer is the only possibility. As expected, this rate is extremely slow, the lowest of those measured.

4.4 Vibrational Transfer

The rate of vibrational transfer in the excited state manifold is a determining factor in the analysis of efficiency and feasibility in a potential chemical laser. A chemical excitation mechanism will populate a range of vibrational levels. These must be thermalized by collisions with either laser medium gases or buffer gases added for this purpose. The work described in this section verified that vibrational transfer in BrF, induced by the mix, is predicted by a particular theoretical description, the Montroll-Shuler model (Montroll, 1957). This was used to predict the vibrational relaxation of BrF in laser conditions.

4.4.1 Background Theory. Vibrational energy transfer is a collisional process that imparts vibrational energy of the excited state molecule to the vibrational or translational energy of a buffer gas molecule. It is studied experimentally by employing spectrally and temporally resolved LIF to observe the population evolution of the vibrational levels. After an initial vibrational level is excited, the emission from another vibrational level is isolated and observed with a monochromator. The time evolution of the emission intensity from the observed level is characteristic of its population and can be used to determine vibrational energy transfer rates.

The following coupled set of first order differential equations describes both electronic quenching and vibrational energy transfer:

$$\begin{aligned} \frac{dN(v')}{dt} = & -\Gamma(v') N(v') - \sum_{\tilde{v}'} k^{v-T}(v', v'+\Delta v') N(v') M \\ & + \sum_{\Delta v'} k^{v-T}(v'+\Delta v', v') N(v'+\Delta v') M - \sum_{\tilde{v}'} k^{v-v}(v', v'+\Delta v') N(v') M(\tilde{v}) \\ & + \sum_{\Delta v'} k^{v-v}(v'+\Delta v', v') N(v'+\Delta v') M(\tilde{v}+\Delta \tilde{v}) \end{aligned} \quad (4.7)$$

where: k^{v-T} = The rate coefficient for the transfer of vibrational energy to the translational energy of the collision partner.

k^{v-v} = The rate coefficient for the transfer of vibrational energy to the vibrational energy of a multi-atomic collision partner.

$\Gamma(v')$ = A total first order decay coefficient accounting for both radiative and electronic quenching depopulation of the v' vibrational level.

$N(v')$ = The population of the v' vibrational level.

M = The concentration of the collision partner.

\tilde{v} = The vibrational level of the buffer gas molecule,

The inverse problem, obtaining rate coefficients from experimental data, is difficult to solve analytically. This problem can be solved numerically in the following manner. A set of coefficients are assumed and the rate equations are integrated. The rates are then systematically varied until a fit to the population data is obtained. Computer codes are

available. However, this process is complex, time intensive, and expensive in computer time. Clearly, some simplifications are desirable.

4.4.1.1 Montroll-Shuler Model. One approach that leads to an analytic solution of the vibrational transfer problem is the Montroll-Shuler model (Montroll, 1957). This approach describes vibrational transfer by modeling a system of harmonic oscillators immersed in an inert heat bath. A number of assumptions are made to allow solution. Excited state populations are considered small so that only interactions between heat bath molecules and the excited oscillators are treated. Thus, the energy transfer processes become first order with respect to electronically excited vibrational populations. When applied to an actual molecular system, radiative lifetimes and electronic quenching rates are assumed to be independent of the vibrational level. Finally, vibrational transfer is limited to $\Delta v = \pm 1$.

The Montroll-Shuler model relates the different vibrational transfer rate coefficients in accordance with the Landau-Teller theory for V-T transfer probabilities (Landau, 1936):

$$k^v(v', v'-1) = v' k^v(1, 0) \quad (4.8)$$

Where $k^v(1, 0)$ is a fundamental vibrational transfer rate coefficient describing vibrational transfer from $v'=1$ to $v'=0$. In general V-V transfer is not described by Landau-Teller scaling. At the same time, the principle of detailed balance yields (Levine, 1987:177-179):

$$k^v(v'-1, v') = k^v(v', v'-1) \exp(-h\nu/kT) \quad (4.9)$$

Where ν and k are, respectively, the fundamental oscillator frequency and Boltzmann's constant.

These two equations, taken together, relate all of the vibrational transfer rates to a single fundamental rate coefficient $k^v(1,0)$. The radiative and electronic quenching effects are included by making a change in variables, transforming the initial population $x_n(t)$ of vibrational level n :

$$z_n(t) = x_n(t) \exp(t/\tau) \quad (4.10)$$

where

$$1/\tau = 1/\tau_r + k^{EQ} M \quad (4.11)$$

This transformation, along with the assumptions made earlier reduce the overall rate equation to the form:

$$\frac{dz_n}{dt} = k^v(1,0) \left[n e^{-\theta} z_{n-1} - \left[n + (n+1) e^{-\theta} \right] z_n + (n+1) z_{n+1} \right] \quad (4.12)$$

Where $\theta = h\nu/kT$.

For an instantaneous δ -function excitation of a single vibrational state m , the Montroll-Shuler solution of equation (4.12) for the population of a state n is:

$$z_n(t) = \left[\frac{(1-e^{-\theta}) e^{m\theta}}{(e^{-t'} - e^{-\theta})} \right] \left(\frac{e^{-t'} - 1}{e^{-t'} - e^{-\theta}} \right)^{m+n} F(-n, -m, 1; U^2) \quad (4.13)$$

where:

$$t' = k^v(1,0) t (1-e^{-\theta}) M$$

$$U = \sinh(\theta/2)/\sinh(t'/2)$$

F = hypergeometric function

The great advantage of this technique is that it reduces the required kinetic data to one experiment: observing the population evolution, at a range of pressures, of a vibrational level after populating a single initial state. In other words, the determination of one rate coefficient provides $k^v(1,0)$ and thus all the others.

When this study was initiated, it seemed that the characteristics of BrF would make it well suited for a Montroll-Shuler analysis. The model

is based on harmonic oscillators; therefore any anharmonicity in the behavior of the real molecule would cause its behavior to deviate from the model. For BrF(B), the anharmonicity is quite low ($\omega_{ex}/\omega_e=.009$), nearly as low as that of IF ($\omega_{ex}/\omega_e=.007$) which is well described by the Montroll-Shuler model (Wolf, 1987). The model assumes $\Delta v=\pm 1$, thus multi-quantum effects are not considered. This assumption appears valid since the vibrational level spacing for BrF(B) is relatively large ($h\nu/kT=1.7$) at 300°K, again close to IF ($h\nu/kT=2$). The model assumes that electronic quenching and radiative lifetimes are independent of vibrational level. This is the case for BrF(B) radiative lifetimes for $v'<6$. At this level predissociation begins to shorten effective lifetimes, but only at rotational levels $J'\geq 49$ (Clyne, 1980). In the work discussed in section 4.3, electronic quenching rate coefficients for BrF(B) show little dependence on vibrational level.

In view of these factors, the initiation of this research the Montroll-Shuler model seemed to be an appropriate analytic tool for vibrational transfer.

4.4.2 Vibrational Transfer Experimental Results. This section discusses the results of an experimental study of vibrational transfer in the BrF(B) vibrational manifold. The goal of this study was to determine if BrF(B) vibrational transfer induced by the BrF production mix did indeed follow the Montroll-Shuler theoretical prediction.

4.4.2.1 Experimental Procedures. In this study, a single initial excitation level, $v'=5$ was populated. A vibrational transfer spectrum was recorded by tuning the monochromator across a 5200-7200 \AA range, for a fixed excitation wavelength (Figure 27). This was used to identify which $v'-v''$ transition, for each v' level, would be observed in LIF vibrational transfer studies. Transitions were observed from all v' levels ($6 \rightarrow 0$). Signal to noise limitations required a monochromator resolution of 22.4 \AA . At this width no observed vibrational band was completely free of overlap from competing bands. The overlap fractions were computed for each observation wavelength used. The selected bands and overlap fractions are given in Table IV. The procedure used to calculate these fractions is discussed in Appendix D.

The spectrum shown in Figure 27 shows that considerable vibrational transfer has occurred at a total pressure of 701 mtorr as evidenced by emission bands originating from $v'=0$. Even at lower pressures (100 mtorr), emissions from vibrational levels other than the originally populated level were still evident.

Ten fluorescence waveforms were recorded at a wide range of BrF production mix pressures for each observation band. Each recorded waveform represented at least a 1000 laser shot summed average. Before data collection, an averaged waveform with no mix was recorded. This was stored in the oscilloscope and used as an on-line baseline subtraction as each data waveform was recorded. On the lowest pressure data 4000 shot averages were required. A summed signal to noise ratio of four was the minimum in any recorded waveform.

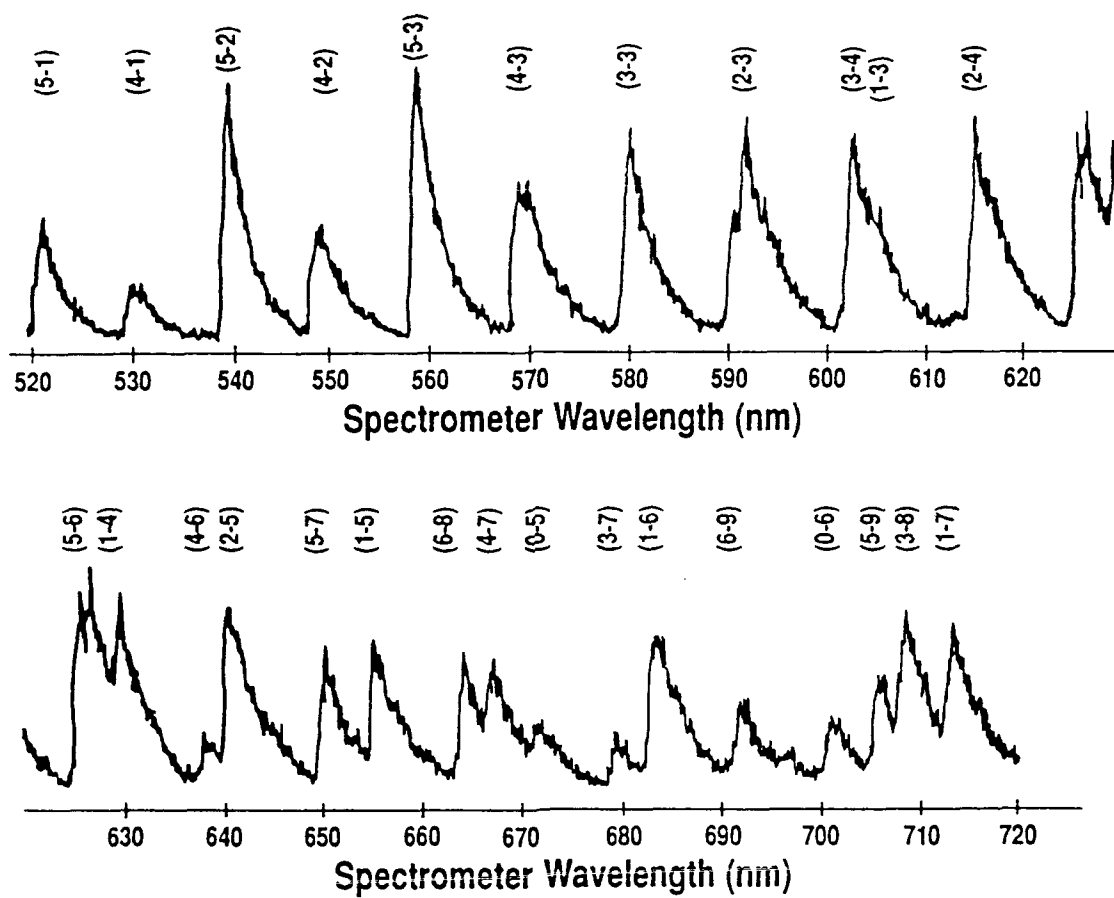


Figure 27. Vibrational Transfer Spectrum observed through 250 μm diameter slits after populating $v'=5$ at a mix pressure of 701 mtorr.

Table IV.
Computed Spectral Overlap Fractions

Observation	Percentage of Overlap								
Band	$v' =$	0	1	2	3	4	5	6	7
(6-9)		.00	.39	.00	.00	.21	.00	.39	.00
(5-2)		.00	.00	.00	.14	.04	.82	.00	.00
(4-3)		.00	.00	.16	.00	.84	.00	.00	.00
(3-3)		.00	.10	.00	.80	.00	.09	.00	.00
(2-2)		.00	.00	.74	.00	.01	.00	.25	.00
(1-6)		.00	.88	.00	.12	.00	.00	.00	.00
(0-6)		.87	.00	.00	.00	.07	.00	.06	.00

A computational version of the Montroll-Shuler theoretical model was developed for use on the Zenith model 248 microcomputer (see Appendix B). This model was used to make a least squares fit to the spectrally resolved waveforms. The parameter of this fit was $k^v(1,0)$, the fundamental vibrational transfer rate coefficient. This parameter was converted to a lifetime by:

$$1/\tau_v = k^v(1,0)M \quad (4.14)$$

Where M in this set of experiments is the number density of the BrF mix. These inverse lifetimes were plotted as a function of the mix number density in a Stern-Volmer plot. The data should be linear, where the slope is the average $k^v(1,0)$ for the range of observed pressures.

4.4.2.2 Montroll-Shuler Data Fits. A computational version of the Montroll-Shuler model, MNTFIT (Appendix B), was used to fit the observed fluorescence waveforms. This model could consider overlapping emissions from up to three vibrational levels. Figures 28-34 show the typical quality of the fit to waveforms from each vibrational level. In general the fits are excellent. In Figure 29, showing emission from $v'=5$ the pump level, the initial decay is slightly more rapid than that predicted. This can be attributed to any process that would deplete the pump level not considered in the Montroll-Shuler model. Examples include multi-quantum transfer and V-V transfer. In two cases, $v'=3$ (Figure 31) and $v'=0$ (Figure 34), the experimental waveforms show the greatest divergence from the Montroll-Shuler prediction. The model does not account for the initial rise in the data in Figure 31. This rise can not be due to multi-quantum vibrational transfer. In levels $v'=2$ and $v'=1$ where the effect should be larger since more collisions are required to populate these levels, the fits are almost perfect. The most likely explanation for the initial rise in Figure 31 is overlap with the distant 4-3 band not predicted by the overlap calculation. High J' levels from this band fall within the monochromator resolution. The population in $v'=4$ is higher than that in $v'=3$ so that even a slight contribution from this level would be significant. In the $v'=0$ data shown in Figure 34, the prediction based on the calculated overlap fraction reproduced the primary features but but with some error in the relative heights. The calculated

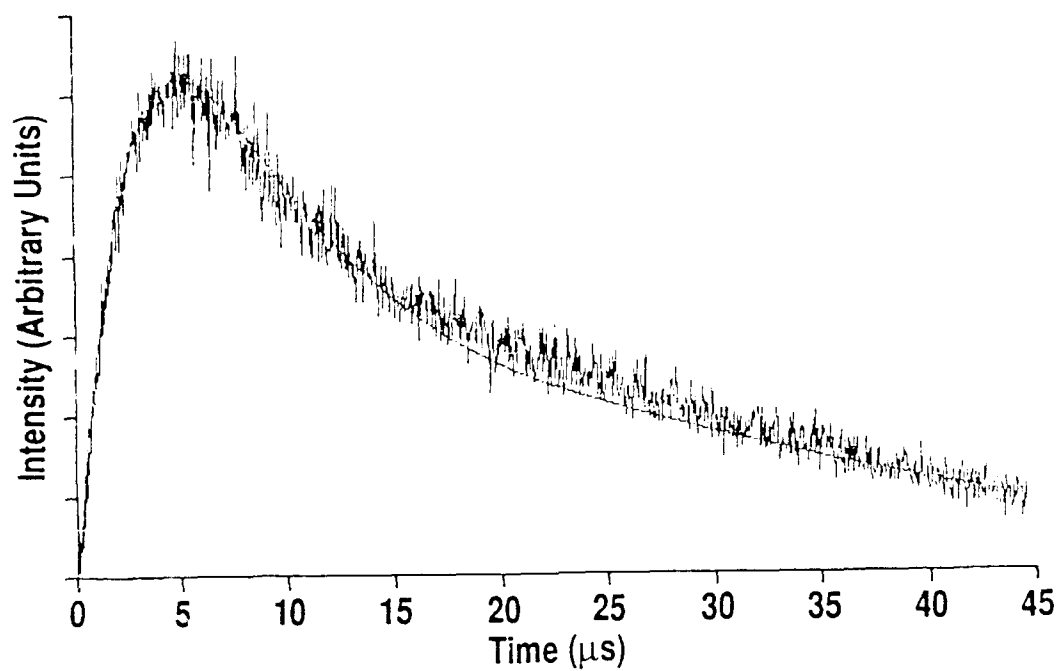


Figure 28. Montroll-Shuler fit to the (6-9) band fluorescence waveform observed at a mix pressure of 357 mtorr.

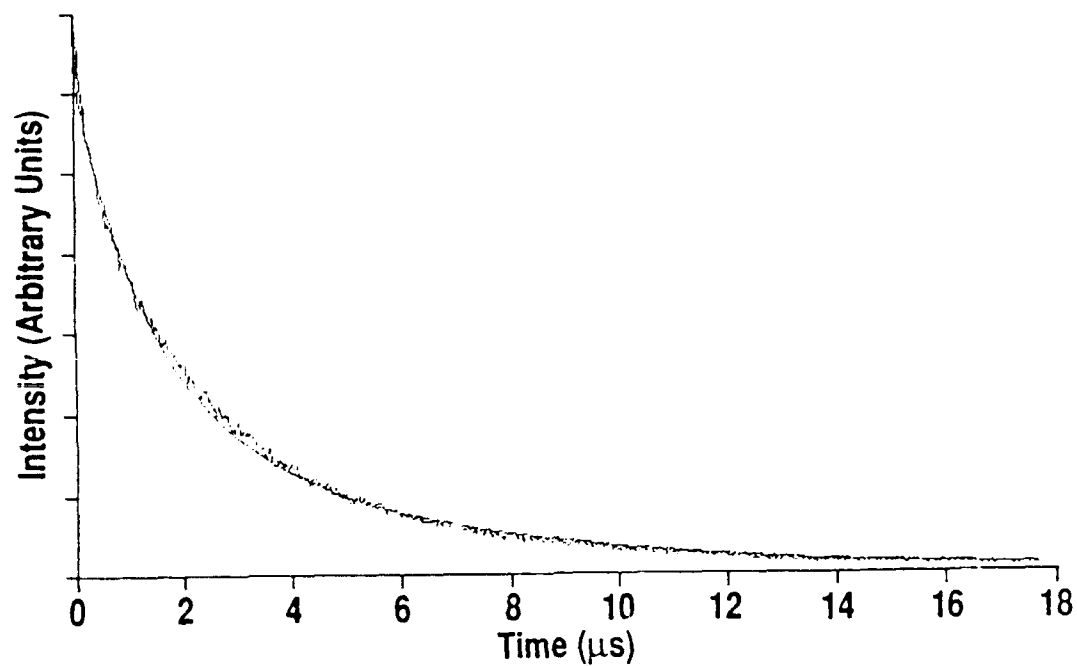


Figure 29. Montroll-Shuler fit to the (5-2) band fluorescence waveform observed at a mix pressure of 531 mtorr.

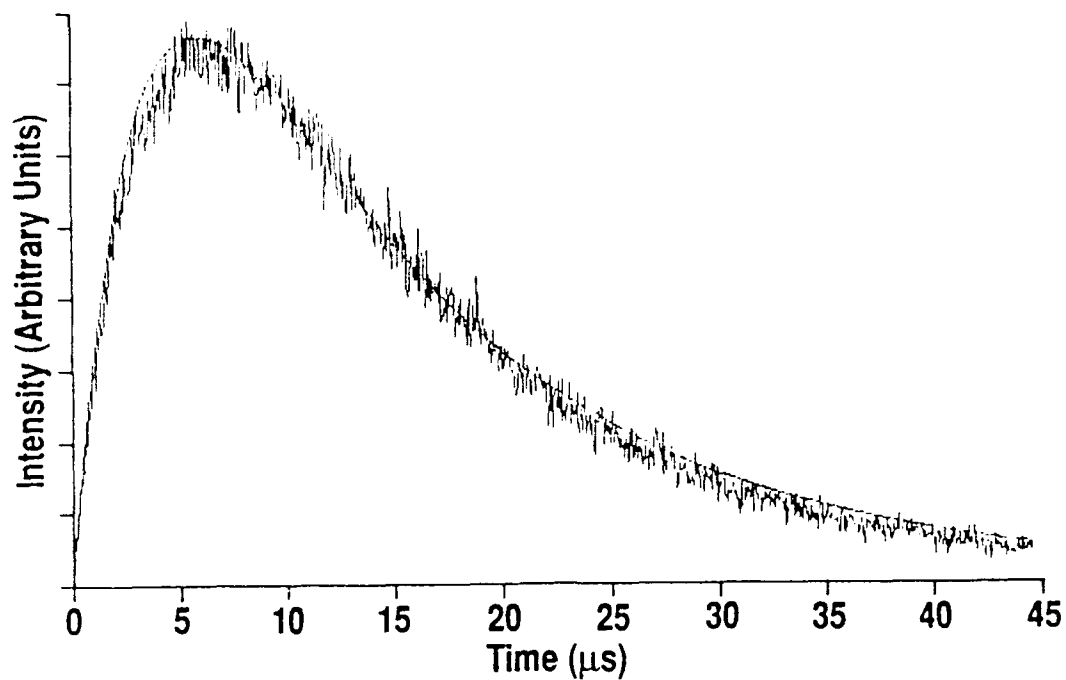


Figure 30. Montroll-Shuler fit to the (4-3) band fluorescence waveform observed at a mix pressure of 237 mtorr.

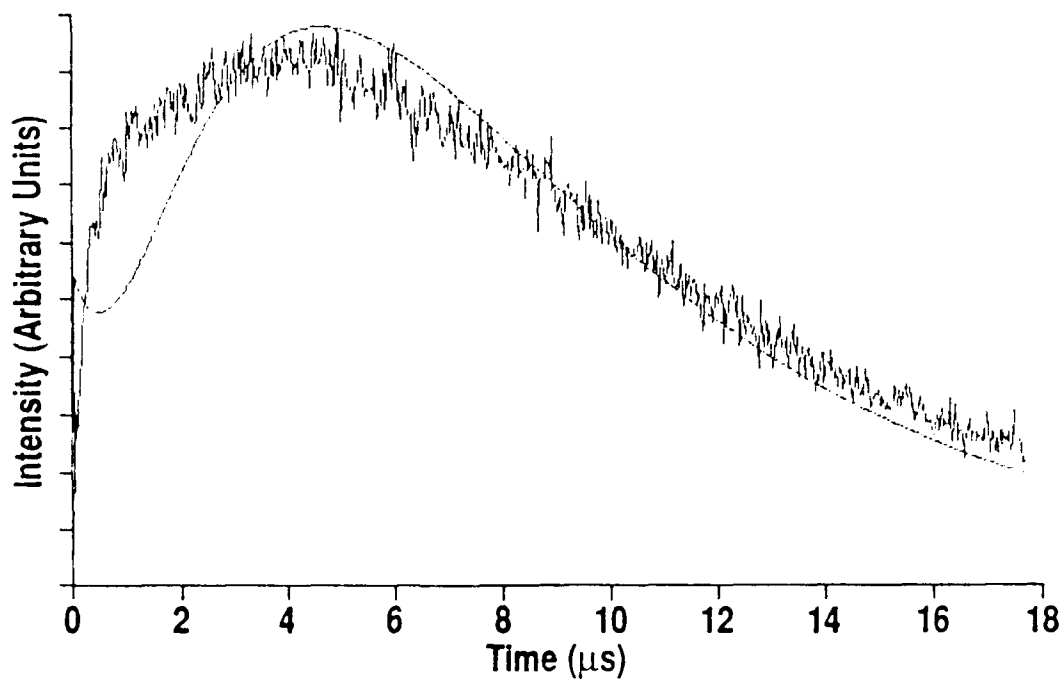


Figure 31. Montroll-Shuler fit to the (3-3) band fluorescence waveform observed at a mix pressure of 599 mtorr.

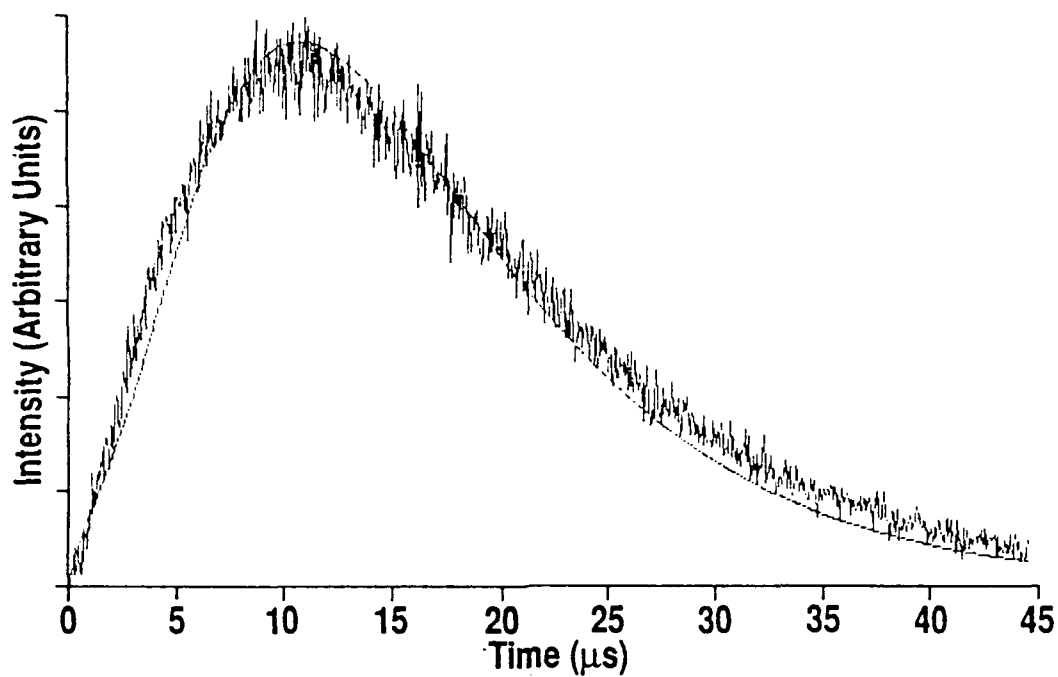


Figure 32. Montroll-Shuler fit to the (2-2) band fluorescence waveform observed at a mix pressure of 462 mtorr.

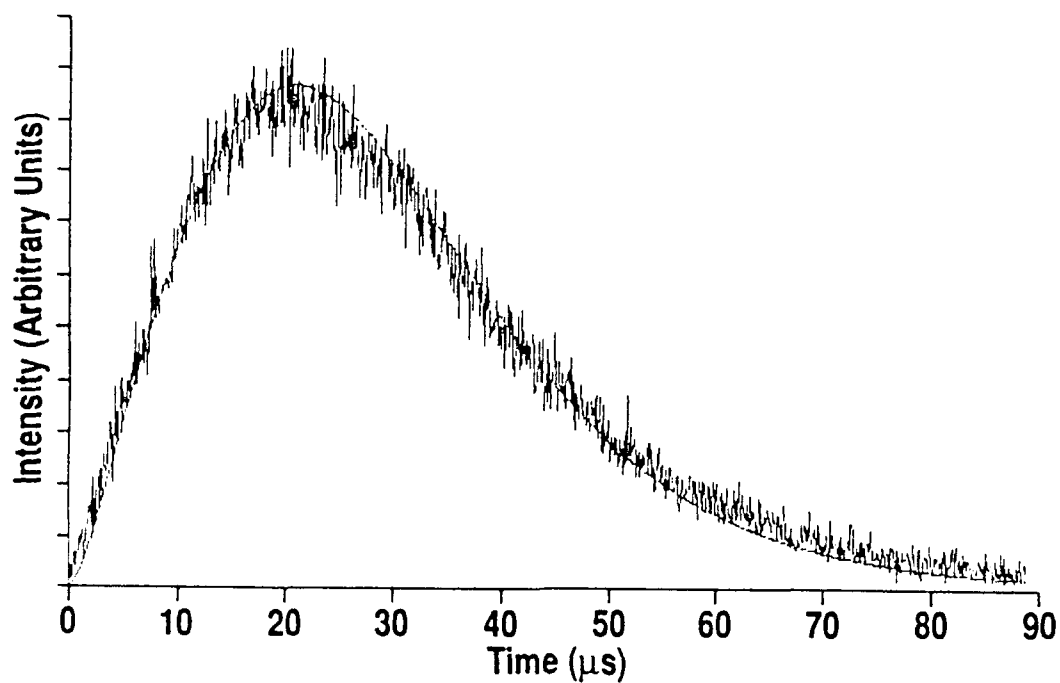


Figure 33. Montroll-Shuler fit to the (1-6) band fluorescence waveform observed at a mix pressure of 403 mtorr.

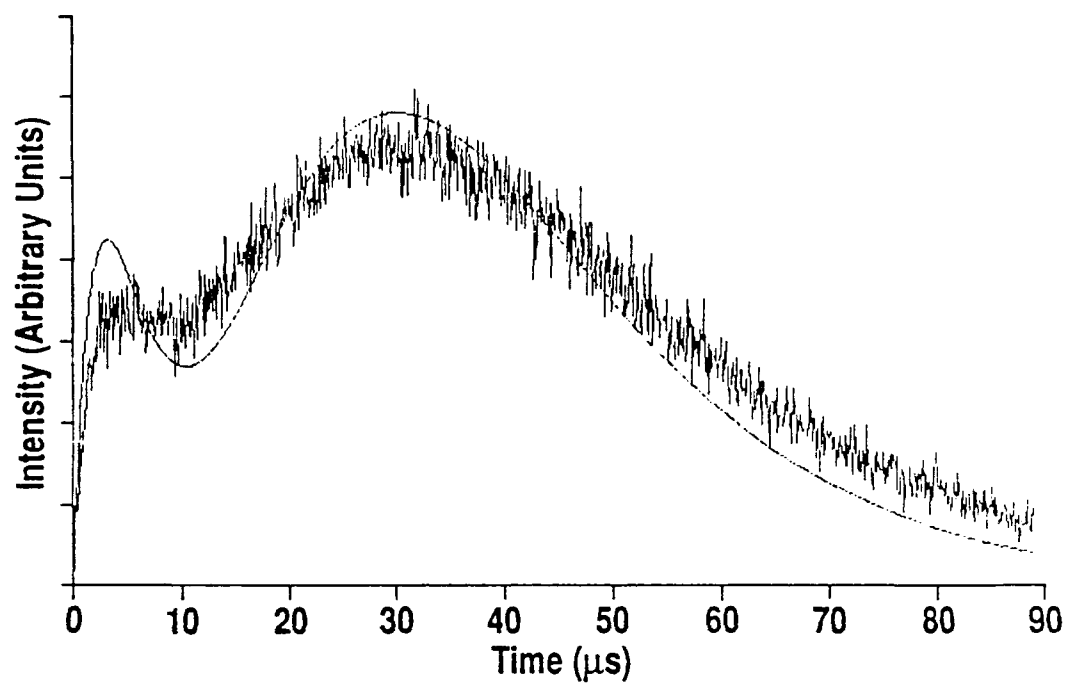


Figure 34. Montroll-Shuler fit to the (0-6) band fluorescence waveform observed at a mix pressure of 557 mtorr.

overlap from $v'=4$ is from a low Franck-Condon factor transition. The population in $v'=4$ is much greater than that in $v'=0$ so that any error in the $(v',v'')=(4,8)$ Franck-Condon factor and thus in the overlap fraction would be enhanced.

It must be emphasized that a single procedure was used to calculate the overlap fractions. The fits are the result of varying only $k(1,0)$ and a scale factor.

4.4.2.3 Stern-Volmer Analysis. Each band was examined at a range of pressures. The $k^v(1,0)$ values from the Montroll-Shuler fits were converted to $1/\tau_v$ values (eqn. 4.14) and plotted versus mix density in a Stern-Volmer analysis. The linearity in these plots is excellent as seen in Figure 35. Ideally the intercepts of these plots should be zero. In practice, factors such as overlap fraction errors and differences in radiative lifetime can cause a positive intercept.

The slopes of the Stern-Volmer plots provided the average $k^v(1,0)$ rate coefficients seen in Table V. The error quoted is the standard deviation of these slopes.

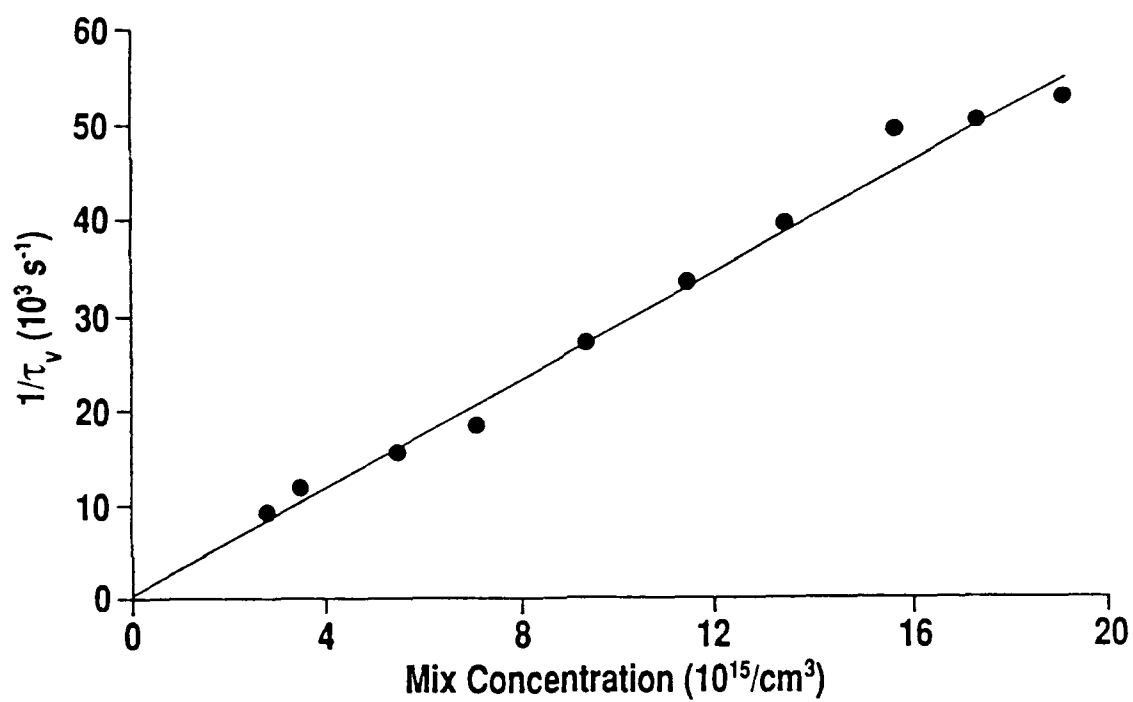


Figure 35. Stern-Volmer plot of the Montroll-Shuler fits to the (6-9) band emission.

Table V.
Fundamental vibrational transfer rate coefficients in BrF(B)
induced by the mix ($10^{-12} \text{ cm}^3/(\text{molecule}\cdot\text{s})$).

v'	$k^v(1,0)$	$k^v(v',v'-1)$
6	$2.80 \pm .10$	$16.8 \pm .6$
5	$4.50 \pm .20$	22.5 ± 1.0
4	$3.54 \pm .03$	$14.2 \pm .1$
3	$4.00 \pm .10$	$12.0 \pm .3$
2	$3.77 \pm .06$	$7.54 \pm .12$
1	$2.55 \pm .06$	$2.55 \pm .06$
0	$3.70 \pm .10$	

4.4.3 Discussion of Vibrational Transfer Results. The experiments discussed in the last section show that the Montroll-Shuler model is an adequate description of vibrational transfer in the BrF B-state manifold. Table V shows a summary of the fundamental vibrational transfer rate coefficients, induced by the BrF production mix, for each vibrational level. There is only a small scatter in these coefficients and no trend with vibrational level. Thus, one final rate coefficient $k^v(1,0) = (3.5 \pm .6) \times 10^{-12} \text{ cm}^3/(\text{molecule}\cdot\text{s})$, describes the vibrational transfer for all levels at any mix pressure. This number is the average of those found in all vibrational levels. The quoted error is the standard deviation in

this average. The table also shows the $k(v',v'-1)$ rate coefficients corresponding to the fundamental rate coefficients. These are plotted versus v' in Figure 36. There is no apparent curvature in this plot showing that Landau-Teller scaling, $k(v',v'-1) = v'^V k^V(1,0)$, is valid. The Montroll-Shuler model does not consider V-V transfer. Although the bulk of the production mix was CF_4 , the excellence of the fits indicates that V-V transfer to CF_4 is not significant. This is reasonable since the lowest energy vibrational mode in CF_4 is 437 cm^{-1} (Herzberg, 1945:167), considerably larger than that of $BrF(B)$ ($\omega_e=372\text{ cm}^{-1}$) (Clyne, 1972).

It is interesting to contrast these results to the only other examination of vibrational transfer in $BrF(B)$ (Clyne, 1980). Clyne measured total vibrational transfer removal rates in $BrF(B)$ induced by oxygen. His measurements were observations of fluorescence decay from initially populated levels through colored glass filters. The signal was too low to allow the use of a monochromator. No observations of the other v' levels were made. His measured vibrational transfer rate coefficients, as seen in Table VI, do not follow Landau-Teller scaling. Thus the Montroll-Shuler model would not be valid for oxygen induced transfer. $BrF(B)$ vibrational transfer with oxygen is being examined in work currently underway at AFIT.

The reduction of the vibrational transfer problem to one final rate coefficient greatly simplifies examinations of BrF as a potential lasing species. Chemical excitation mechanisms populate a number of B-state vibrational levels. Rapid vibrational thermalization is required for efficient lasing. Figures 37 and 38 show the speed and efficiency of

Table VI.

BrF(B) total vibrational transfer rate coefficients with
oxygen ($10^{-11} \text{ cm}^3/(\text{molecule}\cdot\text{s})$) (Clyne, 1980).

v'	$k^v(\text{tot})$
3	3.6
4	2.2
5	2.1
6	3.4
7	12.5

vibrational thermalization in BrF at a mix pressure of 5 torr, predicted using the rate coefficients obtained in this research. This was a reasonable operating pressure for a gas laser. In Figure 37, $v'=5$ is the initially populated level. The $v'=0$ population peaks $3.16 \mu\text{s}$ after the excitation but at a population only 5 % that of the initial $v'=5$ level. This would represent a loss of 95% of the pump energy in a laser. As seen in Figure 38, this situation is only slightly improved when $v'=3$ is the initially pumped level. Here the $v'=0$ population peaks $2.4 \mu\text{s}$ after the excitation at a population 8.3% that of the initial $v'=3$ level. Clearly the vibrational transfer induced by the production mix is not satisfactory for laser applications. Electronic quenching depletes the excited state population faster than multiple collisions can populate $v'=0$. The

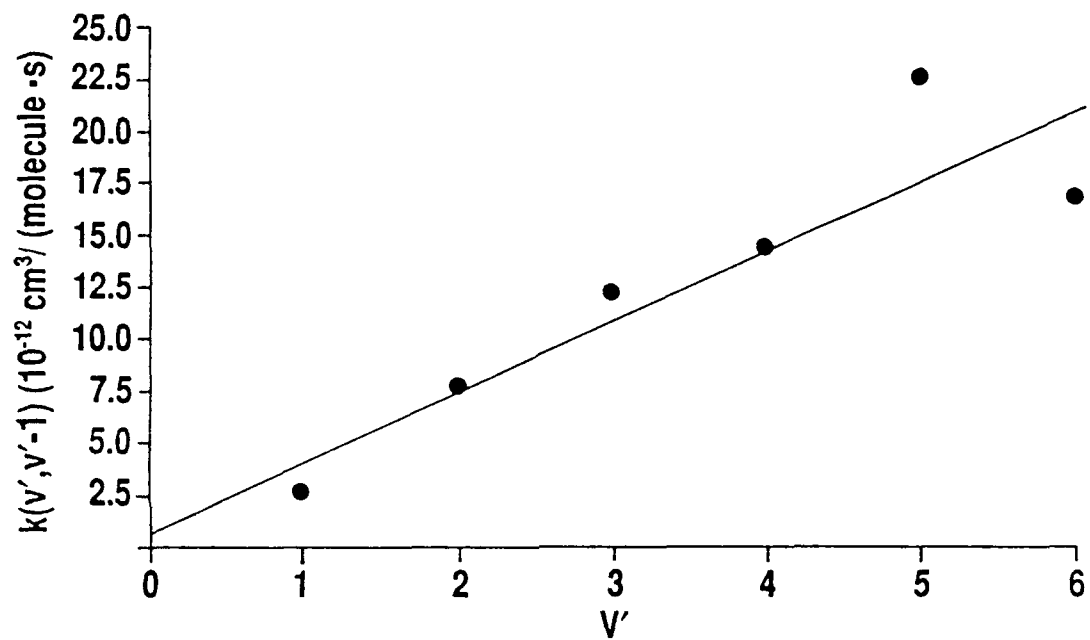


Figure 36. Demonstration of Landau-Teller scaling of vibrational transfer rate constants.

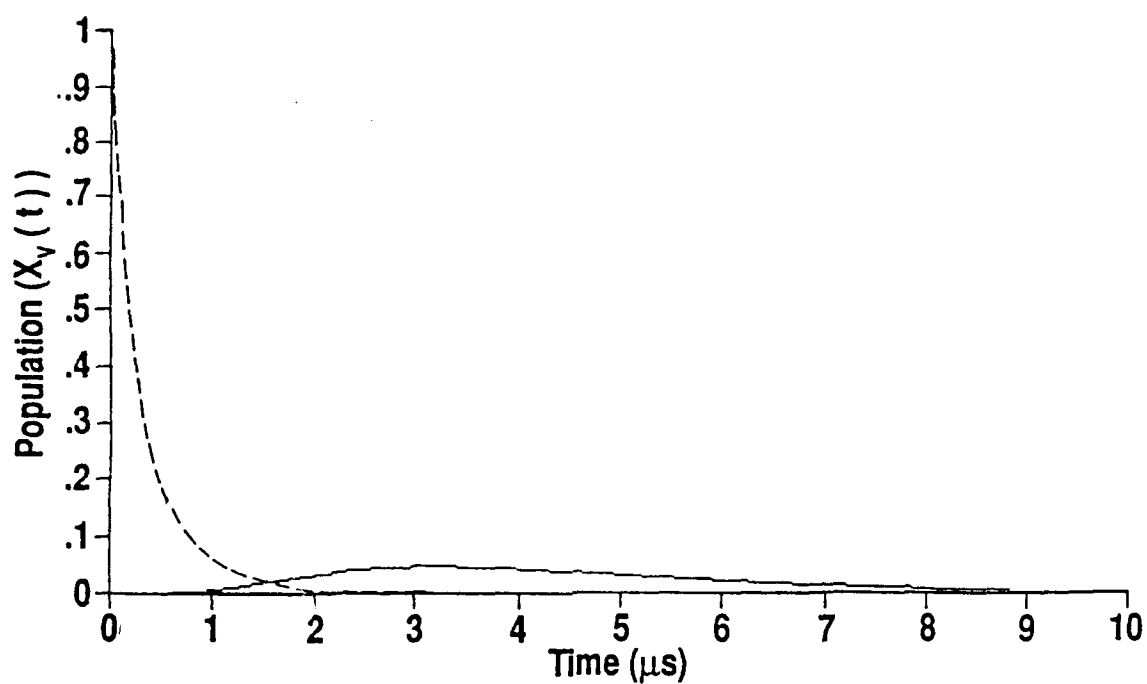


Figure 37. Vibrational thermalization of BrF(B) after initial excitation of $v'=5$. $x_5(t)=(---)$, $x_0(t)=(—)$.

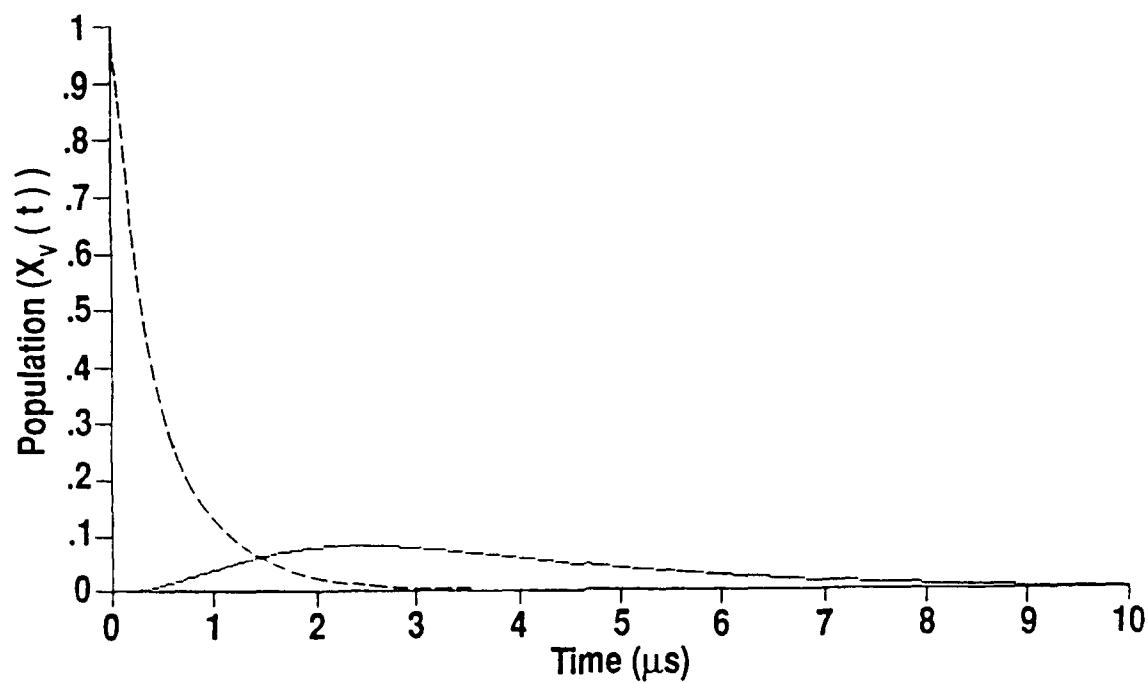


Figure 38. Vibrational Thermalization of BrF(B) after initial excitation of $v'=3$. $x_3(t)=(---)$, $x_0(t)=(—)$.

thermalization is limited since the electronic quenching rate is on the order of the V-T transfer rate.

One way of correcting this problem is the addition of a bath gas to enhance vibrational transfer. One example, based on this research is SF_6 . This gas has a high fundamental vibrational transfer rate coefficient $k^v(1,0) \approx 1.8 \times 10^{-11} \text{ cm}^3/(\text{molecule} \cdot \text{s})$, and an extremely low electronic quenching rate coefficient $k_{\text{SF}_6}^{\text{EQ}} < 8 \times 10^{-14} \text{ cm}^3/(\text{molecule} \cdot \text{s})$. Therefore large amounts of SF_6 could be added to the laser medium to enhance thermalization, without increasing electronic quenching.

4.5 Conclusions

Two fundamental energy transfer processes, electronic quenching and vibrational transfer were examined in this chapter.

4.5.1 Electronic Quenching. Spectrally unresolved laser induced fluorescence was used to study the electronic quenching of BrF(B) for three vibrational levels and a number of collision partners (Br_2 , CO_2 , O_2 , N_2 , CF_4 , SF_6 , Ar). The measured rate coefficients range over three orders of magnitude from $< 6 \times 10^{-14} \text{ cm}^3/(\text{molecule} \cdot \text{s})$ for argon to $(6.86 \pm 0.18) \times 10^{-11} \text{ cm}^3/(\text{molecule} \cdot \text{s})$ for Br_2 . Initial rapid decays were observed for $v'=5$ and $v'=6$ in bromine quenching were attributed to ro-vibrational transfers to predissociated energy levels. The high measured quenching rate coefficients for Br_2 and CO_2 are most likely cases where electronic excitation energy is transferred to vibrational energy in the collision partner. Total fluorescence waveforms with SF_6 as the collision partner show strong peaks, due to a non-linear detector response

to different v' emissions. This behavior was used to estimate a vibrational transfer rate coefficient for SF_6 of $k^v(1,0) \approx 1.8 \times 10^{-11} \text{ cm}^3/(\text{molecule} \cdot \text{s})$. Curvature was observed in the O_2 Stern-Volmer analysis plots, and a description of the mechanism awaits spectrally resolved data.

The most critical factor, in terms of a BrF laser, is the high electronic quenching rate of bromine. Efficient laser operation will require that molecular bromine levels after BrF production be as low as possible. Therefore BrF production should always take place with a surplus of atomic fluorine.

4.5.2 Vibrational Transfer. The Montroll-Shuler model was found to be an adequate description of the BrF(B) vibrational energy transfer induced by the BrF production mix. This greatly reduces data collection and analysis difficulties. A single fundamental rate coefficient $k^v(1,0) = (3.5 \pm 0.6) \times 10^{-12} \text{ cm}^3/(\text{molecules} \cdot \text{s})$ predicts vibrational transfer rates for all levels, at any mix pressure.

Analysis showed that vibrational thermalization due to the mix is inefficient in typical laser operating pressures (5 torr). At this pressure the majority of the initial excitation energy is lost through electronic quenching. This does not eliminate BrF as a chemical laser candidate. A bath gas can be used to enhance vibrational without significantly increasing electronic quenching. SF_6 , examined in this dissertation, is one possible choice.

V. Conclusions

Two broad areas of BrF kinetics were examined in this dissertation. In chapter III, the production of BrF $B^3\Pi(0^+)$, when molecular bromine and atomic fluorine are added to discharged oxygen, was examined in chemiluminescent flow tube studies. In chapter IV, the kinetics of two collisional energy transfer processes within the BrF $B^3\Pi(0^+)$ state, electronic quenching and vibrational transfer, were studied using pulsed laser induced fluorescence (LIF) techniques.

5.1 Summary of Singlet Oxygen Excitation of BrF(B)

An important consideration in evaluating a potential chemical laser medium is the availability of chemical excitation methods. One popular approach has been energy transfer from energetic metastable species such as the singlet states of oxygen or NF.

When Br_2 is combined with F atoms and discharged oxygen in a flow tube an orange-yellow flame is produced persisting for 15-25 ms in the flow direction. Emission spectra of this flame show features characteristic of BrF(B-X) transitions. BrF(B) is produced in a highly non-thermal distribution peaking at $v'=3$. The emission was linearly dependent on the $O_2(b^1\Sigma)$ concentration. The observed dependence of the BrF(B) emission on molecular bromine and atomic oxygen is inconsistent with a steady state prediction of a sequential excitation mechanism, where BrF(X) is excited by successive collisions with singlet oxygen. The experimental data are consistent with a three body mechanism involving Br

and F atoms. A rate constant of $7 \times 10^{-31} \text{ cm}^6/(\text{molecule}^2 \cdot \text{s})$ for this recombination in the presence of molecular oxygen was determined. The observed concentration ratio of $[\text{BrF(B)}]/[\text{O}_2(\text{b})] = 5 \times 10^{-4}$ indicates that this is a relatively efficient process.

5.2 Summary of Collisional Energy Transfer in BrF(B)

Two BrF(B) state collisional energy transfer processes, electronic quenching and vibrational transfer, were examined in LIF studies. Electronic quenching depopulates the electronic state non-radiatively and is thus a major loss mechanism in a laser system. The electronic quenching of a number of collision partners (Br_2 , CO_2 , O_2 , N_2 , CF_4 , SF_6 , Ar) was examined for three vibrational levels. The measured rate constants ranged in magnitude from $< 6 \times 10^{-14} \text{ cm}^3/(\text{molecule} \cdot \text{s})$ as an upper limit for argon quenching, to $(6.96 \pm 1.8) \times 10^{-11} \text{ cm}^3/(\text{molecule} \cdot \text{s})$ for Br_2 . The high quenching rate constants for Br_2 and CO_2 were attributed to the transfer of electronic excitation energy into the vibrational modes of the collision partner. Initially rapid decays observed in Br_2 quenching of BrF $v'=5$ and $v'=6$ are attributed to ro-vibrational population transfer to predissociated energy levels. The BrF(B-X) total fluorescence wave forms induced by SF_6 show initial peaks at high SF_6 pressures, due to differences in detector response to total emission from the different v' bands. This response was calculated and used to estimate a vibrational transfer rate constant for SF_6 of $k^v(1,0) = 1.8 \times 10^{-11} \text{ cm}^3/(\text{molecule} \cdot \text{s})$.

Any chemical excitation mechanism will populate a range of excited-state population levels. Rapid thermalization of the B-state manifold is required for efficient lasing. Vibrational transfer in

BrF(B), induced by the BrF production mix, the bulk of which is CF₄, obeys a relatively simple theoretical prediction, the Montroll-Shuler model. A single fundamental rate constant $k^v(1,0) = (3.5 \pm 0.6) \times 10^{-12} \text{ cm}^3/(\text{molecule} \cdot \text{s})$ predicts vibrational transfer rates for all levels at any mix pressure through Landau-Teller scaling and the principle of detailed balance. Multi-quantum vibrational transfer was not a significant feature in this study.

5.3 Implications for Chemical Laser Development

It is unfortunate that singlet oxygen excitation of BrF(B) was found to proceed through a three-body recombination mechanism. Typically excitation rates of $10^{19} \text{ molecules}/(\text{cm}^3 \cdot \text{s})$ are required to reach threshold in visible chemical lasers (Perram, 1990). It is unlikely that the slow three-body mechanism can produce such rates in the low pressures found in the supersonic cavities of chemical lasers. Thus, another chemical excitation scheme must be found.

The high quenching rate of molecular bromine on BrF will require that free bromine levels after BrF production be as low as possible. Therefore, BrF production should always take place with a surplus of atomic fluorine.

The vibrational thermalization in BrF was found to be inefficient at typical chemical laser operating pressures (5 torr). At this pressure, the bulk of the initial excitation energy is lost through electronic quenching. This does not eliminate BrF as a chemical laser candidate. A bath gas can be added to enhance vibrational transfer without affecting electronic quenching. Other BrF production mixes may have higher

fundamental vibrational transfer rates and thus thermalize BrF(B) more rapidly.

5.4 Further Studies

An efficient chemical excitation scheme for BrF(B) must be found. Other potential energy carriers such as NF(a), NF(b) and $N_2(A)$ should be examined. One promising candidate is NF(b) with an energy ($18,868\text{ cm}^{-1}$) (Herbelin, 1986) sufficient to excite the BrF(B) state directly. NF(b) is reasonably stable with a lifetime of 23 ms.

Spectroscopic examinations must be performed to determine the energy and characteristics of the BrF(A) state. This intermediate state may be involved in several of the processes examined in this dissertation.

Vibrational transfer studies in BrF(B) are underway for the noble gases and all of collision partners examined in the electronic quenching studies. Studies of oxygen and SF_6 are particularly important given the unusual results observed for these gases in total fluorescence examinations.

Demonstration of lasing through optical excitation should be attempted. This will yield information on gain, saturation and lasing threshold.

Bibliography

- Andrews, L.C. *Special Functions for Engineers and Applied Mathematicians*.
New York: MacMillan Publishing Co. (1985).
- Arnold, S.J. et.al. "Relaxation and Reactivity of Singlet Oxygen,"
Advan Chem Ser. 77: 133 (1968).
- Aviles, R.G. et.al. "Quenching of Laser Excited $O_2(b^1\Sigma_g^+)$ by CO_2 , H_2O and I_2 ," *Applied Physics Letters*. 37: 358 (1980).
- Babcock, H.D. and L. Herzberg. "Fine Structure of the Red System of
Atmospheric Oxygen Bands," *Astrophysical Journal*. 108, 167 (1948).
- Badger, R.M. et.al. "Absolute Intensities of the Discrete and Continuous
Absorption Bands of Oxygen Gas at 1.26 and 1.065 μ and the Radiative
Lifetime of the $^1\Delta_g$ State of Oxygen," *Journal of Chemical Physics*,
43: 4345 (1965).
- Becker, K.H. et.al. "The Quenching of Metastable $O_2(^1\Delta_g)$ and $O_2(^1\Sigma_g^+)$
Molecules," *Chemical Physics Letters*. 8: 259 (1971).
- Bemand, P.P. and M.A. Clyne. "Kinetic Spectroscopy in the Far Ultraviolet.
Part 2 F Atom Resonance Spectroscopy and Measurement of F^{2P} Atom
Concentrations," *Journal of the Chemical Society, Faraday
Transactions II*, 72: 191 (1976).
- Broderson, P.H., and J.E. Sicre. "Das Spektrum des BrF und Seine
Dissoziationsenergie," *Zeitschrift fur Physik*. 141: 515 (1955).
- Byer, R.L. et.al. "An Optically Pumped Molecular Iodine Laser," *Applied
Physics Letters*. 20: 463 (1972).

- Clyne, M.A.A. and H.W. Cruse. "Studies of Ground State $^2P_{3/2}$ Halogen Atoms Using Atomic Resonance Absorption," *Transactions of the Faraday Society*. 67: 2869 (1971).
- Clyne, M.A.A., J.A. Coxon, and C.W. Townsend. "Formation of the $B^3\Pi(o^+)$ States of BrF and IF by ($^1\Delta_g$, $^1\Sigma_g^+$) Oxygen," *Journal of the Chemical Society Faraday Transactions II*. 68: 2134 (1972).
- Clyne, M.A.A., A.H. Curran and J.A. Coxon. "Studies of Labile Molecules with a Tunable Dye Laser- Laser Excitation Spectrum of BrF ($B^3\Pi(o^+) - X^1\Sigma^+$)," *Journal of Molecular Spectroscopy*. 63: 43 (1976).
- Clyne, M.A.A. and I.S. McDermid. "Kinetics of Excited $B^3\Pi(o^+)$ States of BrF, ICl, and IF> Fluorescence Decay Lifetimes and Quenching Cross-Sections," *Journal of the Chemical Society, Faraday Transactions II*. 73: 1094 (1977).
- Clyne, M.A.A. and I.S. McDermid. "Quantum Resolved Dynamics of Excited States- Part 1: Predissociation in the $B^3\Pi(o^+)$ State of BrF," *Journal of the Chemical Society Faraday Transactions II*. 74: 644 (1978a).
- Clyne, M.A.A. and I.S. McDermid. "Quantum Resolved Dynamics of Excited States - Part 2: Stable Levels of the $B^3\Pi(o^+)$ State of BrF," *Journal of the Chemical Society Faraday Transactions II*. 74: 664 (1978b).
- Clyne, M.A.A. and I.S. McDermid. "Quantum Resolved Dynamics of Excited States - Part 3: Collision Free Lifetimes of BrF(B)," *Journal of the Chemical Society Faraday Transactions II*. 74: 1376 (1978c).

- Clyne, M.A.A. and J.P. Liddy. "Quantum Resolved Dynamics of Excited States - Part 6: Radiative Lifetime and Collisional Deactivation Rates in BrF," *Journal of the Chemical Society Faraday Transactions II*. 76: 1569 (1980).
- Coxon, J.A. "Dissociation Energies of Diatomic Halogen Fluorides," *Chemical Physics Letters*. 33: 136 (1975).
- Coxon, J.A. and A.H. Curran. "High Resolution Analysis of the $B^3\Pi(0^+) \leftarrow X^1\Sigma^+$ Absorption Spectrum of BrF," *Journal of Molecular Spectroscopy*. 75: 270 (1979).
- Coxon, J.A. and M.A. Wickramaarachchi. "The $B^3\Pi(0^+) \rightarrow X^1\Sigma^+$ Emission Spectrum of ^{79}BrF and ^{81}BrF in the Range 6250-8700 Å," *Journal of Molecular Spectroscopy*. 87: 85 (1981).
- Davidson, J. and E. Ogryzlo. "The Quenching of Singlet Molecular Oxygen," *Chemiluminescence and Bioluminescence*, edited by M.J. Cromier et.al., Plenum Press, New York (1977).
- Davis, S.J. "Potential of Halogen Molecules as Visible Chemical Laser Systems," AFWL-TR-79-104: 167, (1979).
- Davis, S.J., L. Hanco and R.F. Shea. "Iodine MonoFluoride $B^3\Pi(0^+) \rightarrow X^1\Sigma^+$ Lasing From Collisionally Populated States," *Journal of Chemical Physics*. 78: 172 (1983).
- Davis, S.J., L. Hanco, and P.J. Wolf. "Continuous Wave Optically Pumped Iodine Monofluoride $B^3\Pi(0^+) \rightarrow X^1\Sigma^+$ Laser," *Journal of Chemical Physics*, 82: 4831 (1985).
- Davis, S.J. "Short-Wavelength Chemical Lasers," *Gas Flow and Chemical Lasers*, Springer Verlag (1987).

- Davis, S.J. and A.M. Woodward. "Excitation of IF $B^3\Pi(0^+)$ by Metastable O_2 , Studies Involving IF(X,v), PSI -2000/ SR - 395, Andover MA: Physical Sciences Inc. (1989a).
- Davis, S.J. et.al. *Excitation of IF $B^3\Pi(0^+)$ by Singlet O_2 : Energy Transfer from $O_2(^1\Sigma)$* , PSI 2000/SR - 364, Andover, MA: Physical Sciences Inc. (1989b).
- Derwent, R.G. and B.A. Thrush. "Excitation of Iodine by Singlet Molecular Oxygen. Part 1 - Mechanism of the I_2 Chemiluminescence," *Journal of the Chemical Society Faraday Transactions II*. 68: 720 (1972).
- Durie, R.A. "The Visible Emission Spectra of Iodine and Bromine Monofluorides and their Dissociation Energies," *Proceedings of the Royal Society A*. 207: 288 (1951).
- Frank, J. "Elementary Processes of Photochemical Reactions, *Transactions of the Faraday Society*. 21: 536 (1925).
- Herbelin, J.M. "Prospects of a Visible (green) Chemical Laser." *Applied Optics*. 25: 2138 (1986).
- Herzberg, G. *Infrared and Raman Spectra*. New York: Van Nostrand Reinhold Co., (1945).
- Herzberg, G. *Molecular Spectra and Molecular Structure I. Spectra of Diatomic Molecules*. New York: Van Nostrand Reinhold Co. (1950).
- Herzberg, G. *Electronic Spectra of Polyatomic Molecules*. New York: B. Van Nostrand Co., (1966).
- Kessler, W.S. and S.J. Davis. "Vibrationally Assisted Transfer Laser Concept," Conference on Lasers and Electro-Optics. Baltimore, MD. 15 May 1991.

- Kolb, C.E. and M Kaufman. "Molecular Beam Analysis Investigation of the Reaction between Atomic Fluorine and Carbon Tetrachloride," *Journal of Physical Chemistry* 76: 947 (1972).
- Landau, V.L. and E. Teller. *Phys Z Sowj Un.* 10: 35 (1936).
- Levine R.D. and R.B. Bernstein. *Molecular Reaction Dynamics and Chemical Reactivity*. New York: Oxford University Press, (1987).
- Lilenfeld, H.V. et.al. "Energy Pooling Reactions in the Oxygen Iodine System," *Journal of Chemical Physics*. 70: 3434 (1979).
- Lowe, B.F. "Energy Transfer in Singlet Oxygen and Bromine Monofluoride," AFIT GEP - 90D, Master's Thesis, (Unpublished), (1990).
- McAffee, K.B. and R.S. Hozack. "Lifetimes and Energy Transfer Near the Dissociation Limit in Bromine," *Journal of Chemical Physics*. 64: 2491 (1976)
- Montroll, E.W. and K.E. Shuler. "Studies in Nonequilibrium Rate Processes. I The Relaxation of a System of Harmonic Oscillators," *Journal of Chemical Physics*. 26: 454 (1957).
- Mulliken, R.S. "The Interpretation of Band Spectra, Part III," *Reviews of Modern Physics*, 4: 1 (1932).
- Nakagawa, K. et.al. "Infrared Diode Laser Spectroscopy of BrF and BrCl," *Journal of Molecular Spectroscopy*, 131: 233 (1988).
- Perram, G.P. "Collisional Dynamics of the $B^3\Pi(0^+)$ State of Bromine Monochloride," Dissertation, AFIT DS-86, (1986).
- Perram, G.P. and G.D. Hager. *The Standard Chemical Oxygen Iodine Laser Kinetics Package*. AFWL-TR-88-50 Air Force Weapons Laboratory, Kirtland AFB, NM (1988).

- Perram, G.P. "Visible Chemical Lasers," *Proceedings of the International Conference on Lasers, 1989*, STS Press (1990).
- Pines, D. "APS Study: Science and Technology of Directed Energy Weapons," *Reviews of Modern Physics*, 59: 34 (1987).
- Samsonov, G.V. ed. *Handbook of Physiochemical Properties of Elements*. IFI Plenum, New York (1968) pg. 254.
- Singh, J.P. et.al. "Electronic to Vibrational Energy Transfer Studies of Singlet Oxygen; 1. $O^2(a^1\Delta_g)$," *Journal of Photochemistry*, 89: 5347 (1985a).
- Singh, J.P. and D.W. Setser. "Electronic to Vibrational Energy Transfer Studies of Singlet Oxygen; 2 $O_2(b^1\Sigma_g^+)$," *Journal of Photochemistry*, 89: 5353 (1985b).
- Slanger, T.G. and G. Black. "Interactions of $O_2(b^1\Sigma_g^+)$ with O (3P) and O_3 ," *Journal of Chemical Physics*. 81: 5730 (1984).
- Steinfeld, J.I. *Molecules and Radiation*. Cambridge: The MIT Press, 1985.
- Steinfeld, J.I. "Rate Data for Inelastic Collision Processes in Diatomic Halogens," *Journal of Physical and Chemical Reference Data*. 13: 445 (1984).
- Swartz R.N., Z.I. Slawsky and K.F. Herzfeld. "Calculation of Vibrational Relaxation Times in Gases," *Journal of Chemical Physics*. 20: 1591 (1952).
- Takehisa, Y. and N. Ohasi. "Dye Laser Excitation Spectroscopy of the 3-3 Band in the $B^3\Pi(0^+) \leftarrow X^1\Sigma^+$ Transition of BrF," *Journal of Molecular Spectroscopy*. 128: 304 (1988).

- Taatjes, C.A. et.al. "Laser Doubled Resonance Measurements of the Quenching Rates of Br with H₂O, HDO and O₂. Unpublished (1991).
- Whitefield, P.D., R.F. Shea and S.J. Davis. "Singlet Molecular Oxygen Pumping of IF B³Π(0⁺)," *Journal of Chemical Physics*. 78: 6793 (1983).
- Wodarczyk, F.J. and H.R. Schlossber. "An Optically Pumped Molecular Iodine Laser," *Applied Physics Letters*. 20: 4476 (1977).
- Wolf, P.J. and S.J. Davis. "Collisional Dynamics of the IF B³Π(0⁺) State. II Electronic Quenching at Low Pressures." *Journal of Chemical Physics*. 83: 91 (1985).
- Wolf, P.J. and S.J. Davis. "Collisional Dynamics of the IF B³Π (0⁺) State. III Vibrational and Rotational Energy Transfer," *Journal of Chemical Physics*. 87: 3492 (1987).
- Ultee, C.J. "The Homogeneous Recombination Rate Constant of F Atoms at Room Temperature," *Chemical Physics Letters*. 46: 366 (1977).

Appendix A. BrF Spectroscopic Data

This appendix summarizes the body of BrF spectroscopic data at the start of this dissertation. The data base has been well developed through absorption (Brodersen, 1958) (Coxon, 1979), emission (Durie, 1951) (Clyne, 1972) (Coxon, 1981) and laser induced fluorescence (LIF) spectroscopy (Takehisa, 1988) (Nakagawa, 1988). The most current values of the spectroscopic values for BrF are those found by Coxon (Coxon, 1981) in emission spectroscopy. He found that the BrF(X) ground state vibrational manifold is well represented by a classic Dunham polynomial expansion in $(v+1/2)$ giving the vibrational constants shown in table A.I.

Table A.I.
Vibrational spectroscopic constants (cm^{-1}) for $^{79}\text{BrF(X)}$ and $^{81}\text{BrF(X)}$
(Coxon, 1981)

	^{79}BrF	^{81}BrF
ω_e''	669.823	668.227
ω_{e_e}''	3.753	3.739
ω_{e_e}''	-8.7×10^{-3}	-7.8×10^{-3}
ω_{e_e}''	-1.6×10^{-4}	-2.0×10^{-4}

Although vibrational constants for the BrF(B) state have been published in the past (Clyne, 1972), Coxon found that a single set of constants was not a completely accurate picture for the B-state

vibrational manifold. Instead, as shown in Table A.II, the energies of the vibrational levels are given as T_v' term values. This value includes both the electronic and vibrational energies.

Table A.II
Term Values (cm^{-1}) for $^{79}\text{BrF(B)}$ and $^{81}\text{BrF(B)}$ (Coxon, 1981)

	<u>^{79}BrF</u>	<u>^{81}BrF</u>
T_8'	21038.809	21033.625
T_7'	20771.368	20766.342
T_6'	20482.367	20477.727
T_5'	20176.215	20172.067
T_4'	19855.327	19851.792
T_3'	19521.244	19518.385
T_2'	19175.037	19172.933
T_1'	18817.572	18816.324
T_0'	18449.496	18449.084

Similarly, he found that while a single set of rotational constants was adequate in the ground state (See Table A.III). This was not the case in the B-state. Here he gives a separate set of rotational constants for each vibrational level (see Table A.IV).

Table A.III

Rotational Constants for $^{79}\text{BrF}(\text{X})$ and $^{81}\text{BrF}(\text{X})$ (Coxon, 1981)

	^{79}BrF	^{81}BrF
B_e	0.3558193	0.3541193
α_e	2.5826×10^{-3}	2.5703×10^{-3}
γ_e	-1.060×10^{-5}	-1.025×10^{-5}

Coxon included the most accurate values for the RKR turning points. These were used as inputs to a computer code acquired from Phillips Laboratory to calculate a set of Franck-Condon factors for ^{79}BrF (Table A.V).

Table A.IV

Rotational Constants (cm^{-1}) for the Vibrational Levels of $^{79}\text{BrF(B)}$ and $^{81}\text{BrF(B)}$ (Coxon, 1981)

v'	^{79}BrF			^{81}BrF		
	B_v'	$10^7 D_v'$	$10^{11} H_v'$	B_v'	$10^7 D_v'$	$10^{11} H_v'$
0	0.255609	4.806		0.254375	4.811	
1	0.252426	4.886		0.251144	4.723	
2	0.249089	5.297		0.247955	5.477	
3	0.245527	5.715		0.244391	5.719	
4	0.241671	6.204		0.240541	6.101	
5	0.237479	6.891		0.236410	6.863	
6	0.232728	7.835		0.231683	7.706	
7	0.227111	9.154	-1.39	0.226135	9.044	-1.33
8	0.219749	11.39	-8.59	0.218863	11.13	-8.39

Table A.V
Franck-Condon Factors of ^{79}BrF

v'	0	1	2	3	4
v''					
0	1.5445E-5	1.1966E-4	4.8959E-4	1.3974E-3	3.1188E-3
1	2.1606E-4	1.4001E-3	4.7702E-3	1.1283E-2	2.0759E-2
2	1.4464E-3	7.6189E-3	2.0862E-2	3.9106E-2	5.6029E-2
3	6.1916E-3	2.5539E-2	5.3406E-2	7.3812E-2	5.5207E-2
4	1.9043E-2	5.8433E-2	8.6108E-2	7.6353E-2	4.0487E-2
5	4.4641E-2	9.4618E-2	8.4906E-2	3.3285E-2	1.2660E-3
6	8.2835E-2	1.0795E-1	4.1805E-2	1.7712E-4	2.0442E-2
7	1.2516E-1	8.1424E-2	2.4322E-3	2.4885E-2	5.2424E-2
8	1.5671E-1	3.1506E-2	1.5062E-2	6.0264E-2	2.7870E-2
9	1.6449E-1	6.6587E-4	6.0865E-2	4.1162E-2	1.9670E-5
10	1.4411E-1	1.8042E-2	7.5189E-2	2.6541E-3	3.0173E-2
11	1.1048E-1	7.0836E-2	3.8212E-2	1.6740E-2	5.3237E-2
12	7.1595E-2	1.1890E-1	1.7748E-3	6.1311E-2	1.9527E-2
13	3.9961E-2	1.5231E-1	1.7122E-2	6.1071E-2	1.7076E-3
14	1.9217E-2	1.1071E-1	7.3143E-2	1.7305E-2	4.1296E-2
15	7.9625E-3	7.3679E-2	1.1943E-1	2.1556E-3	6.4795E-2

Table A.V continued

v'	5	6	7
v''			
0	5.7963E-3	9.3243E-3	1.3373E-2
1	3.1637E-2	4.1544E-2	4.8438E-2
2	6.5051E-2	6.3317E-2	5.2794E-2
3	5.5207E-2	2.9690E-2	9.7643E-3
4	9.1821E-3	9.6752E-5	8.8721E-3
5	8.8180E-3	2.9819E-3	3.7742E-2
6	4.4265E-2	3.5939E-2	1.2960E-2
7	2.8778E-2	2.1832E-3	5.0289E-3
8	1.2130E-6	1.7899E-2	3.3716E-2
9	2.7952E-2	3.8088E-2	1.3455E-2
10	4.2356E-2	7.0495E-3	4.2645E-3
11	7.2523E-3	1.0442E-2	3.3700E-2
12	1.0552E-2	4.0656E-2	1.5542E-2
13	4.7469E-2	1.6775E-2	3.0408E-3
14	3.1416E-2	2.8878E-3	3.4986E-2
15	9.9271E-5	3.9384E-2	2.2232E-2

The radiative lifetimes of BrF are included in this appendix due to the importance of these values in the calculation of vibrational transfer rate constants. The latest estimates are those of Clyne and Liddy (Clyne, 1980). These values, quoted in table A.VI, are approximately thirty percent higher than those from previous studies (Clyne, 1978). The change is due to correction of diffusion problems in the test chamber.

Table A.VI

BrF(B) Radiative Lifetimes (μs), Mean Standard Deviation $\sigma = 1.2 \mu\text{s}$ (Clyne, 1980)

<u>v'</u>	<u>J'</u>	<u>^{79}BrF</u>	<u>^{81}BrF</u>
7	28	59.4	57.3
	27	60.1	60.1
	20	65.2	65.5
	11	63.2	62.8
6	48	10.4	52.7
	47	58.3	58.6
	46	58.8	58.5
	45	62.1	58.0
	21	62.6	62.2
	10	63.0	62.7
5	21	58.9	----
4	21	59.0	----
3	21	55.5	----

APPENDIX B. Montroll-Shuler Computer Model

One important requirement in this dissertation was the development of a computer model to calculate the Montroll-Shuler solution to vibrational transfer. Two final versions were written, the first MONT to predict the Montroll-Shuler solution for a set of input conditions, and MNTFIT which calculates the fundamental rate constant that best matches the Montroll-Shuler prediction to an experimental waveform. These models were coded in PASCAL and implemented on a Zenith-248 microcomputer with a math co-processor.

The Montroll-Shuler equation, incorporating radiative and electronic quenching losses is:

$$x_n(t) = \left[\frac{(1-e^{-\theta}) e^{m\theta}}{(e^{-t'} - e^{-\theta})} \right] \left(\frac{e^{-t'} - 1}{e^{-t'} - e^{-\theta}} \right)^{m+n} F(-n, -m, 1; U^2) e^{(-t/\tau)} \quad (B.1)$$

Where:

$$1/\tau = 1/\tau_r + k^{EQ} M$$

$$t' = k^v(1,0) t (1-e^{-\theta})$$

$$U = \sinh(\theta/2)/\sinh(t'/2)$$

$$F = \text{hypergeometric function}$$

The parameters of this equation are as defined in section 4.4.1.1. The

most challenging aspect of encoding this equation was the hypergeometric function $F(-n, -m, 1, U^2)$. The general form of the hypergeometric function is (Andrews, 1985 :276):

$$F(a, b; c; x) = \sum_{n=0}^{\infty} \frac{(a)_n (b)_n}{(c)_n} \frac{x^n}{n!} \quad |x| < 1 \quad (B.2)$$

Where $(a)_n$ etc. are called Pochhammer symbols:

$$(a)_n = a(a+1)\dots(a+n-1), \quad n = 1, 2, 3, \dots \quad (B.3)$$

The hypergeometric function $F(a, b; c; x)$ can be simplified by the observation that when either 'a' or 'b' or both is zero or a negative integer, the series is finite, converging for all x. In other words, if 'a' = -m (m = 0, 1, 2, ...) then $(m)_n = 0$ for all $n > m$ and the general form of the hypergeometric function reduces to the hypergeometric polynomial (Anderson, 1985:277):

$$F(-m, b; c; x) = \sum_{n=0}^m \frac{(-m)_n (b)_n}{(c)_n} \frac{x^n}{n!} \quad (B.4)$$

In the Montroll-Shuler solution the first two indices of the hypergeometric function are always negative integers. Therefore the simplified form, the hypergeometric polynomial was encoded.

The MONT program calculates the $x_n(t)$ values for a specified input range of time. The required inputs are $k^v(1,0)$, k^{EQ} , ν_{fund} , τ_r ,

temperature and M.

To test this program a 5 level rate equation matrix was directly solved to generate a synthetic population spectrum. Figure 39 shows the Montroll-Shuler and the rate matrix solutions for the input parameters given in table B.I.

MONT was then incorporated as a module in another program MNTFIT. Given an experimental waveform MNTFIT determines the $k^v(1,0)$ value that provides the best Montroll-Shuler fit to the experimental data.

The model first asks for an initial guess for $k^v(1,0)$ which is used to calculate an initial set of $x_n(t)$ solutions for a specified range of time. The peak value from this list is then compared to the highest point in the experimental data to determine a normalization factor. This factor is used to convert the $x_n(t)$ values to the intensity scale of the experimental observations. The model then varies $k^v(1,0)$ to minimize a least squares merit function:

$$\text{MERIT} = \sum_t \left(x_{\text{data}}(t) - \left[(\text{scale}) (x_n(t)) \right] \right)^2 \quad (\text{B.5})$$

Where $x_{\text{data}}(t)$ is an experimental data point at time t , and scale is the calculated scale factor.

Table B.I

Input parameters for the rate matrix comparison.

$k^v(1,0) = 3.4 \times 10^{-12} \text{ cm}^3/(\text{molecule} \cdot \text{s})$	Temp = 300 °K
$k^{EQ} = 3.5 \times 10^{-12} \text{ cm}^3/(\text{molecule} \cdot \text{s})$	$\tau_r = 59 \text{ } \mu\text{s}$
$\nu_{\text{fund}} = 1.12 \times 10^{13} \text{ hz}$	$M = 1.0 \times 10^{16} \text{ cm}^{-3}$
$\nu_{\text{initial}} = 3$	$\nu_{\text{final}} = 0$

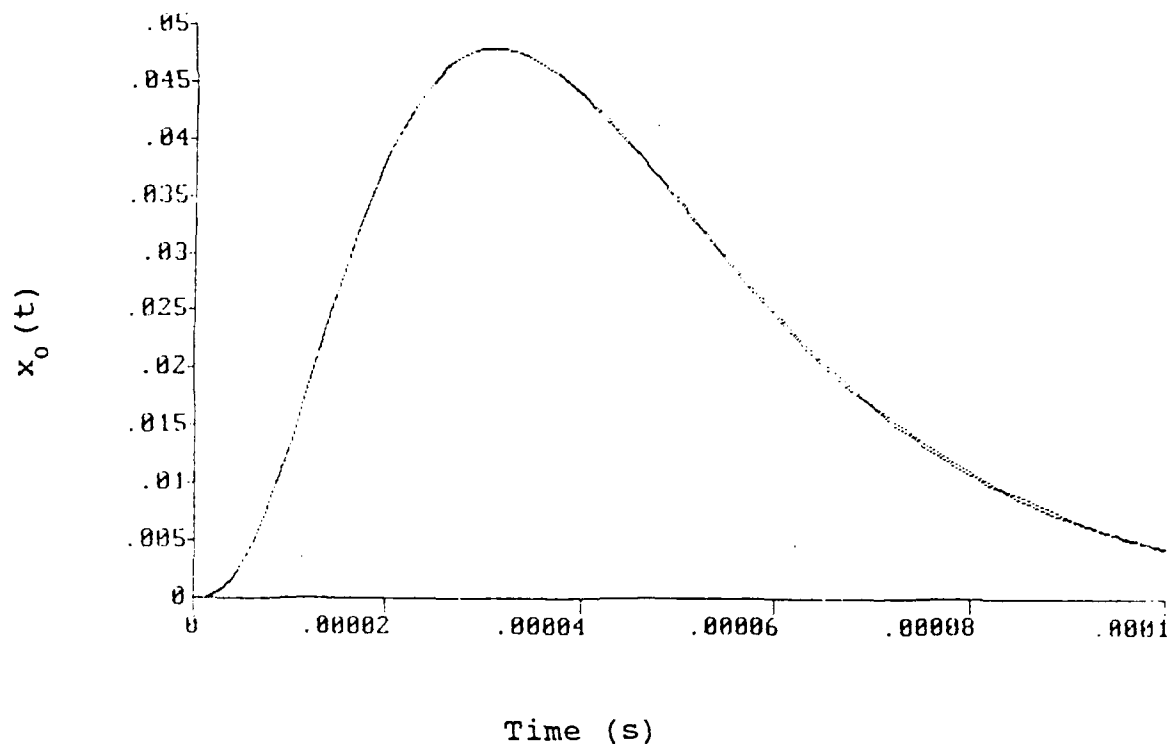


Figure 39. Montroll-Shuler comparison to rate equation result.

This minimization proceeds by a simple stepping function, calculating the MERIT with each change in $k^v(1,0)$. This step size is chosen by the user to produce the desired accuracy in the final estimate of the rate constant.

Once the best $k^v(1,0)$ has been selected, the scale factor is adjusted and the process repeated. The final output of the model is a fundamental rate constant $k^v(1,0)$, a scale factor and a list of output values for $x_n(t)$.

This fitting procedure was tested by using a known list of input data scaled by an arbitrary factor. The model produced the correct $k^v(1,0)$ rate within the limits of the chosen step size.

Appendix C. Experimental Calibrations and Calculations

I. Monochromator Resolution

The spectral resolution of the McPherson 0.3 m monochromator used in the singlet oxygen excitation studies (chapter III), is shown as a function of slit width in Figure 40. The resolution was measured as the full width at half maximum (FWHM) of a spectral line from a neon lamp. Extrapolating from this figure gives a FWHM resolution of 7 \AA at the $300 \text{ }\mu\text{m}$ slit widths used during most of these studies.

The spectral resolution of the ISA HR-360 0.64 m monochromator, used in the spectrally resolved laser induced fluorescence (LIF) studies was determined in the same way. Figure 41 shows spectral resolution of this device as a function of slit width. In this case the resolution is the FWHM of a spectral feature from a Hg lamp. Slit widths of 1 mm were used in the vibrational transfer studies to maximize the LIF signal. Extrapolating from Figure 41 shows that the spectral resolution at 1 mm slit widths was 22.4 \AA .

The absolute wavelength calibration for both instruments was determined from the known spectra of the test lamps.

II. Spectral Response

a. Singlet Oxygen Excitation Studies. The relative spectral response of the detector system, consisting of the 0.3 m monochromator and the RCA C31034A-02 photomultiplier tube (PMT), was a factor in relating

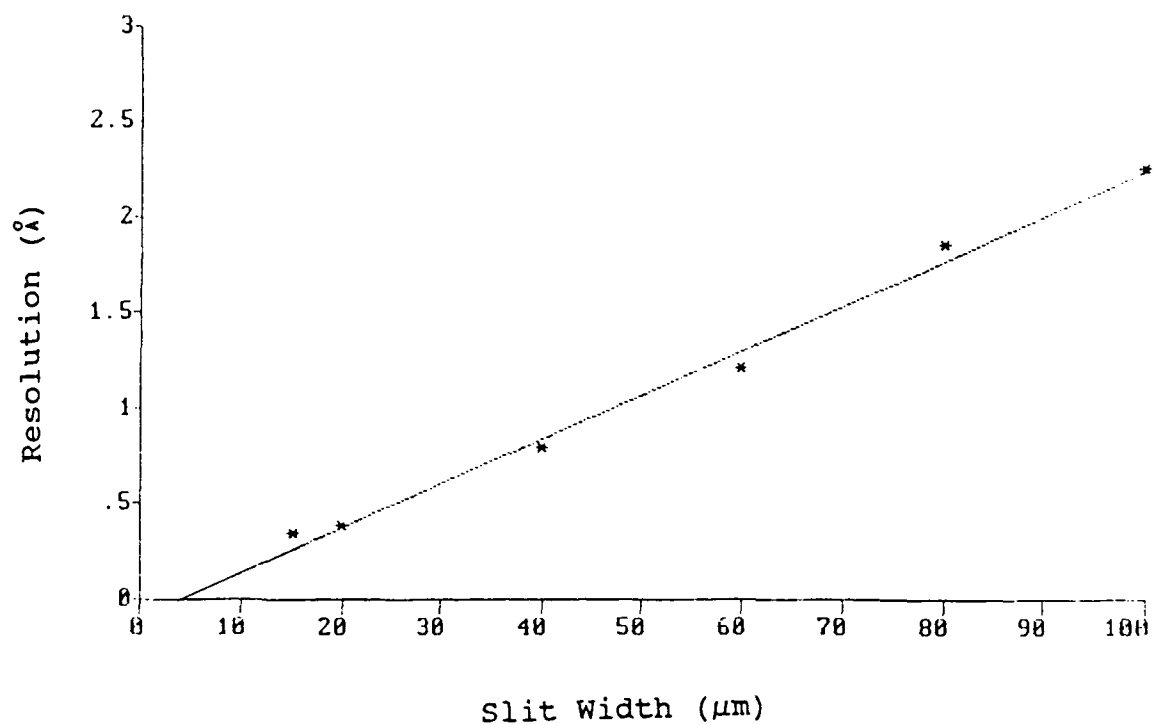


Figure 40. Spectral resolution of the McPherson 0.3 m monochromator.

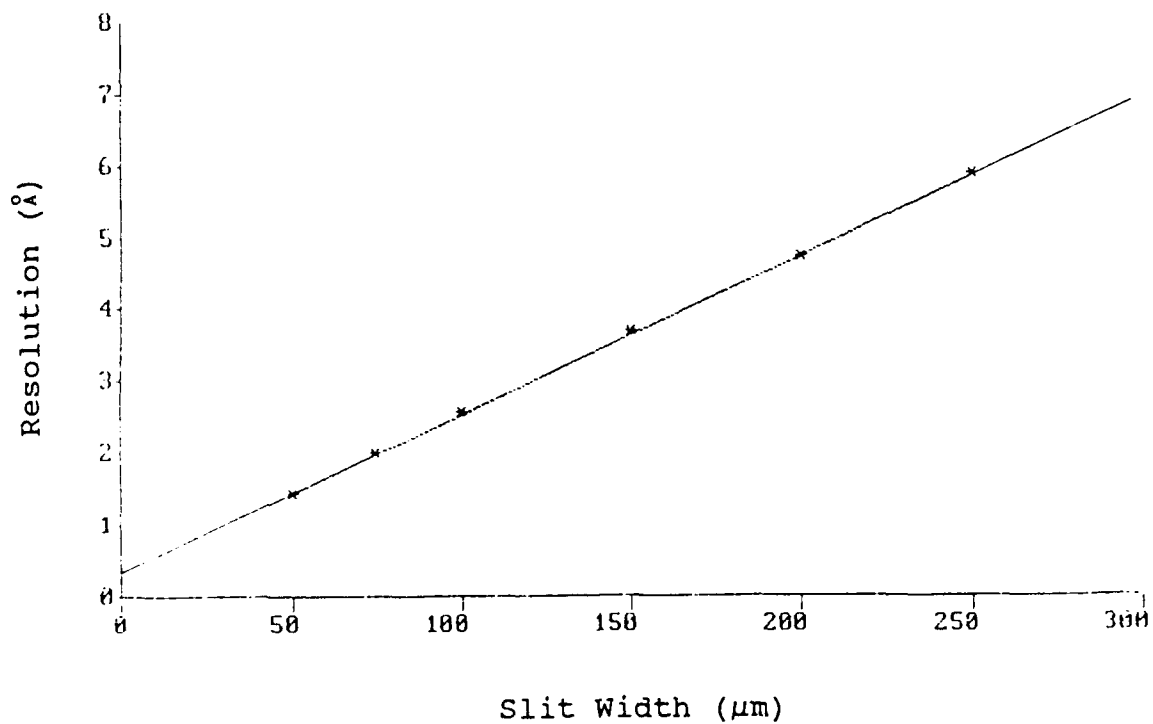


Figure 41. Spectral Resolution of the ISA HR-360 0.64 m monochromator.

observed line intensities to excited state population densities. This calculation was fundamental to the determination of BrF B-state vibrational populations in these emission experiments. The response of the detector system was evaluated by recording the emission spectrum of a blackbody source at 1000 °C and comparing it to the predicted spectrum calculated from the Planck Blackbody Radiation Law. This work was performed by an AFIT master's student, Barrett F. Lowe, and described in detail in his thesis (Lowe, 1990).

b. Electronic Quenching Studies. In this work, the total fluorescence excited by the laser pulses was observed directly by a C31034 PMT. It was not feasible to perform a blackbody calibration in this circumstance since no monochromator was utilized. A 6300 Å long wavelength pass colored-glass filter was used to block scattered laser light. The published spectral response of the PMT is flat across the visible spectrum to a wavelength of 8800 Å, after which it falls off abruptly. The relative response to the total emission from each BrF(B) vibrational state is an important consideration. Although the wavelength response is flat, differing fractions of the total emission from each ν' level fall within the 6300-8800 Å effective bandpass of the detection system. This is an important consideration in interpreting non-exponential total fluorescence waveforms such as those for SF₆.

The relative response was calculated by first noting the Franck-Condon factors for all transitions from a particular ν' level falling within the effective bandpass. These were then scaled by ν^4 (frequency) and then normalized by the center frequency of the bandgap.

This scaling was required since:

$$I_{\text{emission}} = \left(\frac{64 \pi^4}{3} \right) c \nu^4 q_{\nu', \nu''} S_J |R_e|^2 N_{\nu'} \quad (\text{C.1})$$

Where:

ν = emission frequency

$q_{\nu', \nu''}$ = Franck-Condon factor

S_J = Hönl-London factor (rotational line strength)

$|R_e|^2$ = electronic transition moment

$N_{\nu'}$ = Number density in the ν' level

In electronic transitions, only frequency and Franck-Condon Factor would differ among the (ν', ν'') emission bands from a particular ν' level. The results of this analysis are shown in Figure 42, where the relative response is plotted as a function of ν' level. This figure demonstrates that emission from the lowest ν' levels is detected most efficiently in total fluorescence observations.

c. Vibrational Transfer Studies. Spectral response of the detection system was not an issue in these spectrally resolved observations. No information was extracted from the relative intensities of spectrally resolved features.

III. Calculation of Overlap Fractions

The vibrational bands in the BrF(B-X) emission spectrum are severely overlapped. This combined with the spectral resolution required in the

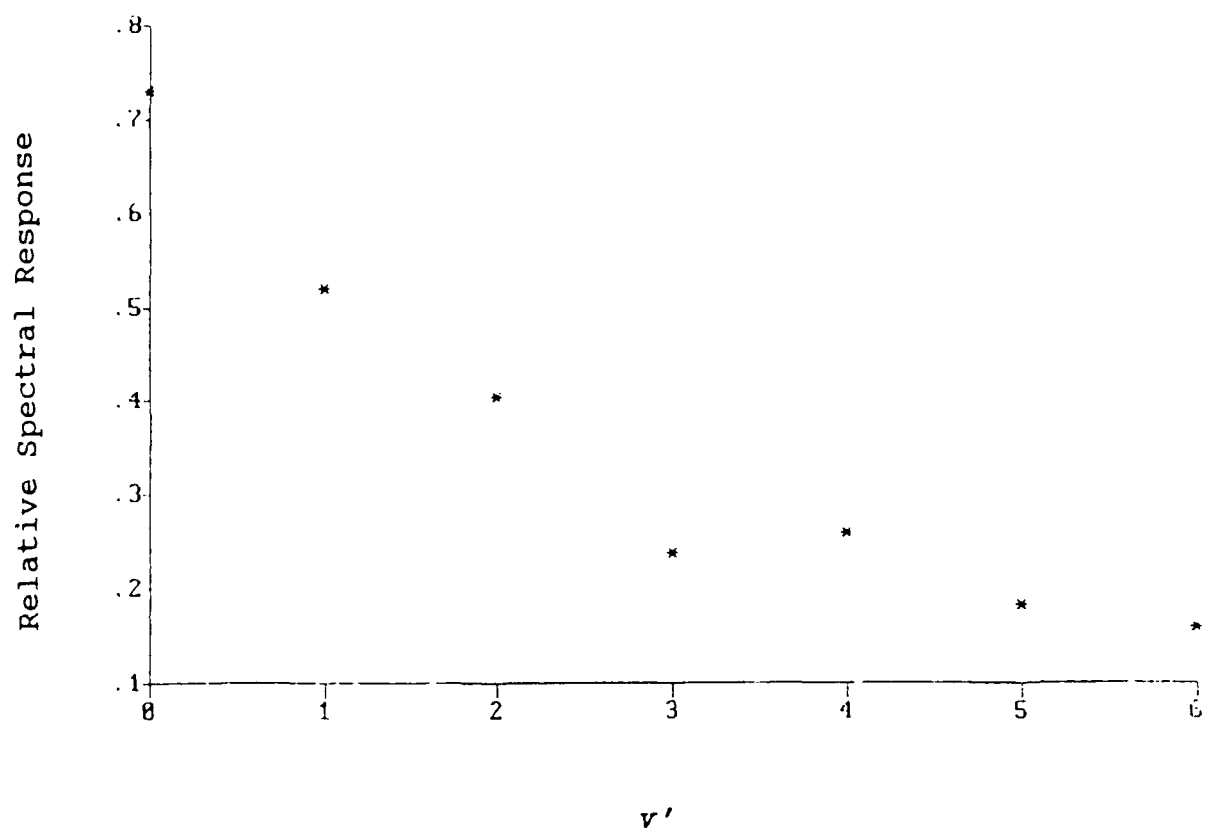


Figure 42. Relative spectral response to total fluorescence emitted from BrF(B) v' levels.

Table C.I

Observation Wavelengths (\AA) Used in the Vibrational Transfer Experiments

<u>v'</u>	<u>Wavelength</u>
6	6915
5	5403
4	5694
3	5847
2	6181
1	6850
0	7015

vibrational transfer studies, 22.4 \AA , precluded the isolation of individual v' levels. The vibrational transfer spectrum generated by scanning the monochromator for a fixed pump laser wavelength (Figure 27) was used to select, and quantify the degree of band overlap at, observation wavelengths (Table C.I).

The intensity observed at a particular observation wavelength is the sum of the emission from all v' levels falling within the resolution of the monochromator:

$$I_{\text{obs}} = C \sum_{v', v''} q_{v', v''} N_{v'} h(\lambda_{\text{obs}} - \lambda_{v', v''}) \quad (\text{C.2})$$

Where C is an arbitrary constant and $h(\lambda_{\text{obs}} - \lambda_{v',v''})$ is a response function describing the intensity at the observation wavelength in comparison to the intensity at the bandhead. The other variables are as defined in equation (C.1). The response function was estimated from a vibrational transfer spectrum recorded at the same monochromator resolution as in the vibrational transfer kinetic experiments. A triangular vibrational band intensity distribution was assumed.

$$h(\lambda_{\text{obs}} - \lambda_{v',v''}) = \begin{cases} 1 - (\lambda_{\text{obs}} - \lambda_{v',v''}) / 120 \text{ \AA} & 120 \text{ \AA} > \lambda_{\text{obs}} - \lambda_{v',v''} > 0 \\ 1 - (\lambda_{v',v''} - \lambda) / 34 \text{ \AA} & -34 \text{ \AA} < \lambda_{\text{obs}} - \lambda_{v',v''} < 0 \\ 0 & \text{elsewhere} \end{cases} \quad (\text{C.3})$$

The effective Franck-Condon factor $h(\lambda_{\text{obs}} - \lambda_{v',v''}) \cdot q_{v',v''}$ was calculated for each overlap band at an observation wavelength. The effective Franck-Condon factors are used as inputs in MNTFIT, the Montroll-Shuler fitting model. The evolution of the population densities is calculated in the model. The effective Franck-Condon factors are the basis for the band overlap percentages given in Table IV in chapter IV.

Appendix D. Systematic Error

The quoted errors in chapter IV are the standard deviations in the the Stern-Volmer plots used to assign rate constants. There is a more global systematic error present that can cause variations in the rates determined from different data sets.

There are two sources of error in the electronic quenching experiments. The first is the measurement of buffer gas pressures. The total pressure measurements are accurate, the capacitance manometer error is rated as 0.12 % of the pressure reading. The zero for this instrument was set by evacuating the system to 10^{-6} torr with a diffusion pump. All electronic quenching measurements were performed with an argon background pressure of ≈ 200 mtorr. The mix and added buffer gas partial pressures are measured on top of this background. Small shifts in the argon pressure over the time required to take a data set can causes inaccuracies in pressure measurements of added buffer gas. Shifts as high as 2 mtorr in argon pressure have been observed over the course of a set of measurements. When the total added buffer gas pressures are small (15 mtorr), in the case of efficient quenchers, these shifts can cause errors of up to 20 % in the rate constant measurement. Added buffer gas was measured as the difference between successive observations to minimize this problem.

Another error source is in BrF production. Small shifts in Br₂ flow or microwave discharge efficiency can change the amount of BrF produced. This can be significant in examining gases with low quenching rates. The

BrF production mix is overwhelmingly CF₄. BrF is only $\approx 1\%$ of the mix. Br₂ and most likely BrF have large quenching rate constants. The measured quenching rate constant for the mix was $3.43 \times 10^{-12} \text{ cm}^3/(\text{molecule} \cdot \text{s})$, yet the measured rate constant for CF₄ is only 2.07×10^{-12} . Thus the small percentage of added Br₂/BrF changed the rate constant by 65%. A small change of 20% in Br₂ flow or BrF production could change the measured quenching rate constant for a low quencher by $\approx 10\%$.

Considering both error sources a total systematic error of 20% is estimated for all measured electronic quenching rate constants.

In the vibrational transfer experiments, the largest source of error is in the calculation of band overlap fractions. The effects of this error is incorporated in the standard deviation in the final fundamental vibrational transfer rate constant for the BrF mix $(3.5 \pm .6) \times 10^{-12} \text{ cm}^3/(\text{molecule} \cdot \text{s})$.

Abstract

When Br_2 is combined with F atoms and discharged oxygen in a flow tube, $\text{BrF } B^3\Pi(0^+)$ is produced in a highly non-thermal distribution peaking at $v'=3$. The emission was linearly dependent on the $\text{O}_2(b^1\Sigma)$ concentration. The observed dependence of the $\text{BrF}(B)$ emission on Br_2 and atomic oxygen is inconsistent with a steady state prediction of a sequential excitation mechanism, where $\text{BrF}(X)$ is excited by successive collisions with singlet oxygen. The experimental data are consistent with a three body mechanism involving Br and F atoms.

Electronic quenching of $\text{BrF}(B)$ by a number of collision partners (Br_2 , CO_2 , O_2 , N_2 , CF_4 , SF_6 , Ar) was examined for three vibrational levels using laser induced fluorescence (LIF) techniques. The rate coefficients ranged from $<6 \times 10^{-14} \text{ cm}^3/(\text{molecule} \cdot \text{s})$ as an upper limit for argon, to $(6.86 \pm 1.18) \times 10^{-11} \text{ cm}^3/(\text{molecule} \cdot \text{s})$ for Br_2 .

Vibrational transfer in $\text{BrF}(B)$, induced by the BrF production mix ($\text{CF}_4, \text{Br}_2, \text{F}$) was measured by observing the spectrally resolved LIF emission from each vibrational level after an initial excitation of $\text{BrF}(B) v'=5$. This vibrational transfer obeyed a simple theoretical prediction, the Montroll-Shuler model. A single fundamental rate coefficient $k^v(1,0) = (3.5 \pm 0.6) \times 10^{-12} \text{ cm}^3/(\text{molecule} \cdot \text{s})$ characterizes vibrational transfer.